

$$ZF\hat{I}T_{ER}$$

An Analytical Program for Fermion Pair Production in e^+e^- Annihilation

D. Bardin¹, M. Bilenky^{1,2,†}, A. Chizhov¹, O. Fedorenko³, S. Ganguli⁴,
A. Gurtu⁴, M. Lokajicek¹, G. Mitselmakher¹, A. Olshevsky¹, J. Ridky¹,
S. Riemann^{5,‡}, T. Riemann^{5,6}, M. Sachwitz⁵, A. Sazonov¹, A.D. Schaile⁷,
Yu. Sedykh¹, I. Sheer⁸, L. Vertogradov¹

¹ Joint Institute for Nuclear Research, Dubna, Russia

² Universität Bielefeld, Germany

³ Petrosavodsk State University, Petrosavodsk, Russia

⁴ Tata Institute of Fundamental Research, Bombay, India

⁵ DESY – Institut für Hochenergiephysik, Zeuthen, Germany

⁶ Theory Division, CERN, Geneva, Switzerland

⁷ Albert-Ludwigs-Universität, Freiburg, Germany

⁸ University of California, San Diego, USA

Abstract

We describe how to use $ZF\hat{I}T_{ER}$, a program based on a semi-analytical approach to fermion pair production in e^+e^- annihilation and Bhabha scattering. A flexible treatment of complete $\mathcal{O}(\alpha)$ QED corrections, also including higher orders, allows for three calculational **chains** with different realistic sets of restrictions in the photon phase space. $ZF\hat{I}T_{ER}$ consists of several **branches** with varying assumptions on the underlying hard scattering process. One includes complete $\mathcal{O}(\alpha)$ weak loop corrections with a resummation of leading higher-order terms. Alternatively, an ansatz inspired from S-matrix theory, or several model-independent effective Born cross sections may be convoluted. The program calculates cross sections, forward-backward asymmetries, and for τ pair production also the final-state polarization. Various **interfaces** allow fits to be performed with different sets of free parameters.

[†] Alexander-von-Humboldt Fellow

[‡] Partly supported by the German Bundesministerium für Forschung und Technologie

Contents

1	Introduction	4
1.1	$z_F \overline{I} T_{ER}$ Chains	6
1.2	$z_F \overline{I} T_{ER}$ Branches	6
1.3	$z_F \overline{I} T_{ER}$ Interfaces	7
2	Chains of $z_F \overline{I} T_{ER}$: Photonic Corrections with Different Cuts	8
2.1	No Cuts	10
2.2	Convolution Integral with Cut on the Invariant Mass of the Outgoing Fermion Pair (s'_{\min})	11
2.3	Convolution Integral with Cuts on Fermion Energies and Acollinearity (E_f^{\min}, ξ^{\max})	11
2.4	Photonic Corrections for Bhabha Scattering	13
3	The Hard Scattering Process: (I) The Standard Model Branch	15
3.1	$\mathcal{O}(\alpha)$ Corrections to Δr	17
3.2	$\mathcal{O}(\alpha)$ Corrections to Γ_Z	17
3.3	$\mathcal{O}(\alpha)$ Corrections to Fermion Pair Production	20
3.4	Higher-Order Corrections	26
4	The Hard-Scattering Process: (II) Model-Independent Branches	31
4.1	Effective Couplings	31
4.2	Partial Z Widths	32
4.3	S-Matrix	33
5	Beyond the Standard Model	36
6	Initialization of $z_F \overline{I} T_{ER}$	39
6.1	Subroutine ZUINIT	39
6.2	Subroutine ZUFLAG	39
6.3	Subroutine ZUWEAK	44
6.4	Subroutine ZUCUTS	45
6.5	Subroutine ZUINFO	46
7	Interface Routines of $z_F \overline{I} T_{ER}$	46
7.1	Subroutine ZUTHSM	46
7.2	Subroutine ZUTPSM	47
7.3	Subroutine ZUXSA	47
7.4	Subroutine ZUXSA2	48
7.5	Subroutine ZUTAU	49
7.6	Subroutine ZUXSEC	49
7.7	Subroutine ZUSMAT	50
8	Comparisons	50
8.1	Weak Mixing Angles and Partial Z Widths	51
8.2	Cross Sections and Asymmetries	54
8.3	Conclusions	59

References	60
A Common Blocks	65
A.1 ZF^{T}_{ER} Common Blocks	65
A.2 DIZET Common Blocks	66
B Subroutine ZFTEST	66
B.1 Subroutine ZFTEST	67
B.2 ZFTEST Results	71

List of Figures

1	Scattering angle ϑ in e^+e^- annihilation.	4
2	Real photon emission.	8
3	Photonic vertex corrections.	9
4	Box diagrams with virtual photons.	9
5	Dalitz plot for the photon phase space with a cut on s'	11
6	Dalitz plot for the photon phase space with cuts on E^f and ξ	12
7	Top-quark exchange diagrams which contribute to Γ_b	19
8	Photon and Z self energies.	20
9	Vertex corrections to the Z matrix element.	21
10	Box diagrams contributing to the Z matrix element.	21
11	Matrix element in the approach with effective Z couplings.	31
12	Matrix element for the Z resonance scattering.	32
13	Scattering in the S-matrix approach.	34
14	The structure of ${}_{ZF}I^T T_{ER}$	40
15	Cross section ratios from ${}_{ZF}I^T T_{ER}$ and ZSHAPE for muon and hadron production; both programs with their ‘recommended’ choice of flags.	56
16	Cross section ratios from ${}_{ZF}I^T T_{ER}$ and ZSHAPE for muon and quark production; flags are chosen such that the theoretical assumptions of both programs are as similar as possible.	57
17	Comparisons of σ^μ and A_{FB}^μ as predicted by ${}_{ZF}I^T T_{ER}$ and ALIBABA.	58
18	Same as in foregoing figure, at LEP I energies.	58
19	Same as in foregoing figure, for Bhabha scattering at LEP I energies.	59

List of Tables

1	Weak mixing angle and partial and total Z widths.	19
2	The running QED coupling as a function of the centre-of-mass energy.	20
3	Leptonic form factors $\rho_{ef}, \kappa_e, \kappa_f, \kappa_{ef}$ as functions of the centre-of-mass energy.	22
4	Differential cross sections in nb for $\mu^+\mu^-$ production both with and without weak box contributions for selected LEP I energies.	23
5	The weak mixing angle, muon pair production cross section and asymmetry both with and without leading $\mathcal{O}(\alpha^2 m_t^4)$ terms.	28
6	Λ_{MS} for different energy regions.	29
7	Running $\alpha_s(q^2)$ versus $ q $	29
8	The dependence of the form factors ρ_{ef} and $\kappa_e, \kappa_f, \kappa_{ef}$ at the Z peak on different treatments of $\mathcal{O}(\alpha\alpha_s)$ corrections.	30
9	Flag settings for ${}_{ZF}I^T T_{ER}$	41
10	Indices used by ${}_{ZF}I^T T_{ER}$ interface routines to select the final-state fermion pair.	45
11	Comparison of $\sin^2 \theta_W, s_W^{2,\text{eff}}$ and $\sin^2 \theta_W^{\text{MS}}$ as calculated by ${}_{ZF}I^T T_{ER}$ and by programs from Hollik and Degrassi, Fanchiotti, Sirlin.	52
12	Partial and total widths of the Z boson from ${}_{ZF}I^T T_{ER}$, Hollik, and Degrassi, Sirlin.	53
13	Flag settings in ${}_{ZF}I^T T_{ER}$ for comparisons of cross sections and asymmetries.	54

1 Introduction

There is a growing demand for flexible programs to fit the very precise data on fermion pair production from experiments at the e^+e^- storage ring LEP I:

$$e^+e^- \longrightarrow f\bar{f}(n\gamma), \quad (1.1)$$

including Bhabha scattering,

$$e^+e^- \longrightarrow e^+e^-(n\gamma). \quad (1.2)$$

It is important that such programs allow for model-independent and Standard Model [1] fits to the data. In addition, it is interesting to be able to fit the data to theories that go beyond the Standard Model. Because experimental cuts tend to be more complicated than can be realized with semi-analytic programs, typically Monte Carlo programs are used to correct for such cuts and detector inefficiencies before fitting.

In this article, we describe the subroutine package $ZFI^T T_{ER}$. This program [2] is based on a semi-analytical approach to the radiative corrections that are needed for the analysis of reactions (1.1) and (1.2).

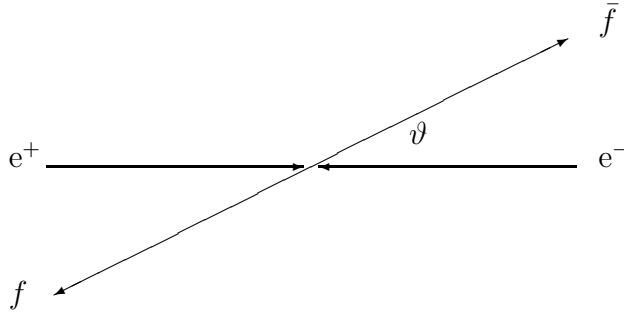


Figure 1: *Scattering angle ϑ in e^+e^- annihilation.*

The $ZFI^T T_{ER}$ package employs an approach which relies on formulae that are analytically integrated over a finite angular region with respect to the scattering angle, as shown in fig. 1. The program directly calculates predictions for observable quantities and *not* corrections to Born approximations. The total cross section, σ_T , and the forward-backward asymmetry, A_{FB} , may be calculated in a non-symmetric angular interval, $c_1 < \cos \vartheta < c_2$:

$$\sigma_T(c_1, c_2) = \int_{c_1}^{c_2} d \cos \vartheta \frac{d\sigma}{d \cos \vartheta}, \quad (1.3)$$

$$A_{FB}(c_1, c_2) = \frac{\sigma_{FB}(c_1, c_2)}{\sigma_T(c_1, c_2)}, \quad (1.4)$$

where

$$\sigma_{FB}(c_1, c_2) = \left[\int_0^{c_2} d \cos \vartheta - \int_{c_1}^0 d \cos \vartheta \right] \frac{d\sigma}{d \cos \vartheta}. \quad (1.5)$$

These expressions are constructed from the following integrals:

$$\sigma(0, c) \equiv \int_0^c d \cos \vartheta \frac{d\sigma}{d \cos \vartheta} = \frac{1}{2} [\sigma_T(c) + \sigma_{FB}(c)]. \quad (1.6)$$

Here $\sigma_T(c)$ and $\sigma_{FB}(c)$ are two special cases of $\sigma_A(c_1, c_2)$, which will be the basis of the discussion in the following chapters:

$$\sigma_T(c) = \int_{-c}^c d \cos \vartheta \frac{d\sigma}{d \cos \vartheta}, \quad (1.7)$$

$$\sigma_{FB}(c) = \left[\int_0^c d \cos \vartheta - \int_{-c}^0 d \cos \vartheta \right] \frac{d\sigma}{d \cos \vartheta}. \quad (1.8)$$

By simple algebraic combinations of the above constructs, one may derive various measurable cross sections and asymmetries. One must, of course, take into account the possible beam polarizations and final-state helicities within the hard subprocess description ($\sigma_{T,FB}^o$) as explained below.

For reaction (1.1), excluding Bhabha scattering which will be discussed in section 2.4, both functions σ_T and σ_{FB} may be split into different contributions from initial-state radiation, σ^{ini} , final-state radiation, σ^{fin} , and their interference, σ^{int} ($A = T, FB$):

$$\sigma_A(c) = \sigma_A^{\text{ini}}(c) + \sigma_A^{\text{int}}(c) + \sigma_A^{\text{fin}}(c). \quad (1.9)$$

Common soft photon exponentiation for initial- and final-state radiation, which relies on a more compact (but also more sophisticated) formula, has been realized in ${}_{ZF}I^T T_{ER}$:

$$\sigma_A(c) = \sigma_A^{\text{ini+fin}}(c) + \sigma_A^{\text{int}}(c). \quad (1.10)$$

Alternatively, the program allows the user to choose a simplified treatment of the (small) contribution from final-state radiation:

$$\sigma_A(c) = \sigma_A^{\text{ini}}(c) \left(1 + \frac{3}{4} \frac{\alpha}{\pi} Q_f^2 \right) + \sigma_A^{\text{int}}(c). \quad (1.11)$$

The expressions introduced in (1.10) and in (1.11) are realized in ${}_{ZF}I^T T_{ER}$ as one-dimensional numeric integrations over a photon phase space variable s' .

Photonic corrections to the cross sections and asymmetries are implemented by convoluting the Born cross sections ($\sigma_A^{a,o}$) with radiator functions (R_A^a):

$$\sigma_A^a(c) = \frac{1}{d_A} \Re \int_0^\Delta dv \sigma_A^{a,o}(s, s') R_A^a(v, c), \quad (1.12)$$

where $a = \text{ini, ini+fin, int}$; $d_T = \frac{4}{3}$, $d_{FB} = 1$; $s' = (1 - v)s$; and v is the energy of the radiated photon in units of the beam energy. Further, σ_A^o contains the dynamics of the basic process to be studied, and the functions R_A^a depend on the treatment of the QED effects. There are several ways to describe ${}_{ZF}I^T T_{ER}$. It contains:

- three calculational *chains* with a different handling of QED corrections plus the Bhabha *chain*,
- four *branches* which differ by the theoretical description of the hard scattering process,
- seven *interfaces* with different choices of input/output parameters.

1.1 $ZF\overline{f}T_{ER}$ Chains

No cuts - a fast option

In this chain, the cross sections are calculated with formulae that assume that there are no cuts applied to the photon phase space.

Phase-space cut on the minimum invariant mass of the $f\bar{f}$ pair

The underlying formulae may be found in [3],[4] and in references quoted therein. This chain allows for a cut on the minimum invariant mass of the final-state $f\bar{f}$ pair, which can be reinterpreted as a cut on the maximum of the allowed energy of the bremsstrahlung photon.

Cuts on energies and acollinearity of final-state fermions

This treatment of the photon phase space follows the basic lines of that of the above chain. The restriction on the maximal photon energy is replaced by a simultaneous cut on both the energies of the produced fermions and on their acollinearity [5]. This chain also allows the calculation of differential and integrated cross sections for Bhabha scattering using the BHANG package [6], which has been incorporated into $ZF\overline{f}T_{ER}$.

Furthermore, in both the latter chains one can impose a restriction on the maximum production angle of the outgoing antifermion¹.

1.2 $ZF\overline{f}T_{ER}$ Branches

Analytic Standard Model formulae with higher-order corrections

This is the central branch of the program. The calculations of the partial and total Z and W widths follow [7] and [8] respectively. The explicit formulae for the improved Born cross sections with electroweak corrections are described in [9]. In addition, improvements have been realized in the program by including various higher-order corrections, which will be described in detail later. The electroweak loop corrections are determined in $ZF\overline{f}T_{ER}$ using the DIZET package [10] for all channels including Bhabha scattering [11].

Model-independent ansatz using effective couplings

This approach assumes that the effective axial-vector and vector couplings of fermions to the Z are real, constant, process- and energy-independent as in [12, 13]. It is known from comparisons with Standard Model predictions that these assumptions allow for quite a good approximation.

Model-independent ansatz using partial decay widths

Following general arguments of field theory, one can describe resonance scattering with the help of the partial decay widths of the resonance. This is particularly advantageous since measuring the Z line shape allows for a very precise determination of the partial decay widths. A compact description of the underlying formalism may be found in [12].

S-matrix ansatz

The cross section ansatz due to general S-matrix ideas as described in [14] has been implemented in the program. The main advantage of this branch is that it gives the mass and total

¹ As a matter of convention this cut is imposed on the antifermion only. Because of CP invariance the cut could equally well be applied on the fermion instead.

width of the Z with minimal assumptions on the underlying dynamics. As with the other branches some additional degrees of freedom are available; however, the physical information, which can be extracted from them is limited.

The advantage of the various model-independent branches is the simple picture of the dynamics and the gain in flexibility compared with the Standard Model. Such model-independent approaches also allow for pragmatic checks of Standard Model predictions and practical gains in computing time. If different branches give statistically significant differences with respect to the various parameters then perhaps a strong indication of New Physics exists!

Thanks to the flexibility of the convolution approach to QED corrections in ${}_{ZF}I_{ER}^T$, it is relatively easy to make different assumptions on the hard scattering process. While the above branches cover some of the most important theoretical tools for LEP I physics, it is a straight-forward job to add new branches so that predictions for New Physics can be made within the ${}_{ZF}I_{ER}^T$ framework. One such example is described in [15], where the mixing of the Z with an additional heavy Z' is implemented. In addition, other possibilities, which cover some New Physics by extensions of the weak form factors will also be discussed.

1.3 ${}_{ZF}I_{ER}^T$ Interfaces

Subroutine ZUTHSM

Calculation of Standard Model *cross sections* and *forward-backward asymmetries* as functions of M_Z, m_t, M_H , and α_s .

Subroutine ZUTPSM

Calculation of Standard Model τ *polarization*, A_{pol} , and τ *polarization forward-backward asymmetry*, A_{FB}^{pol} , as functions of M_Z, m_t, M_H , and α_s .

Subroutine ZUXSA

Calculation of model-independent *cross sections* and *asymmetries* as functions of the normalization form factors ($\hat{\rho}$), effective vector (\hat{v}) and axial-vector (\hat{a}) couplings, respectively.

Subroutine ZUTAU

Calculation of model-independent *final-state polarization* in τ pair production as functions of the normalization form factors, effective vector and axial-vector couplings.

Subroutine ZUXSA2

Calculation of model-independent *cross sections* and *asymmetries* as functions of the squares of the normalization form factors, effective vector and axial-vector couplings.

Subroutine ZUXSEC

Calculation of model-independent *cross sections* as functions of the partial (Γ_f) and total Z widths.

Subroutine ZUSMAT

Calculation of model-independent *cross sections*, based on an S-matrix inspired ansatz, as functions of M_Z, Γ_Z , etc.

The above interfaces have been designed with the analysis of LEP I data in mind. In fact, the accuracy of the Standard Model branch of $ZFI^T T_{ER}$ has been optimized near the Z pole. Nevertheless, the Standard Model branch of the package can be used at PETRA, TRISTAN, and linear collider energies without changes. Many examples of the use of the $ZFI^T T_{ER}$ package exist in the literature (see e.g. [16]). We will thus make no attempt to describe how to use $ZFI^T T_{ER}$ to fit data.

The organization of the article is as follows: section 2 describes the treatment of photonic corrections; the description of the various theoretical treatments of the hard scattering process is given in section 3 for the Standard Model *branch* and in section 4 for the other *branches*; the search for effects of New Physics with $ZFI^T T_{ER}$ is commented in section 5; initialization is described in section 6; section 7 documents the interface structure; finally section 8 compares $ZFI^T T_{ER}$ results with those of other programs for weak mixing angles [17, 18] and widths [19, 20], and also cross sections in an energy range covering both PETRA and LEP I energies and beyond (ZSHAPE [21, 22], ALIBABA [23]). The appendices contain a description of the contents of some of the common blocks of $ZFI^T T_{ER}$ and an example of the use of the package.

2 Chains of $ZFI^T T_{ER}$: Photonic Corrections with Different Cuts

In this section, we will describe the functions $\sigma_T(c)$ and $\sigma_{FB}(c)$, which were introduced in (1.7) and (1.8). A complete treatment of photonic corrections would also include the running of the electromagnetic coupling constant, which will be discussed in section 3, on the hard subprocess description.

In order to get a finite, gauge-invariant result, real photon bremsstrahlung from the diagrams of fig. 2 has to be combined with photonic vertex corrections of fig. 3 for initial- or final-state radiation and for their interference with the box-diagram corrections of fig. 4.

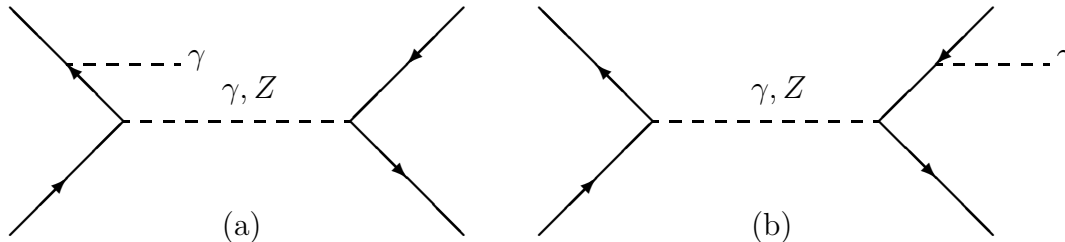


Figure 2: *Real photon emission from initial (a) and final (b) states.*

$ZFI^T T_{ER}$ relies on the following numerical integration for the contributions introduced in (1.10). The common soft photon exponentiation of initial- and final-state radiation is taken into account with:

$$\sigma_A^{\text{ini+fin}}(c) = \frac{1}{d_A} \Re \int_0^\Delta dv \sigma_A^o(s') R_A^{\text{ini}}(v, c) \bar{R}_A^{\text{fin}}(v), \quad (2.1)$$

where $s' = (1 - v)s$. Final-state radiation is described by \bar{R}_A^{fin} , which is more complex than a simple angular integral of $R_A^{\text{fin}}(v, c)$; in [3] it has been shown that \bar{R}_A^{fin} is almost completely

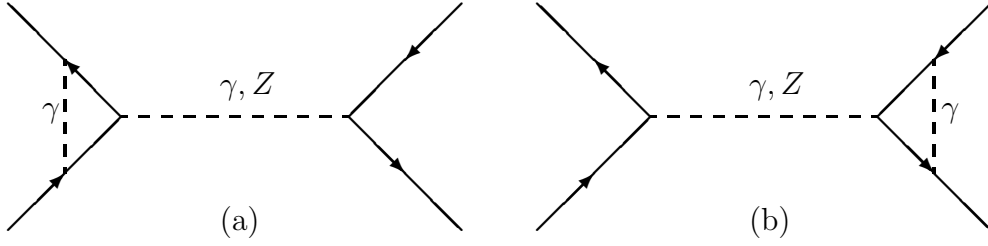


Figure 3: *The photonic vertex corrections for the initial (a) and final (b) states.*

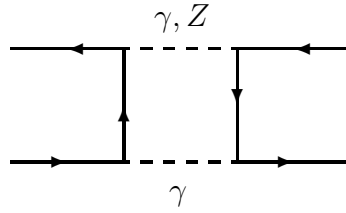


Figure 4: *Box diagrams with virtual photons, which combine with the initial-final interference bremsstrahlung into finite and gauge-invariant contributions.*

angle-independent. For each of the cross section parts, the contributions from γ and Z exchange and from their interference can be separated:

$$\sigma_A^o(s) = \sum_{m,n} \sigma_A^o(s; m, n) \equiv \sigma_A^o(s; \gamma, \gamma) + \sigma_A^o(s; \gamma, Z) + \sigma_A^o(s; Z, Z). \quad (2.2)$$

For the interference of initial and final states, this decomposition is unavoidable. This is due to the differences in the $\gamma\gamma$ and γZ boxes in fig. 3, which regularize the infrared divergence:

$$\sigma_A^{\text{int}}(c) = \frac{1}{d_A} \Re \int_0^\Delta dv \sum_{m,n} \sigma_A^o(s, s'; m, n) R_A^{\text{int}}(v, c; m, n), \quad (2.3)$$

where $m, n = \gamma, Z$. The origin of the complex structure of the initial-final interference bremsstrahlung contribution is two-fold. First, the cross section part originates from the interference of matrix elements with emission of a photon *before* and one *after* the hard-scattering process. This leads to the dependence of the hard-scattering cross section, σ_A^o , on both s and s' . Secondly, the virtual corrections of initial- and final-state radiation or of the interference have different structure (fig. 2). The simple vertex diagrams (fig. 3) of the former factorize into the Born cross section and a universal factor, while the box diagrams (fig. 4) with two-particle exchange do not. This leads to a dependence of the interference radiator functions, R_A^{int} , on m, n .

The radiator functions $R_A^a(v, c)$ are the result of a three-fold analytic integration of the corresponding photon phase space:

$$R_A^a(v, c, m, n) = \int dv_2 \int d \cos \vartheta \int d\phi_\gamma \chi_A^a(s, v, v_2, \cos \vartheta, \phi_\gamma), \quad (2.4)$$

where χ_A^a is the result of a Feynman diagram calculation. Further, $s' = Rs = (1 - v)s = M_{ff}^2$ is the invariant mass of the fermion pair, $v_2 = M_{f\gamma}^2/s$ and ϕ_γ is one of the photon angles in the (γ, f) rest system. Two treatments of the photon phase space are realized in ${}_{ZF}I^T T_{ER}$. These are shown below in the Dalitz plots of figs. 5 and 6. The variable v_2 has been integrated over analytically, while R remains to be numerically integrated by ${}_{ZF}I^T T_{ER}$. Note that the corner of the photon phase space, which corresponds to the emission of a soft photon is located near $R = 1$.

As may be seen from the definitions (1.7) and (1.8), the angular acceptance cut, $c_1 \leq \cos\vartheta \leq c_2$, limits the scattering angle ϑ of the final-state antifermions (see fig. 1). In this case, the scattering angle of the fermion f remains unrestricted if the other cut(s) do not imply an implicit restriction (see section 2.3).

In ${}_{ZF}I^T T_{ER}$, the QED contributions include the complete $\mathcal{O}(\alpha)$ corrections and soft photon exponentiation. It should be mentioned that the radiator functions (flux factors), R_A^a , differ for different observables ($A = T, FB$) and for different bremsstrahlung origin ($a = \text{ini, fin, int}$). In addition, the radiator functions for the integrated cross sections and the differential cross sections are not the same [3]. Only at LEP I, around the Z resonance, do all the radiator functions agree approximately [24, 25]. Some other semi-analytic programs use equal radiator functions for the total cross section and for A_{FB} . At LEP I energies, where hard photon emission is suppressed, and for loose cuts (thus not enhancing the initial-final interference terms), this is numerically acceptable. ${}_{ZF}I^T T_{ER}$, however, uses the *correct* radiator functions; the underlying formalism thus allows an application of ${}_{ZF}I^T T_{ER}$ at energies far away from the Z peak. No part of our treatment of the bremsstrahlung is specific to physics near the Z resonance peak.

Higher order QED corrections have been implemented in ${}_{ZF}I^T T_{ER}$ for initial-state radiation contributions, besides the above-mentioned soft photon exponentiation, to σ_T as in [21] and to A_{FB} as in [26]. For the two calculational chains, which involve an angular acceptance cut, these higher-order corrections are treated with an approximation that assumes a Born-like angular behavior.

When no acceptance cut is applied, $c = 1$, the expressions for $\sigma_T(1)$ and $A_{FB}(1)$ approach well-known formulae for σ_T [27, 28, 21] and A_{FB} [25, 26].

2.1 No Cuts

Of the various calculational chains contained in the ${}_{ZF}I^T T_{ER}$ package the simplest to describe is the one where no cuts are allowed. This chain has been realized with special formulae in order to make it as computationally fast as possible. Here the photon may have any energy, Δ , up to the kinematic limit:

$$\Delta \equiv E_\gamma^{\text{max}}/E_{\text{beam}}, \quad \Delta \leq \Delta^{\text{max}} = 1 - 4m_f^2/s. \quad (2.5)$$

Thus, the radiative corrections depend on the fermion masses even for the light quarks and leptons. This dependence can be important when total cross sections are determined from experimental data, and *is* of special importance when comparing results from other semi-analytic programs. The latter will be discussed in section 8.2.

2.2 Convolution Integral with Cut on the Invariant Mass of the Outgoing Fermion Pair (s'_{\min})

${}_{ZF}I^T T_{ER}$ allows for a constraint on the minimum allowed invariant mass of the outgoing fermion pair, s'_{\min} :

$$s'_{\min} = (1 - \Delta)s. \quad (2.6)$$

This is easily re-interpreted as a cut on the maximum allowed energy of the bremsstrahlung photon, Δ . In this calculational chain the s'_{\min} cut may be combined with an angular acceptance cut:

$$c_1 \leq \cos \vartheta \leq c_2. \quad (2.7)$$

The Dalitz plot shown in fig. 5 corresponds to a Δ cut of $\Delta = 1 - R^{\min}$.

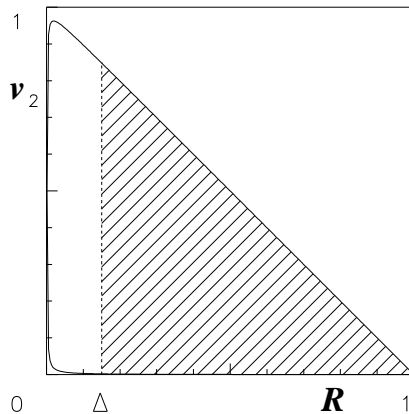


Figure 5: *Dalitz plot for the photon phase space with a cut on s' .*

The allowed region is a triangle in the ultra-relativistic limit. Note that v_2 is not influenced by the cut. This simplifies the analytical integration over v_2 .

Explicit expressions for the radiator functions $R_A^a(v, c)$ discussed above may be found in the literature. For initial-state radiation and initial-final interference, they may be found in eqs. (8), (18) in [4], respectively. For final state radiation, the angular dependence is relatively simple and eqs. (132-134) in [3] are valid. The radiator functions for common exponentiation of initial- and final-state soft-photon emission implemented in ${}_{ZF}I^T T_{ER}$ are derived from eq. (157) in [3], as has been described in section 4 of [4].

2.3 Convolution Integral with Cuts on Fermion Energies and Acollinearity (E_f^{\min}, ξ^{\max})

As an alternative to the s'_{\min} cut, one can apply another set of cuts on the outgoing $f\bar{f}$ pair [5]. Cuts on the minimum energy, E_f^{\min} , and the maximum acollinearity, ξ^{\max} , of the $f\bar{f}$ pair in addition to angular acceptance cuts have been implemented in ${}_{ZF}I^T T_{ER}$.

Figure 6 shows a Dalitz plot of the allowed phase space for the two energy variables R and v_2 , introduced above.

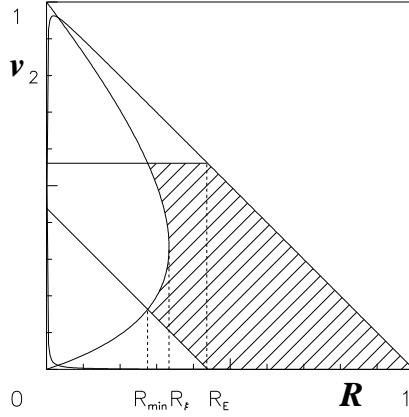


Figure 6: *Dalitz plot for the photon phase space with cuts on E^f and ξ as explained in the text.*

The boundaries of the allowed phase-space region are defined by the following conditions:

$$v_2^{\max} = 1 - R_{\bar{E}}, \quad (2.8)$$

$$v_2^{\min}(R) = R_E - R, \quad (2.9)$$

$$R^{\min}(v_2) = \frac{4R_\xi v_2(1 - v_2)}{(1 - R_\xi)^2 + 4R_\xi v_2}, \quad (2.10)$$

where

$$R_{\bar{E}} = \frac{2E_f^{\min}}{\sqrt{s}}, \quad R_E = \frac{2E_f^{\min}}{\sqrt{s}}, \quad R_\xi = \frac{1 - \sin(\xi^{\max}/2)}{1 + \sin(\xi^{\max}/2)}. \quad (2.11)$$

The absolute minimum of R is given by²

$$R^{\min} = \min(R_E, R_{\bar{E}}) \left(1 - \frac{\sin^2(\xi^{\max}/2)}{1 - R_E \cos^2(\xi^{\max}/2)} \right). \quad (2.12)$$

Further, the upper integration limit in (1.12) becomes

$$\Delta = 1 - R^{\min}. \quad (2.13)$$

The above relations are independent of the scattering angle and are, thus, compatible with an angular acceptance cut:

$$c_1 \leq \cos \vartheta \leq c_2. \quad (2.14)$$

The turning point, P_t in fig. 6, of the acollinearity bound of the integration region is:

$$P_t \equiv [R_t; v_{2,t}] = \left[R_\xi; \frac{1}{2}(1 - R_\xi) \right]. \quad (2.15)$$

This is significant since it allows the user to apply a reasonable approximation of the acollinearity cut in terms of the simpler Δ cut; this can be achieved by using Δ_ξ for the definition of the integration limit (2.6) in section 2.2:

$$\Delta_\xi \equiv 1 - R_\xi = \frac{2 \sin(\xi^{\max}/2)}{1 + \sin(\xi^{\max}/2)}. \quad (2.16)$$

²The current implementation of $zF^T T_{ER}$ assumes that $E_f^{\min} = E_{\bar{f}}^{\min}$.

The quality of such an approximation depends critically on the values of the E_{\min}^f cut and the ξ^{\max} cut; for loose cuts it improves.

Because of the approximations that have been implemented in the QED calculational chain, the user must be cautious in applying severe cuts. Since the approximation is ultra-relativistic one should restrict oneself to the region of the phase space:

$$E^{\min} \gg m_f, \quad \xi^{\max} \ll \left(1 - \frac{8m_f}{\sqrt{s}}\right) \pi. \quad (2.17)$$

Near the turning point P_t introduced in (2.15) the validity of the soft photon exponentiation approximation comes into question³. To avoid any such problems the following restrictions should be observed:

$$E^{\min} < 0.95 E_{\text{beam}}, \quad \xi^{\max} > 2^\circ. \quad (2.18)$$

This last limitation guarantees that the second-order terms $[\beta \log(1 - R_{\text{cut}})]^2$ with $\beta = 2(\alpha/\pi)$ $[\log(s/m_e^2) - 1]$ and $R_{\text{cut}} = R_E, R_\xi$ do not become too large:

$$|\beta \log(1 - R_{\text{cut}})| \ll 1. \quad (2.19)$$

This corresponds to

$$E^{\min} \ll \frac{\exp(\beta^{-1}) - 1}{\exp(\beta^{-1})} E_{\text{beam}}, \quad \xi^{\max} \ll \exp(-\beta^{-1}). \quad (2.20)$$

Finally, we would like to point out that the acollinearity cut has an indirect influence on the acceptance cut. It is easy to see that the maximal scattering angle of the second fermion (which is unrestricted by the user's acceptance cut) becomes limited by an acollinearity cut, i.e. the scattering angle of the second fermion is limited to $[-(\xi^{\max} + \vartheta^{\max}), (\xi^{\max} + \vartheta^{\max})]$.

2.4 Photonic Corrections for Bhabha Scattering

The Bhabha scattering cross section (1.2) arises from the sum of s- and t-channel exchange cross sections and from their interference. The s-channel part needs no further comment since it corresponds completely to ordinary fermion pair production. In the t channel the energy variables, which correspond to (s, s') are (t, t') , where:

$$t = -\frac{1}{2}s(1 - \cos \vartheta) \quad (2.21)$$

and

$$t' = t \frac{s'}{s}. \quad (2.22)$$

The t-channel propagator for a massless photon is proportional to $1/t$ or $1/t'$; it thus becomes divergent in the forward direction, i.e. as $\vartheta \rightarrow 0$:

$$\frac{d\sigma^{\text{Bhabha}}}{d \cos \vartheta} \sim \frac{1}{\vartheta^4}. \quad (2.23)$$

Such a divergence is common in calculations of the Bhabha scattering cross section and it prevents a reasonable definition of a total cross section without at least an acceptance cut, even at the level of the Born approximation.

³A more advanced exponentiation procedure [29] circumvents these limitations.

For *large-angle* Bhabha scattering [30], $\vartheta \geq 10^\circ$, this problem is absent. Near the Z peak, such a condition guarantees that the photonic t-channel exchange contributions, including the QED corrections (with an effective $t' = s'(1 - \cos \vartheta) \leq t$ in the hard-scattering process), are at most of the same order as the non-resonating terms from the s channel. Of course, an acceptance cut does not prevent t' from becoming small because of the emission of a hard initial-state photon, in which case the t channel dominates. This divergence can, however, be circumvented by excluding very hard photons from the observed cross section with an E_f^{\min} cut. In any case, the hard photon corrections to these contributions must be carefully taken into account.

At LEP I energies, terms with Z exchange in the t channel are strongly suppressed owing to the form of the Z propagator ($\sim 1/(t' + M_Z^2)$) and contribute less than 1% to the cross section. In summary, the contributions, which arise from photon exchange in the t channel, compete with those of the s channel; however, near the Z resonance it is clear that the s channel must dominate.

An explicit description of the QED corrections to Bhabha scattering which have been implemented in ${}_{ZF}I^T T_{ER}$ will be presented elsewhere [6]. In order to discuss some features of the present implementation, we give an explicit example for the general structure of the Bhabha cross section:

$$\frac{d\sigma^{\text{Bhabha}}}{d\cos\vartheta} = \frac{d\sigma^{(s)}(s, \cos\vartheta)}{d\cos\vartheta} + \int_0^{1-R^{\min}} dv \sum_a \sum_{V_1, V_2} \sigma^{a,o}(s, s'; V_1, V_2) R^a(v, \cos\vartheta; V_1, V_2). \quad (2.24)$$

Here the first term corresponds to the s-channel part. The sum under the integral extends over a , denoting in the s-channel diagrams initial- and final-state radiation, in the t-channel up and down radiation, and in the interferences the corresponding combinations. Further, a sum extends over (V_1, V_2) , the possible combinations of propagators $\gamma_s, \gamma_t, Z_s, Z_t$ from the t channel and the interference. In (2.24), all functions R^a have the form

$$R^a(v, \cos\vartheta; V_1, V_2) = \delta(1-v) \left[1 + \frac{\alpha}{\pi} S^a(s, \cos\vartheta; V_1, V_2) \right] \Delta^\beta + \frac{\alpha}{\pi} H^a(v, \cos\vartheta; V_1, V_2), \quad (2.25)$$

where

$$\Delta = 1 - R^{\min}, \quad \beta = 4 \frac{\alpha}{\pi} \left(\log \frac{s}{m_e^2} + \log \frac{1 - \cos\vartheta}{1 + \cos\vartheta} \right), \quad (2.26)$$

and R^{\min} was introduced in (2.13).

The functions S^a in (2.25) contain the soft photon (plus corresponding virtual) corrections, and H^a the complete $\mathcal{O}(\alpha)$ hard photonic corrections. In the s channel, the hard photon part depended on s'/s only, while here, due to the t-channel propagators, it is also dependent on t'/s or on t/s . As a consequence, it loses its universality and depends also on the kind of bosons which are exchanged (i.e. γ or Z). Further, the running QED coupling (if not assigned formally to the radiator functions, it is contained in the hard-scattering cross section $\sigma^{a,o}$) depends, in the t channel, on the scattering angle as well.

These (t, t') dependences have the far-reaching consequence that the integrand in (2.24) depends in a more non-trivial way on the scattering angle compared with the s-channel case – thus preventing an analytic integration over $\cos\vartheta$, which is the basis of the fast computing of ${}_{ZF}I^T T_{ER}$.

In the current implementation of BHANG, the cut conditions of section 2.3 are taken into account in the functions (2.25)⁴.

Further, in (2.25) the leading higher-order corrections due to soft and hard collinear photon radiation with t-channel participation are taken into account in an approximate way. The cross section of the hard process is considered to be independent of the actual energy scale, i.e. assuming $s' = s$ and $t' = t$. At LEP I, the error induced by this is definitely less than 1%. A simple improvement could be the choice of some better scales for the effective s- and t-invariants in the hard cross section, which effectively take into account the change of kinematics due to radiation.

Hard photon radiation is considered in the collinear approximation for the cross section parts which correspond to Z exchange in the t channel, i.e. the appropriate functions $H_A^a(v, \cos \vartheta, Z_t, Z_t)$ are set to zero.

The user of $_{ZF}I^T T_{ER}$ should be aware that the Bhabha cross section returned with the aid of BHANG is to a much larger extent adapted for LEP I physics than for the other fermion channels and contains more approximations in the treatment of the QED corrections.

part.

3 The Hard Scattering Process: (I) The Standard Model Branch

We now describe some general features of the cross section formulae for the hard-scattering subprocesses. In all branches of $_{ZF}I^T T_{ER}$, we can denote:

$$\sigma_A^o(s, s'; m, n) = \mathcal{I}_A(m, n; s, s') \frac{1}{2} [\mathcal{K}_m(s') \mathcal{K}_n^*(s) + \mathcal{K}_m(s) \mathcal{K}_n^*(s')]. \quad (3.1)$$

For initial-state radiation this simplifies to:

$$\sigma_A^o(s', s'; m, n) \rightarrow \sigma_A^o(s'; m, n) = \mathcal{I}_A(m, n; s') \mathcal{K}_m(s') \mathcal{K}_n^*(s'). \quad (3.2)$$

For final-state radiation s' has to be replaced by s . The propagator functions $\mathcal{K}_n(s)$ are:

$$\mathcal{K}_n(s) = \frac{s}{s - \mathcal{M}_n^2 + i\mathcal{M}_n \mathcal{G}_n}. \quad (3.3)$$

Here, \mathcal{M}_n are the masses and \mathcal{G}_n are the widths of the intermediate gauge bosons.

In addition to the QED-corrected cross sections (1.12), $_{ZF}I^T T_{ER}$ can also return (improved or effective) Born cross sections, σ_A^{Born} . These are constructed out of the expressions introduced above:

$$\sigma_A^{\text{Born}}(s, c) = D_A(c) \left\{ \mathcal{I}_A(\gamma, \gamma; s) + \Re e [\mathcal{I}_A(\gamma, Z; s) \mathcal{K}_Z^*(s)] + \mathcal{I}_A(Z, Z; s) |\mathcal{K}_Z(s)|^2 \right\}, \quad (3.4)$$

$$D_A(c) = \begin{cases} 2(c + \frac{1}{3}c^3) & \text{for } a = T \\ 2c^2 & \text{for } A = FB. \end{cases} \quad (3.5)$$

⁴ At present there is a limitation on the allowed value of the scattering angle ϑ ; it must be larger than the acollinearity ξ^{max} . This is due to purely technical reasons and this restriction will be removed in successive versions of the code.

The functions \mathcal{I}_A contain the underlying dynamics of the hard-scattering process. Often, but not necessarily, they are assumed to be inversely proportional to s, s' . The different branches of ${}_{ZF}\overline{I}T_{ER}$ rely on various assumptions with respect to \mathcal{I}_A , as will be discussed later.

For the photon ($n = 0$) the propagator becomes $\mathcal{K}_\gamma = 1$, while for the Z , various possibilities exist in ${}_{ZF}\overline{I}T_{ER}$. In recent years, much influenced by the discussions of the 1989 workshop on physics at LEP I [31], it became common to use the following definitions:

$$\mathcal{K}_Z(s) = \frac{s}{s - \mathcal{M}_Z^2 + i\mathcal{M}_Z\mathcal{G}_Z}, \quad (3.6)$$

$$\mathcal{M}_Z = M_Z, \quad (3.7)$$

$$\mathcal{G}_Z = \Gamma(s) \approx \frac{s}{M_Z^2}\Gamma_Z, \quad (3.8)$$

where M_Z and Γ_Z are considered to be the mass and total width of the Z . This point of view reflects the fact that in a quantum field theory such as the Standard Model the Z width is predicted as a result of quantum corrections (self-energy insertions) and is, thus, naturally s -dependent. This s -dependence of \mathcal{G} becomes important only because the very narrow Z peak may be scanned with extreme precision, leading to errors of a few MeV for mass and width of the Z .

The definitions (3.6)-(3.8) may be related to an alternate resonance description, which assumes a constant width:

$$\bar{\mathcal{K}}_Z(s) = \frac{s}{s - \bar{M}_Z^2 + i\bar{M}_Z\bar{\Gamma}_Z}. \quad (3.9)$$

The following equality holds as long as the approximate relation in (3.8) may be considered to be exact⁵ [32]:

$$G_\mu \mathcal{K}_Z(s) \equiv \bar{G}_\mu \bar{\mathcal{K}}_Z(s), \quad (3.10)$$

Compared to (3.6)-(3.8), (3.9) corresponds to another ansatz for mass, width, and coupling constant:

$$\bar{\mathcal{M}} = \bar{M}_Z = \left[1 + (\Gamma_Z/M_Z)^2\right]^{-\frac{1}{2}} M_Z \approx M_Z - \frac{1}{2} \frac{\Gamma_Z^2}{M_Z} \approx M_Z - 34 \text{ MeV}, \quad (3.11)$$

$$\bar{\mathcal{G}} = \bar{\Gamma}_Z = \left[1 + (\Gamma_Z/M_Z)^2\right]^{-\frac{1}{2}} \Gamma_Z \approx \Gamma_Z - \frac{1}{2} \frac{\Gamma_Z^3}{M_Z^2} \approx \Gamma_Z - 1 \text{ MeV}, \quad (3.12)$$

$$\bar{G}_\mu = \frac{G_\mu}{1 + i\Gamma_Z/M_Z}. \quad (3.13)$$

A naïve use of a constant width in (3.6)-(3.8) would lead to a wrong determination of what has been introduced there to be the Z mass. In fact, one can put forward a completely different point of view [33]-[14] (see also references cited therein and [36]-[38]). There is no physical reason to consider (3.6)-(3.8) as the final result of a perturbative calculation. After so many formal manipulations, including renormalization, one could consider the transformations (3.9)-(3.12) as part of the renormalization procedure. In doing so, one is in complete agreement with the ideas of S-matrix theory: Unstable particles are described by simple poles of the S-matrix

⁵ In the Standard Model, this is the case if two conditions are fulfilled: (i) there are no opening new Z decay channels (production thresholds) near $s = M_Z^2$; (ii) radiative corrections to \mathcal{G} are practically independent of s in a region where \mathcal{G} essentially influences the cross sections.

in the complex energy plane whose location is defined by the particle's mass (real part) and its width (imaginary part). Such an approach automatically anticipates the propagator $\bar{K}_Z(s)$ with mass (3.11) and width (3.12).

The default mass and width definition for the S-matrix branch of the ${}_{ZF}I^T T_{ER}$ package is (3.9)-(3.12), while (3.6)-(3.8) should be used for all other branches. The final choice of the definition of the Z mass and width is left to the user (see flag **GAMS**).

For the t channel of Bhabha scattering, the above discussion regarding the propagators is also of some relevance. Of course, here the width of the resonance is absent. Furthermore, one must replace s by t and s' by t' in the propagator functions.

For the corresponding Standard Model calculations, ${}_{ZF}I^T T_{ER}$ relies on the DIZET [10] package. The following parameters are passed to DIZET:

$$\alpha, \alpha_s, G_\mu, M_Z, M_H, m_f, \quad (3.14)$$

which returns M_W ; the total and partial Z widths; the weak form factors, etc. Thus, one arrives at improved Born cross sections, which are used as building blocks of the QED formulae discussed in the foregoing sections; ${}_{ZF}I^T T_{ER}$ *does not* calculate bare Born cross sections since definitions of the latter tend to be ambiguous. The weak mixing angle also will not be considered as a quantity of physical relevance (although one could do so), but will only be used for book-keeping of intermediate results.

In the remainder of this section and in the next, we discuss the various assumptions regarding the functions $\mathcal{I}_A(m, n; s)$ that have been implemented in ${}_{ZF}I^T T_{ER}$.

3.1 $\mathcal{O}(\alpha)$ Corrections to Δr

In the on-mass-shell renormalization scheme [39] that is used in ${}_{ZF}I^T T_{ER}$, the weak mixing angle is defined uniquely through the gauge-boson masses:

$$\sin^2 \theta_W \equiv 1 - \frac{M_W^2}{M_Z^2}, \quad (3.15)$$

$$\sin^2 \theta_W M_W^2 = \frac{\pi\alpha/(\sqrt{2}G_\mu)}{1 - \Delta r}. \quad (3.16)$$

In subroutine **SEARCH** of DIZET, Δr is calculated to order $\mathcal{O}(\alpha)$ as defined in [39], where the heavy top contribution is calculated as in [7]. Recently, a careful comparison [40] of two independent $\mathcal{O}(\alpha)$ calculations of (3.16) showed agreement in 12 digits.

3.2 $\mathcal{O}(\alpha)$ Corrections to Γ_Z

Electroweak corrections to the Z width have been calculated to order $\mathcal{O}(\alpha)$ in [7]. The partial decay width of the Z into fermions of type f is given by:

$$\begin{aligned} \Gamma_f &= \frac{G_\mu M_Z^3}{\sqrt{2} 12\pi} \mu R_{\text{QED}} c_f R_{\text{QCD}}(M_Z^2) \rho_f^Z \times \\ &\quad \left\{ \left[1 - 4|Q_f| \sin^2 \theta_W \kappa_f^Z + 8(|Q_f| \sin^2 \theta_W \kappa_f^Z)^2 \right] \left(1 + 2\frac{m_f^2}{M_Z^2} \right) - 3\frac{m_f^2}{M_Z^2} \right\}, \\ &= \frac{G_\mu M_Z^3}{\sqrt{2} 24\pi} \mu R_{\text{QED}} c_f R_{\text{QCD}}(M_Z^2) \left\{ [(\bar{v}_f^Z)^2 + (\bar{a}_f^Z)^2] \left(1 + 2\frac{m_f^2}{M_Z^2} \right) - 6(\bar{a}_f^Z)^2 \frac{m_f^2}{M_Z^2} \right\}. \end{aligned} \quad (3.17)$$

The renormalized vector and axial-vector couplings⁶ are defined as follows:

$$\bar{a}_f^Z = \sqrt{\rho_f^Z}, \quad (3.18)$$

$$\bar{v}_f^Z = \bar{a}_f^Z [1 - 4|Q_f| \sin^2 \theta_W \kappa_f^Z]. \quad (3.19)$$

The bare Born vector and axial-vector couplings, v and a , correspond to $\rho = \kappa = 1$. The weak form factors, ρ and κ , are real, constant, and depend slightly on the decay channel. They contain the electroweak corrections to the process, including the dependence on m_t and M_H . Since ${}_{ZF} I_{ER}^T$ exactly follows [7], we need not go into details here. However, it must be mentioned that the Z width depends on the choice of the definition of the Z mass (see the discussion presented at the beginning of this section).

Sometimes, the combination

$$s_W^{2,\text{eff}} = \kappa_e^Z \sin^2 \theta_W \quad (3.20)$$

is used as a definition of the ‘effective’ weak mixing angle; see e.g. [41, 42] and the recent discussion on possible alternatives in [43] and references quoted therein. Such a definition can also rely on the other decay channels:

$$s_W^{2,\text{f}} = \kappa_f^Z \sin^2 \theta_W. \quad (3.21)$$

Several factors contain additional corrections:

$$\mu \equiv \mu(M_Z^2),$$

$$\mu(s) = \sqrt{1 - 4m_f^2/s}, \quad (3.22)$$

$$R_{\text{QED}} = 1 + \frac{3}{4} \frac{\alpha}{\pi} Q_f^2 = 1 + 0.0017 Q_f^2, \quad (3.23)$$

$$c_f = \begin{cases} 3 & \text{for quarks} \\ 1 & \text{for leptons,} \end{cases} \quad (3.24)$$

$$R_{\text{QCD}} = \begin{cases} 1 + c_1(m_f^2) \frac{\alpha_s(M_Z^2, \Lambda_{\overline{\text{MS}}})}{\pi} + \dots & \text{for quarks} \\ 1 & \text{for leptons.} \end{cases} \quad (3.25)$$

The corrections R_{QED} and R_{QCD} contain the photonic and gluonic corrections, respectively. The factor c_1 is of relevance only for the b-quark channel. The exact definition of R_{QCD} will be given in section 3.4.

Owing to the large mass splitting between the t and b quark, there are two vertex diagrams for the Z decay into b quarks (fig. 7), which contribute additional m_t -dependent corrections that are absent in the cases of light quarks [7, 44] (see also [45, 46]). The matrix element for the decay of the Z boson into d and s quarks (and similarly, for u and c quarks) may be written as follows:

$$\mathcal{M}_d \sim \sqrt{\frac{G_\mu}{\sqrt{2}}} M_Z^2 \epsilon^\beta \bar{u} [\gamma_\beta \bar{v}_d^Z + \gamma_\beta \gamma_5 \bar{a}_d^Z] u. \quad (3.26)$$

⁶The Born axial-vector coupling is often defined to be equal to the weak isospin, $a_f = I_3^L(f)$, e.g. $a_e = -\frac{1}{2}$.

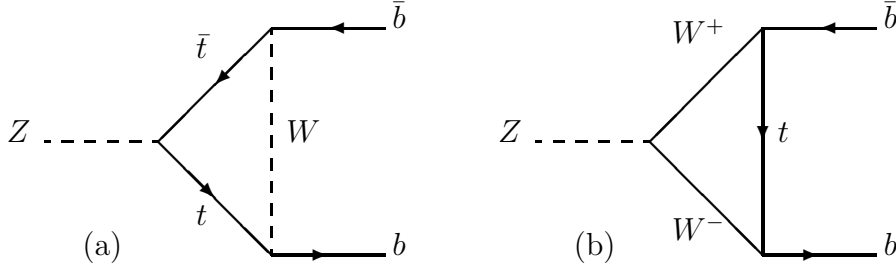


Figure 7: *Top quark exchange diagrams which contribute to Γ_b .*

$\sin^2 \theta_W$	Γ_ν	Γ_e	Γ_μ	Γ_τ	Γ_u	Γ_d	Γ_c	Γ_s	Γ_t	Γ_b	Γ_{tot}
0.2282	166.6	83.6	83.6	83.4	296.6	382.9	296.2	382.9	0.	375.7	2484.7

Table 1: *Weak mixing angle and partial and total Z widths; widths are given in MeV.*

The corresponding matrix element for b quarks has an additional left-handed contribution:

$$\begin{aligned}
\mathcal{M}_b &\sim \sqrt{\frac{G_\mu}{\sqrt{2}}} M_Z^2 \epsilon^\beta \bar{u} \left[\gamma_\beta \bar{v}_d^Z + \gamma_\beta \gamma_5 \bar{a}_d^Z + \Delta_b(m_t^2) \gamma_\beta (1 + \gamma_5) \right] u \\
&\sim \sqrt{\frac{G_\mu}{\sqrt{2}}} M_Z^2 \epsilon^\beta \sqrt{\rho_b^Z} a_b \bar{u} \left[\gamma_\beta (1 + \gamma_5) - 4 \sin^2 \theta_W \kappa_b^Z \gamma_\beta \right] u.
\end{aligned} \tag{3.27}$$

Here, Δ_b vanishes for $m_t \rightarrow 0$. By simple algebra, one can show that

$$\rho_b^Z = \rho_d^Z - 2 \frac{\Delta_b(m_t^2)}{a_b}, \tag{3.28}$$

$$\kappa_b^Z = \kappa_d^Z + \frac{\Delta_b(m_t^2)}{a_b}. \tag{3.29}$$

These exact form factors have been implemented in ${}_{ZF}I^T T_{ER}$. In the limit of large t-quark masses, the leading terms are given by [7]:

$$\frac{\Delta_b(m_t^2)}{a_b} = \frac{\alpha}{4\pi \sin^2 \theta_W} |V_{tb}|^2 \frac{1}{2} \left[\frac{m_t^2}{M_W^2} + \left(\frac{8}{3} + \frac{1}{6 \cos^2 \theta_W} \right) \log \frac{m_t^2}{M_W^2} \right], \tag{3.30}$$

where V_{tb} is the (t, b) Kobayashi-Maskawa mixing matrix element. ${}_{ZF}I^T T_{ER}$ calculations use the normalization $a_b = 1$ in (3.27).

The calculation of the W width [8] follows the same principles as that of the Z width and is realized in subroutine **ZWRATE** of **DIZET**. Since the W width is not that important for the description of fermion pair production, we do not go into details.

The partial and total widths, returned by $_{ZF}F_{ER}^T$ ⁷, are summarized in table 1. In addition the weak mixing angle is given in the table.

3.3 $\mathcal{O}(\alpha)$ Corrections to Fermion Pair Production

Fermion pair production in the Standard Model gets contributions from self-energy insertions, vertex corrections and box diagrams. We divide these into two gauge-invariant subsets.

Fermion loop insertions to the photon propagator are summed together with the photonic Born diagram (see fig. 8a) to form the matrix element \mathcal{M}_γ . In effect these corrections change α into $\alpha(s)$:

$$\mathcal{M}_\gamma(s) \sim \frac{1}{s} \alpha(s) Q_e Q_f \gamma_\beta \otimes \gamma^\beta, \quad (3.31)$$

where the following short notation for bilinear combinations of spinors u_f is used:

$$A_\beta \otimes B^\beta = [\bar{u}_e A_\beta u_e] \cdot [\bar{u}_f B^\beta u_f]. \quad (3.32)$$

After a Dyson summation of the fermion loop insertions $\Delta\alpha(s)$ to the photon self energy, the running electromagnetic coupling constant contains higher-order corrections:

$$\alpha(s) = F_A(s) \alpha \equiv \frac{\alpha}{1 - \Delta\alpha(s)}. \quad (3.33)$$

The function XFOTF1 in DIZET is used to calculate $\Delta\alpha$.

Some numerical examples are given in table 2 as a function of \sqrt{s} .

\sqrt{s}	30	87	89	91	93	95	200
F_A	1.0504	1.0630	1.0633	1.0635	1.0638	1.0640	1.0723
	- i.0186	- i.0188	- i.0188	- i.0188	- i.0188	- i.0189	- i.0191

Table 2: *The running QED coupling, $F_A(s) = \alpha(s)/\alpha$, as a function of the centre-of-mass energy (\sqrt{s} in GeV).*

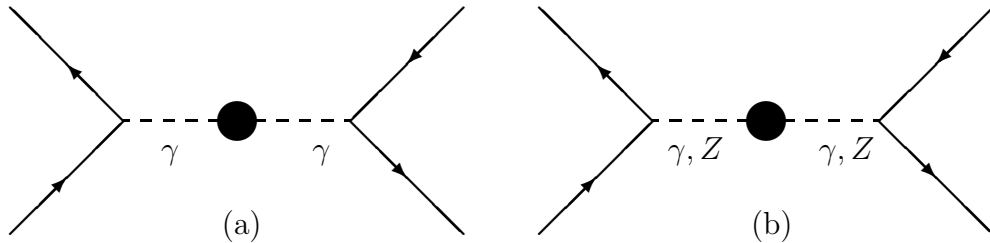


Figure 8: *Photon (a) and Z (b) self energies. In (b), the case γ, γ is not included.*

⁷In the examples we have taken $M_Z = 91.175$ GeV, $M_H = 300$ GeV, $m_t = 140$ GeV, $\alpha_s = 0.12$ and default flag values (see table 9 in section 6.2) unless explicitly stated otherwise.

At $\sqrt{s} = M_Z$ the running coupling constant has the value:

$$\alpha(M_Z^2) = F_A(M_Z^2)\alpha \simeq \frac{1}{137}F_A(M_Z^2) \simeq \frac{1}{128.8}. \quad (3.34)$$

In addition to the running of $\alpha(s)$, there are diagrams with additional internal W and Z boson propagators to the photonic Born amplitude, e.g. a W^\pm -pair insertion or a vertex correction with a Z propagator. These diagrams could be treated as corrections to the photon amplitude as well. However, this would make \mathcal{M}_γ dependent on the gauge. Diagrams of this type form a gauge-invariant subset together with all the insertions to the Z Born diagram as well as with ZZ and WW boxes. So, any diagram with at least one additional massive gauge boson will be combined with the Z exchange Born diagram to form the matrix element \mathcal{M}_Z (see figs. 8b, 9 and 10).

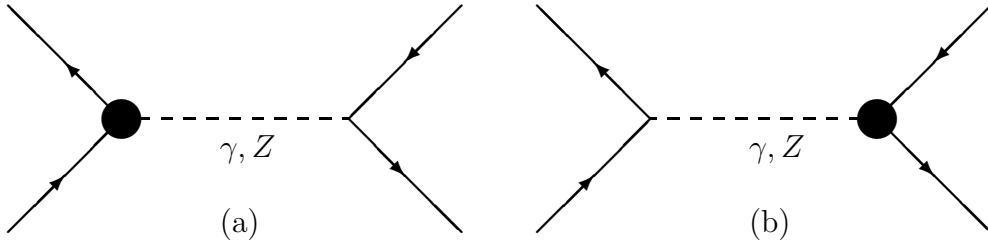


Figure 9: *Vertex corrections to the Z matrix element.*

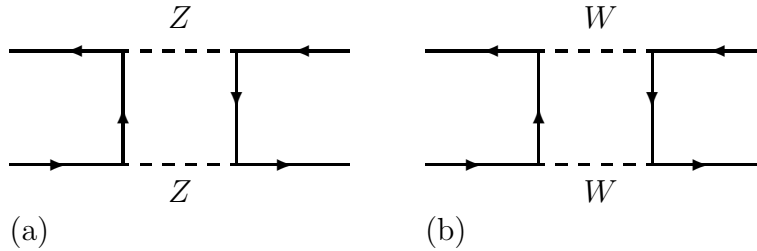


Figure 10: *Box diagrams contributing to the Z matrix element.*

The contributions to the corresponding matrix element \mathcal{M}_Z can be expressed in terms of four weak form factors ($\rho_{ef}, \kappa_e, \kappa_f, \kappa_{ef}$) as introduced to order $\mathcal{O}(\alpha)$ in [9]:

$$\mathcal{M}_Z(s, \cos \vartheta) \sim \frac{G_\mu a_e a_f \rho_{ef}(s, \cos \vartheta)}{s - M_Z^2 + iM_Z \Gamma_Z} \left[L_\beta \otimes L^\beta - 4|Q_e| \sin^2 \theta_W \kappa_e(s, \cos \vartheta) \gamma_\beta \otimes L^\beta - 4|Q_f| \sin^2 \theta_W \kappa_f(s, \cos \vartheta) L_\beta \otimes \gamma^\beta + 16|Q_e Q_f| \sin^4 \theta_W \kappa_{ef}(s, \cos \vartheta) \gamma_\beta \otimes \gamma^\beta \right], \quad (3.35)$$

$$L_\beta = \gamma_\beta(1 + \gamma_5), \quad (3.36)$$

where L_β is the left-handed projector. The $(\rho - 1)$ and $(\kappa - 1)$ are normalized with the factor $\alpha/(4\pi \sin^2 \vartheta_W)$.

The matrix element may be rewritten in terms of renormalized vector (\bar{v}) and axial-vector (\bar{a}) couplings:

$$\mathcal{M}_Z(s, \cos \vartheta) \sim \frac{G_\mu}{s - M_Z^2 + iM_Z\Gamma_Z} [\bar{a}_e \bar{a}_f \gamma_\beta \gamma_5 \otimes \gamma^\beta \gamma_5 + \bar{v}_e \bar{a}_f \gamma_\beta \otimes \gamma^\beta \gamma_5 + \bar{a}_e \bar{v}_f \gamma_\beta \gamma_5 \otimes \gamma^\beta + \bar{v}_e \bar{v}_f \gamma_\beta \otimes \gamma^\beta], \quad (3.37)$$

$$\bar{a}_f = \sqrt{\rho_{ef}(s, \cos \vartheta)} I_3^L(f), \quad (3.38)$$

$$\bar{v}_f = \bar{a}_f [1 - 4|Q_f| \sin^2 \theta_W \kappa_f(s, \cos \vartheta)], \quad (3.39)$$

$$\bar{v}_{ef} = \bar{a}_e \bar{v}_f + \bar{v}_e \bar{a}_f - \bar{a}_e \bar{a}_f [1 - 16|Q_e Q_f| \sin^4 \theta_W \kappa_{ef}(s, \cos \vartheta)]. \quad (3.40)$$

The four form factors are the most general ansatz for the weak radiative corrections. In the Born approximation, $\rho = \kappa = 1$, and $v_{ef} = v_e v_f$. The coupling v_{ef} has no parallel in the Born approximation and is, in principle, completely independent of v_e and v_f . Form factors are calculated in subroutine ROKANC of the DIZET package.

In table 3 we show the s dependence of the weak form factors for lepton production.

\sqrt{s}	30	87	89	91	93	95	200
ρ_{ef}	0.9992 - i.0006	1.0020 - i.0043	1.0021 - i.0045	1.0022 - i.0047	1.0022 - i.0048	1.0023 - i.0050	1.0102 - i.0283
κ_e, κ_f	1.0283 + i.0115	1.0227 + i.0134	1.0226 + i.0135	1.0226 + i.0135	1.0225 + i.0136	1.0225 + i.0137	1.0117 + i.0329
κ_{ef}	1.0552 + i.0204	1.0459 + i.0265	1.0458 + i.0268	1.0456 + i.0271	1.0455 + i.0273	1.0454 + i.0276	1.0355 + i.0560
$\kappa_e \kappa_f$ $-\kappa_{ef}$	0.0020 + i.0032	-0.0002 + i.0008	-0.0002 + i.0007	-0.0002 + i.0006	-0.0002 + i.0005	-0.0001 + i.0004	-0.0010 + i.0110

Table 3: *Leptonic form factors $\rho_{ef}, \kappa_e, \kappa_f, \kappa_{ef}$ as functions of the centre-of-mass energy (\sqrt{s} in GeV).*

The last row in the table shows how well κ_{ef} can be factorized in terms of κ_e and κ_f . The form factors shown in the table have been calculated without the box diagrams of fig. 10. The program DIZET allows for three options: inclusion of these box diagrams into the weak form factors; calculation of them as an extra cross-section piece, σ_{box} , to be added incoherently (see [9]); or neglecting them completely. $ZF^I T_{ER}^I$ allows for the last two options only. This has been arranged in order to make the weak form factors independent of the scattering angle. Thus, the angular integration could be performed analytically. Table 4 shows the influence of the box-diagram corrections on the differential cross section for different angular bins at LEP I energies⁸.

Henceforth, we omit the possibility of an angular dependence of the form factors. Using an alternative parametrization, the axial-vector couplings may be chosen such that they are

⁸ The contributions from box diagrams are non-resonant at LEP I energies. $ZF^I T_{ER}^I$ users should be aware that, off the Z resonance peak, box diagrams may not be neglected with respect to other radiative corrections.

ϑ region	$\sqrt{s} = M_Z$			$\sqrt{s} = 94 \text{ GeV}$		
	$\sigma_\mu - \sigma_{\text{box}}$	σ_μ	$\sigma_{\text{box}} \times 10^7$	$\sigma_\mu - \sigma_{\text{box}}$	σ_μ	$\sigma_{\text{box}} \times 10^7$
$0^\circ - 30^\circ$	0.1410419	0.1410410	9	0.0512613	0.0512605	8
$30^\circ - 60^\circ$	0.2993644	0.2993631	13	0.1042011	0.1041998	13
$60^\circ - 90^\circ$	0.3005794	0.3005789	5	0.0961092	0.0961088	4
$90^\circ - 120^\circ$	0.3016901	0.3016900	1	0.0800074	0.0800073	1
$120^\circ - 150^\circ$	0.3015250	0.3015249	1	0.0721641	0.0721640	1
$150^\circ - 180^\circ$	0.1420456	0.1420456	0	0.0353764	0.0353763	1

Table 4: *Differential cross section in nb for $\mu^+\mu^-$ production both with and without weak box contributions for selected LEP I energies. QED corrections are calculated following section 2.2 with $s'_{\text{min}} = 4m_f^2/s$.*

unchanged by radiative corrections. In this case, the Fermi constant absorbs the weak form factor $\rho(s)$ and becomes dependent on the process and its kinematics:

$$G_\mu \rightarrow \bar{G}_\mu = \rho(s)G_\mu. \quad (3.41)$$

The other form factors may be absorbed into various weak mixing angles:

$$\sin^2 \theta_W = 1 - M_W^2/M_Z^2 \rightarrow \begin{cases} \kappa_e(s) \sin^2 \theta_W \\ \kappa_f(s) \sin^2 \theta_W \\ \sqrt{\kappa_{ef}(s)} \sin^2 \theta_W. \end{cases} \quad (3.42)$$

This is similar to (3.20), even though more involved because of the additional complications presented by the kinematics. The above parametrization of \mathcal{M}_Z allows for a Born-like interpretation of all weak corrections. In this respect, we differ in our intentions from many other definitions of weak form factors and couplings, which try to perform dedicated approximations. Of course, such approximations may be applied to our weak form factors or to quantities derived from them; in sections 4 and 8.1 such approximations will be discussed; see also section 3.2. At LEP I energies, the approximate relations hold:

$$|\rho_{ef}(M_Z^2)|^2 \sim \rho_e^Z \rho_f^Z, \quad (3.43)$$

$$\bar{v}_f(M_Z^2) \sim \bar{v}_f^Z, \quad (3.44)$$

where the second relation may be replaced by:

$$\kappa_f(M_Z^2) \sim \kappa_f^Z. \quad (3.45)$$

So far, we have concentrated on s-channel kinematics, which depend on s and $\cos \vartheta$. It should be noted that for the t channel in Bhabha scattering the energy variable becomes $t = -\frac{1}{2}s(1 - \cos \vartheta)$ instead of s .

For b-quark production, unlike d- and s-quark production, a special contribution to the weak form factors arises from diagrams in fig. 9b, which contain as building blocks the Feynman graphs of fig. 7. This contribution may be of special interest at a high luminosity version of LEP I as is discussed in [47]. In general, the correction is s -dependent. It can be approximated near the Z resonance by the corresponding correction $\Delta_b(m_t^2)$ to the Z width as introduced in (3.27):

$$\rho_{eb} = \rho_{ed} - \frac{\Delta_b(m_t^2)}{a_b}, \quad (3.46)$$

$$\kappa_b = \kappa_d + \frac{\Delta_b(m_t^2)}{a_b}, \quad (3.47)$$

$$\kappa_{eb} = \kappa_{ed} + \frac{\Delta_b(m_t^2)}{a_b}, \quad (3.48)$$

with κ_e unchanged. This approximation has been implemented in $ZF\overline{I}T_{ER}$; it is valid only near the Z resonance and for $m_t > \sqrt{s}/2$. At other energies, since it would be difficult or impossible to measure the effects of this tiny correction due to small cross sections, we assume that the approximation holds there as well.

Higher order corrections in R_{QCD} have been implemented in $ZF\overline{I}T_{ER}$. These and the effects of the higher-order corrections to ρ and κ associated with a potentially large t-quark mass will be discussed in the next section.

We now come to the cross-section formulae, which are calculated in subroutine BORN. Both σ_T and σ_{FB} are sums of three terms:

$$\begin{aligned} \sigma_A^{o,\text{SM}}(s) &= \sigma_A^{o,\text{SM}}(s; \gamma, \gamma) + \sigma_A^{o,\text{SM}}(s; \gamma, Z) + \sigma_A^{o,\text{SM}}(s; Z, Z) \\ &= \mathcal{I}_A^{\text{SM}}(\gamma, \gamma; s) + \Re e \left[\mathcal{I}_A^{\text{SM}}(\gamma, Z; s) \mathcal{K}_Z^*(s) \right] + \mathcal{I}_A^{\text{SM}}(Z, Z; s) |\mathcal{K}_Z(s)|^2. \end{aligned} \quad (3.49)$$

Here, we have written the cross section in a form that is suitable for initial- and final-state radiation. However, the initial-final state interference cross section depends on two different energy scales (s, s'). The correct handling of the propagators can be inferred from (3.1). The generalized couplings \mathcal{I}_A are assumed to be dependent on s in $ZF\overline{I}T_{ER}$ with the exclusion of the running QED coupling where the scale (s or s') can be chosen by a flag⁹. This assumption speeds up the calculations with negligible loss of accuracy. In principle, one can take into account the s and s' dependence, in a trivial way for the factorizing parts of the form factors, and the rest with a little effort.

For unpolarized scattering, σ_T can be expressed by

$$\mathcal{I}_T^{\text{SM}}(\gamma, \gamma; s) = c_m N_\gamma(s) |Q_e|^2 |Q_f|^2 |F_A|^2, \quad (3.50)$$

$$\mathcal{I}_T^{\text{SM}}(\gamma, Z; s) = 2c_m N_\gamma(s) N_Z |Q_e Q_f| [F_A^* \rho_{ef} \bar{v}_{ef}], \quad (3.51)$$

$$\mathcal{I}_T^{\text{SM}}(Z, Z; s) = N_\gamma(s) N_Z^2 \left[c_m (1 + |\bar{v}_e|^2 + |\bar{v}_f|^2 + |\bar{v}_{ef}|^2) - \frac{6m_f^2}{s} (1 + |\bar{v}_e|^2) \right] |\rho_{ef}|^2, \quad (3.52)$$

where

$$N_\gamma(s) = \frac{\pi\alpha^2}{2s} \mu(s) c_f R_{\text{QCD}}(s), \quad (3.53)$$

$$N_Z = \frac{G_\mu M_Z^2}{\sqrt{2} 8\pi\alpha}, \quad (3.54)$$

$$c_m = (1 + 2m_f^2/s). \quad (3.55)$$

The variables $\mu(s)$, c_f , and R_{QCD} have already been introduced in section 3.2, and F_A in (3.33).

⁹ In principle, with initial-state radiation, the form factors depend on s' , with final-state radiation on s and with the small initial-final interference on both s and s' .

The corresponding generalized couplings for the anti-symmetric cross section σ_{FB} are:

$$\mathcal{I}_{FB}^{\text{SM}}(\gamma, \gamma; s) = 0, \quad (3.56)$$

$$\mathcal{I}_{FB}^{\text{SM}}(\gamma, Z; s) = 2\mu(s)N_\gamma(s)N_Z|Q_e Q_f|\rho_{ef} F_A^*, \quad (3.57)$$

$$\mathcal{I}_{FB}^{\text{SM}}(Z, Z; s) = 4\mu(s)N_\gamma(s)N_Z^2(\bar{v}_e\bar{v}_f^* + \bar{v}_{ef})|\rho_{ef}|^2. \quad (3.58)$$

In σ_{FB} , the QCD-factor is set zero, $R_{\text{QCD}} = 0$.

Helicities and polarizations may be included in the Standard Model cross sections σ_A in a compact way for massless fermion production [3, 9]. To do this, one must replace the above couplings, $\mathcal{I}_A(m, n; s)$, with¹⁰

$$\begin{aligned} C_T(m, n; \lambda_1, \lambda_2, h_1, h_2) = \\ \{ \lambda_1[\bar{v}_e(m)\bar{v}_e^*(n) + \bar{a}_e(m)\bar{a}_e^*(n)] + \lambda_2[\bar{v}_e(m)\bar{a}_e^*(n) + \bar{v}_e^*(n)\bar{a}_e(m)] \} \times \\ \{ h_1[\bar{v}_f(m)\bar{v}_f^*(n) + \bar{a}_f(m)\bar{a}_f^*(n)] + h_2[\bar{v}_f(m)\bar{a}_f^*(n) + \bar{v}_f^*(n)\bar{a}_f(m)] \}, \end{aligned} \quad (3.59)$$

$$C_{FB}(m, n; \lambda_1, \lambda_2, h_1, h_2) = C_T(m, n; \lambda_2, \lambda_1, h_2, h_1). \quad (3.60)$$

The vector and axial-vector couplings $\bar{v}_f(0)$ and $\bar{a}_f(0)$ of the fermion to the photon are:

$$\bar{v}_f(0) = Q_f F_A(s), \quad \bar{a}_f(0) = 0. \quad (3.61)$$

Here, we introduce the longitudinal polarizations of the electron (λ_-) and positron (λ_+) and the helicities of the final state fermions h_\pm in the following combinations:

$$\lambda_1 = 1 - \lambda_+\lambda_-, \quad \lambda_2 = \lambda_+ - \lambda_-, \quad (3.62)$$

$$h_1 = \frac{1}{4}(1 - h_+h_-), \quad h_2 = \frac{1}{4}(h_+ - h_-). \quad (3.63)$$

The various parts of the cross section in (3.1, 3.49) now become:

$$\sigma_A^\circ(s, s'; m, n) = \Re \left\{ C_A(m, n; \lambda_1, \lambda_2, h_1, h_2) \frac{1}{2} [\chi_m(s')\chi_n^*(s) + \chi_m(s)\chi_n^*(s')] \right\}, \quad (3.64)$$

$$\chi_\gamma(s) = \sqrt{N_\gamma(s)}\mathcal{K}_\gamma(s), \quad (3.65)$$

$$\chi_Z(s) = \sqrt{N_\gamma(s)}N_Z\mathcal{K}_Z(s), \quad (3.66)$$

where again the QCD-factor R_{QCD} in N_γ is set equal zero for σ_{FB} .

If at least one incoming and one outgoing fermion are polarized, then the contribution to the forward-backward anti-symmetric Standard Model cross section from pure photon exchange does *not* vanish as in (3.56). This can be seen from formulae (3.59)-(3.64).

We have not gone into details that are specific to Bhabha scattering: this is done in [11] and it represents a straight-forward extension of the above formulae.

¹⁰ This is not rigorous with respect to \bar{v}_{ef} , which has been assumed to factorize in order to simplify the notation. The correct expression, implemented in ${}_{ZF}I_{ER}^T$, can be obtained by performing the multiplications in (3.59) and replacing the product $\bar{v}_e(Z)\bar{v}_f(Z)$ with $\bar{v}_{ef}(Z)$. This may be verified by explicitly squaring the matrix element (3.35).

Asymmetries represent a clean and near systematic free measurement with which to test various models. In addition to the forward–backward asymmetry, several other asymmetries are interesting. It is useful to define a generic ‘spin’ asymmetry, $A(h)$:

$$A(h) = \frac{\sigma(h) - \sigma(-h)}{\sigma(h) + \sigma(-h)}, \quad (3.67)$$

where h can denote the polarization of an incoming fermion or the helicity of an outgoing one.

Choosing h to be $h_+ = +1$ the helicity of a final-state τ^+ and $\sigma(h)$ to be $\sigma_T(h_+)$, $A(h)$ becomes the τ polarization, $\lambda_\tau \equiv A_{\text{pol}}$. Similarly, one can define: $A_F^{\text{pol}}, A_B^{\text{pol}}$ as in [48] from (3.67) with $\sigma(h) = \sigma_A(h_+)$, $A = F, B, FB$, respectively. The subscript F (B) is used to indicate that only data from the forward (backward) hemisphere are in the measurement; the corresponding theoretical relations are given by (3.64) and (1.6). The forward–backward polarization asymmetry A_{FB}^{pol} may be defined as follows:

$$A_{FB}^{\text{pol}} = \frac{\sigma_{FB}(h) - \sigma_{FB}(-h)}{\sigma_T}. \quad (3.68)$$

3.4 Higher-Order Corrections

Here, we give a summary of treatment and common resummation of some higher-order weak and QCD corrections in $z_F \overline{I}^T T_{ER}$.

Some higher-order terms are used to correct Δr , ρ and κ . These terms are exclusively due to t -quark mass corrections. $z_F \overline{I}^T T_{ER}$ takes into account the following m_t -dependent corrections:

- complete m_t -dependent $\mathcal{O}(\alpha)$ terms [7],
- leading $\mathcal{O}(\alpha^2 m_t^4)$ terms [49, 11],
- complete (either approximated as a function of energy or exact) $\mathcal{O}(\alpha \alpha_s)$ terms [50, 51] with leading part $\mathcal{O}(\alpha \alpha_s m_t^2)$.

For Δr as introduced in (3.16), a common resummation of these leading terms may be performed as follows [52, 18, 20, 42]¹¹:

$$\frac{1}{1 - \Delta r} = \frac{1}{[1 - \Delta\alpha(M_Z^2)] \left(1 + \frac{\cos^2 \theta_W}{\sin^2 \theta_W} \delta\bar{\rho}\right) - \Delta r_{\text{rem}}}, \quad (3.69)$$

$$\Delta r_{\text{rem}} = \Delta r^{\text{1loop}} - \frac{\cos^2 \theta_W}{\sin^2 \theta_W} \Delta\rho - \Delta\alpha(M_Z^2) + \Delta r_{\text{rem}}^{\alpha\alpha_s}, \quad (3.70)$$

$$\begin{aligned} \Delta\rho &= \Delta\rho^\alpha + \Delta\rho^{\alpha\alpha_s} + X_0 \\ &= \frac{3\alpha}{16\pi \sin^2 \theta_W \cos^2 \theta_W} \frac{m_t^2}{M_Z^2} \left[1 - \frac{2}{3} \left(1 + \frac{\pi^2}{3}\right) \frac{\alpha_s(q^2, \Lambda_{\overline{\text{MS}}})}{\pi} \right] + X_0, \end{aligned} \quad (3.71)$$

¹¹ A detailed discussion of the $z_F \overline{I}^T T_{ER}$ flags which control the implementation of these corrections will be presented in section 6.2.

where the $\Delta\alpha(s)$ is introduced in (3.33) and

$$X_0 = \Re e \left[\frac{\Pi_Z(M_Z^2)}{M_Z^2} - \frac{\Pi_W(M_W^2)}{M_W^2} \right]_{\overline{\text{MS}}}^{\text{1loop}} - \Delta\rho^\alpha. \quad (3.72)$$

In X_0 the UV divergencies are removed according to the $\overline{\text{MS}}$ renormalization scheme with $\mu = M_Z$ ¹². The separation of X_0 is not uniquely defined; it introduces a dependence of the resummation on the renormalization procedure. Further,

$$\begin{aligned} \delta\bar{\rho} &= \delta\bar{\rho}^\alpha + \delta\bar{\rho}^{\alpha^2} + \delta\bar{\rho}^{\alpha\alpha_s} + X \\ &= 3\mathcal{T} \left[1 - (2\pi^2 - 19)\mathcal{T} - \frac{2}{3} \left(1 + \frac{\pi^2}{3} \right) \frac{\alpha_s(q^2, \Lambda_{\overline{\text{MS}}})}{\pi} \right] + X, \end{aligned} \quad (3.73)$$

$$\mathcal{T} = \frac{G_\mu m_t^2}{\sqrt{2} 8\pi^2}, \quad (3.74)$$

$$X = 2 \sin^2 \theta_W \cos^2 \theta_W \frac{G_\mu M_Z^2}{\sqrt{2}\pi\alpha} \left[1 - \Delta\alpha(M_Z^2) \right] X_0. \quad (3.75)$$

For the cross-section form factors, $\rho(s, \cos\vartheta)$ and $\kappa(s, \cos\vartheta)$, and partial Z width form factors, ρ^Z and κ^Z , similar formulae hold:

$$\rho = \frac{\rho^{\text{1loop}} + \rho_{\text{rem}}^{\alpha\alpha_s} - \Delta\rho}{1 - \delta\bar{\rho}}, \quad (3.76)$$

$$\kappa = \left(\kappa^{\text{1loop}} + \kappa_{\text{rem}}^{\alpha\alpha_s} - \frac{\cos^2 \theta_W}{\sin^2 \theta_W} \Delta\rho \right) \left(1 + \frac{\cos^2 \theta_W}{\sin^2 \theta_W} \delta\bar{\rho} \right). \quad (3.77)$$

For the cross section alone, we have additionally:

$$\kappa_{ef} = \left(\kappa_{ef}^{\text{1loop}} + \kappa_{ef,\text{rem}}^{\alpha\alpha_s} - 2 \frac{\cos^2 \theta_W}{\sin^2 \theta_W} \Delta\rho \right) \left(1 + \frac{\cos^2 \theta_W}{\sin^2 \theta_W} \delta\bar{\rho} \right)^2. \quad (3.78)$$

Some numerical examples of the effect of leading $\mathcal{O}(\alpha^2 m_t^4)$ corrections on the weak mixing angle, the $\mu^+\mu^-$ total cross section and forward-backward asymmetry at $s = M_Z^2$ are shown in table 5.

In section 3.2 we introduced the QCD correction factor, R_{QCD} , in (3.25). Its exact definition as implemented in ${}_{ZF}I^T T_{ER}$ is given by [53]:

$$R_{\text{QCD}} = 1 + \frac{\alpha_s}{\pi} + 1.409 \left(\frac{\alpha_s}{\pi} \right)^2 - 12.805 \left(\frac{\alpha_s}{\pi} \right)^3 \text{QCD3}. \quad (3.79)$$

For b quarks, the top- and bottom-quark mass-dependent QCD corrections (c_1, c_2) up to $\mathcal{O}(\alpha_s^2)$ have been taken from [54]:

$$R_{\text{QCD}} = 1 + c_1(m_b) \frac{\alpha_s}{\pi} + c_2(m_b, m_t) \left(\frac{\alpha_s}{\pi} \right)^2 - 12.805 \left(\frac{\alpha_s}{\pi} \right)^3 \text{QCD3}. \quad (3.80)$$

Where QCD3 has the value 0 or 1 as required by the user. In subroutine ZUWEAK , R_{QCD} is calculated and the result is stored in the variables QCDCOR and QCDCOB .

¹² In [39] this corresponds to a replacement of M_W by M_Z in the UV divergence \mathcal{P}_{UV} .

Observable	AMT4	m_t (GeV)				
		100	150	200	250	300
$\sin^2 \theta_W$	0	.2324	.2269	.2199	.2107	.1986
	1	.2324	.2271	.2206	.2128	.2040
	2	.2324	.2270	.2204	.2123	.2025
	3	.2324	.2270	.2205	.2125	.2029
σ_T^μ (nb)	0	1.4845	1.4861	1.4885	1.4920	1.4971
	1	1.4847	1.4867	1.4898	1.4942	1.5004
	2	1.4847	1.4867	1.4895	1.4935	1.4990
	3	1.4847	1.4867	1.4896	1.4935	1.4990
A_{FB}^μ	0	-.0043	-.0024	-.0004	.0015	.0023
	1	-.0045	-.0024	.0004	.0040	.0078
	2	-.0045	-.0023	.0008	.0052	.0115
	3	-.0045	-.0024	.0007	.0050	.0113

Table 5: *The weak mixing angle, muon pair production cross section and asymmetry both with (AMT4 \neq 0) and without (AMT4=0) leading $\mathcal{O}(\alpha^2 m_t^4)$ terms.*

Depending on a flag, the running strong interaction coupling constant [55] $\alpha(q^2, \Lambda_{\overline{\text{MS}}})$ is calculated with functions ALPHA4 or ALPHA5 [56]:

$$\alpha_s(q^2, \Lambda_{\overline{\text{MS}}}) = \frac{4\pi}{b_0 A} \left[1 - \frac{b_1}{b_0^2 A} \ln A + \left(\frac{b_1}{b_0^2 A} \right)^2 \left\{ \left(\ln A - \frac{1}{2} \right)^2 + b_2 \frac{b_0}{b_1^2} - \frac{5}{4} \right\} \right], \quad (3.81)$$

with

$$b_0 = 11 - \frac{2}{3}n_f, \quad b_1 = 102 - \frac{38}{3}n_f, \quad b_2 = \frac{1}{2} \left[2857 - \frac{5033}{9}n_f + \frac{325}{27}n_f^2 \right], \quad (3.82)$$

$$A = \ln \frac{q^2}{\Lambda_{\overline{\text{MS}}}^{(n_f)^2}}. \quad (3.83)$$

Here q^2 represents the energy scale and n_f the number of quark flavors. The corresponding definition of $\Lambda_{\overline{\text{MS}}}$ may be found in table 6.

In R_{QCD} , the α_s is calculated with $q^2 = s$ for cross sections or $q^2 = M_Z^2$ for the Z width. In the $\mathcal{O}(\alpha\alpha_s)$ corrections the scale is chosen to be $q^2 = M_Z^2$ for light quarks and $q^2 = \max\{M_Z^2, m_t^2\}$ for the tb doublet. One can see that in the LEP energy region the difference between the approximate¹³ and exact treatment of the $\mathcal{O}(\alpha\alpha_s)$ corrections is minor.

Table 7 shows the $\alpha_s(q^2, \Lambda_{\overline{\text{MS}}})$ as a function of q^2 .

The dependence of weak parameters on α_s is shown in table 8 as a function of how the $\mathcal{O}(\alpha\alpha_s)$ corrections are applied.

¹³The approximation realized in ${}_Z F^T T_{ER}$ is a Taylor series expansion in s/m_t^2 for s smaller than m_t^2 . The leading term of this expansion is included in (3.73).

q^2	n_f	$\Lambda_{\overline{\text{MS}}}$
$\leq m_c^2$	3	$\Lambda_{\overline{\text{MS}}}^{(4)} \left(\frac{m_c}{\Lambda_{\overline{\text{MS}}}^{(4)}} \right)^{\frac{2}{27}} \ln \left(\frac{m_c^2}{(\Lambda_{\overline{\text{MS}}}^{(4)})^2} \right)^{\frac{107}{2025}}$
$\leq m_b^2$	4	$\Lambda_{\overline{\text{MS}}}^{(4)}$
$\leq m_t^2$	5	$\Lambda_{\overline{\text{MS}}}^{(4)} \left(\frac{\Lambda_{\overline{\text{MS}}}^{(4)}}{m_b} \right)^{\frac{2}{23}} \ln \left(\frac{m_b^2}{(\Lambda_{\overline{\text{MS}}}^{(4)})^2} \right)^{\frac{-963}{13225}}$
$> m_t^2$	6	$\Lambda_{\overline{\text{MS}}}^{(5)} \left(\frac{\Lambda_{\overline{\text{MS}}}^{(5)}}{m_t} \right)^{\frac{2}{21}} \ln \left(\frac{m_t^2}{(\Lambda_{\overline{\text{MS}}}^{(5)})^2} \right)^{\frac{-107}{1127}}$

Table 6: $\Lambda_{\overline{\text{MS}}}$ for different energy regions.

$ q $ (GeV)	50	100	150	200	250	300
α_s	.1193	.1079	.1022	.0985	.0958	.0937

Table 7: Running $\alpha_s(q^2)$ versus $|q|$.

QCDC	ρ_{ef}	κ_e	κ_f	κ_{ef}
$\nu\bar{\nu}$ final state				
0	$1.004 - i0.002$	$1.025 + i0.013$		
1	$1.004 - i0.002$	$1.023 + i0.014$		
2	$1.004 - i0.002$	$1.022 + i0.014$		
ll final state				
0	$1.003 - i0.005$	$1.025 + i0.013$	$1.025 + i0.013$	$1.050 + i0.026$
1	$1.002 - i0.005$	$1.023 + i0.014$	$1.023 + i0.014$	$1.046 + i0.027$
2	$1.002 - i0.005$	$1.022 + i0.014$	$1.022 + i0.014$	$1.045 + i0.027$
$u\bar{u}$ final state				
0	$1.003 - i0.004$	$1.025 + i0.013$	$1.024 + i0.012$	$1.050 + i0.026$
1	$1.003 - i0.004$	$1.023 + i0.014$	$1.022 + i0.013$	$1.045 + i0.026$
2	$1.003 - i0.004$	$1.022 + i0.014$	$1.022 + i0.013$	$1.045 + i0.026$
dd final state				
0	$1.003 - i0.003$	$1.025 + i0.013$	$1.024 + i0.012$	$1.049 + i0.025$
1	$1.003 - i0.003$	$1.023 + i0.014$	$1.022 + i0.012$	$1.045 + i0.026$
2	$1.003 - i0.003$	$1.022 + i0.014$	$1.022 + i0.012$	$1.044 + i0.026$
bb final state				
0	$0.999 - i0.003$	$1.025 + i0.013$	$1.028 + i0.012$	$1.054 + i0.025$
1	$0.999 - i0.003$	$1.023 + i0.014$	$1.026 + i0.012$	$1.049 + i0.026$
2	$0.999 - i0.003$	$1.022 + i0.014$	$1.026 + i0.012$	$1.049 + i0.026$

Table 8: The dependence of the form factors ρ_{ef} and $\kappa_e, \kappa_f, \kappa_{ef}$ at the Z peak on different treatments of $\mathcal{O}(\alpha_s)$ corrections (QCDC=0 - no, 1 - approximate and 2 - exact $\mathcal{O}(\alpha_s)$ corrections are applied).

4 The Hard-Scattering Process: (II) Model-Independent Branches

4.1 Effective Couplings

In a simple quantum mechanical approach, the Z boson may be assumed to have real constant vector (\hat{v}_f) and axial-vector (\hat{a}_f) couplings to fermions (f). This ansatz may be realized by a replacement of the renormalized effective couplings as predicted from the Standard Model by naïve effective couplings in the cross section, see fig. 11.

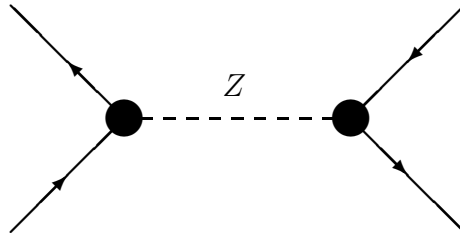


Figure 11: *Matrix element in the approach with effective Z couplings.*

The cross sections for the hard-scattering process are:

$$\begin{aligned}\sigma_A^{o,\text{eff}}(s) &= \sigma_A^{o,\text{eff}}(s; \gamma, \gamma) + \sigma_A^{o,\text{eff}}(s; \gamma, Z) + \sigma_A^{o,\text{eff}}(s; Z, Z) \\ &= \mathcal{I}_A^{\text{eff}}(\gamma, \gamma; s) + \Re \left[\mathcal{I}_A^{\text{eff}}(\gamma, Z; s) \mathcal{K}_Z^*(s) \right] + \mathcal{I}_A^{\text{eff}}(Z, Z; s) |\mathcal{K}_Z(s)|^2.\end{aligned}\quad (4.1)$$

Here, the generalized couplings for the total cross section are:

$$\mathcal{I}_T^{\text{eff}}(\gamma, \gamma; s) = c_m N_\gamma(s) |F_A(s)|^2 Q_e^2 Q_f^2, \quad (4.2)$$

$$\mathcal{I}_T^{\text{eff}}(\gamma, Z; s) = 2c_m N_Z N_\gamma(s) F_A(s) |Q_e Q_f| \hat{v}_e \hat{v}_f, \quad (4.3)$$

$$\mathcal{I}_T^{\text{eff}}(Z, Z; s) = N_Z^2 N_\gamma(s) \left[c_m (\hat{v}_e^2 + \hat{a}_e^2) (\hat{v}_f^2 + \hat{a}_f^2) - \frac{6m_f^2}{s} (\hat{v}_e^2 + \hat{a}_e^2) \hat{a}_f^2 \right], \quad (4.4)$$

where $N_\gamma(s)$ and N_Z are defined in (3.53)-(3.54), c_m in (3.55), and F_A in (3.33).

The asymmetric cross-section part is defined by:

$$\mathcal{I}_{FB}^{\text{eff}}(\gamma, \gamma; s) = 0, \quad (4.5)$$

$$\mathcal{I}_{FB}^{\text{eff}}(\gamma, Z; s) = 2\mu(s) N_Z N_\gamma(s) F_A(s) |Q_e Q_f| \hat{a}_e \hat{a}_f, \quad (4.6)$$

$$\mathcal{I}_{FB}^{\text{eff}}(Z, Z; s) = 8\mu(s) N_Z N_\gamma(s) \hat{v}_e \hat{a}_e \hat{v}_f \hat{a}_f, \quad (4.7)$$

where $\mu(s)$ is defined in (3.22).

One may interpret effective couplings as approximations to the weak form factors of the Standard Model e.g.:

$$\hat{a}_f \equiv 2\hat{g}_a^f \sim \Re e \sqrt{\rho_{ef}(M_Z^2)} a_f, \quad (4.8)$$

$$\hat{v}_f \equiv 2\hat{g}_v^f \sim \Re e \left[\sqrt{\rho_{ef}(M_Z^2)} \bar{v}_f(M_Z^2) \right], \quad (4.9)$$

where the alternate notation $(\hat{g}_a^f, \hat{g}_v^f)$ is favored by the LEP experiments. We neglect here possible dependences on the scattering angle. In ${}_{ZF}I^T T_{ER}$ the normalization $a_f=1$ is used for all fermions. In addition, one may choose an alternative parametrization in terms of the effective weak neutral current amplitude normalization, $\hat{\rho}_f$:

$$\hat{\rho}_f \equiv \frac{\hat{g}_a^f}{g_a^f}, \quad (4.10)$$

$$\hat{\rho}_e \hat{\rho}_f \sim \Re \sqrt{\rho_{ef}(M_Z^2)}, \quad (4.11)$$

$$\hat{v}_f \sim \Re \left[\sqrt{\rho_{ef}(M_Z^2)} \bar{v}_f(M_Z^2) \right]. \quad (4.12)$$

In the present approach, one can leave Γ_Z as a free fundamental parameter of the ansatz. Alternatively, one may define it through the second line of (3.17), replacing there the renormalized (\bar{v}^Z, \bar{a}^Z) couplings by effective (\hat{v}^Z, \hat{a}^Z) ones.

In either case, one must realize that the normalization of the Z width may change depending on the definition of M_Z (see earlier discussion in connection with equations (3.8) and (3.12)). For additional general comments on cross sections and asymmetries we refer to section 3.

In principle, this branch is completely model independent. However, ${}_{ZF}I^T T_{ER}$ users should be aware that the current implementation contains small Standard Model contributions in the form of imaginary parts of weak form factors (see table 8).

4.2 Partial Z Widths

This approach to determining cross sections relies on the assumption that scattering through the Z boson may be considered as subsequent formation and decay of a resonance, see fig. 12. The corresponding net cross section is (see e.g. [12] and references therein):

$$\sigma_T^{o,\Gamma}(s) = \sigma_T^{o,\text{SM}}(s; \gamma, \gamma) + I^\Gamma + \sigma_T^{o,\Gamma}(s; Z, Z), \quad (4.13)$$

$$\sigma_T^{o,\Gamma}(s; Z, Z) = \mathcal{I}_T^\Gamma(Z, Z; s) |\mathcal{K}_Z(s)|^2, \quad (4.14)$$

$$\mathcal{I}_T^\Gamma(Z, Z; s) = \frac{3}{8s} \frac{12\pi c_m \Gamma_e \Gamma_f}{\mu(M_Z R_{\text{QED}})^2}. \quad (4.15)$$

The photonic contribution to the cross section, $\sigma_T^{o,\text{SM}}$, is given in (3.50)-(3.51).

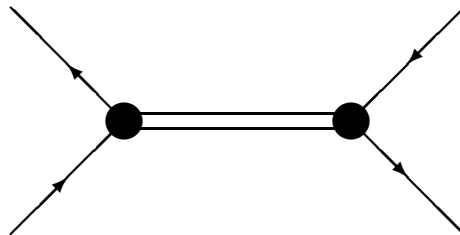


Figure 12: *Matrix element for the Z resonance scattering.*

One of the attractive features of the partial widths approach is the treatment of hadron production. Here one simply replaces Γ_f with Γ_{had} in (4.15). In case of hadron production, we have to use the quark language for the photonic cross-section contribution in (4.13), which is taken over from (3.49) in section 3.3 without changes.

The interference term in (4.13) presents some complications with this approach. There are at least four different ways dealing with this term: an exact calculation, a simple parametrization, ignoring the term completely, or assuming the Standard Model prediction.

A correct handling would rely on partial decay widths into specific helicity states, $\Gamma_{\pm}(f)$, as proposed in [12]:

$$I^{\Gamma} \equiv \sigma_T^{o,\Gamma}(s; \gamma, Z) = \mathcal{I}_T^{\Gamma}(\gamma, Z; s) \Re e \mathcal{K}_Z(s), \quad (4.16)$$

$$\mathcal{I}_T^{\Gamma}(\gamma, Z; s) = \pm \frac{3}{8s} \frac{4\pi Q_e Q_f \alpha(s) c_m}{M_Z R_{\text{QED}}} \left[\Gamma_{+}^{\frac{1}{2}}(e) - \Gamma_{-}^{\frac{1}{2}}(e) \right] \left[\Gamma_{+}^{\frac{1}{2}}(f) - \Gamma_{-}^{\frac{1}{2}}(f) \right]. \quad (4.17)$$

In practice, however, experimental measurements seem not to deliver a sufficiently high number of degrees of freedom to use this formula.

A simple parametrization of the interference term, as has been realized in the S-matrix approach, could be used. This, however, leads to large uncertainties in the Z mass determination [14].

Ignoring the interference term completely (i.e. assuming that it is identically zero) is another possibility, since this term is expected to be small. In addition this removes one degree of freedom.

The last alternative is to assume the interference term from the Standard Model, as defined in (3.49), (3.51):

$$I^{\Gamma} = \sigma_T^{o,\text{SM}}(s; \gamma, Z). \quad (4.18)$$

This is the approach that has been implemented in ${}_{ZF}I^{\Gamma}T_{ER}^{\bar{\Gamma}}$.

In addition to the partial decay widths of the Z , the total Z width and mass are free parameters with this approach. There is an ambiguity in the normalization of the total and partial widths which is due to the different choices for the definition of the Z propagator (see discussion at the beginning of section 3). The energy-dependent total Z width, $\Gamma_Z(s)$, is related to the constant total Z width, $\bar{\Gamma}_Z$, by (3.8), (3.12). In relating the two approaches to the resonance definition, there is no explicit constraint on the partial widths.

They may be related as follows. In the Standard Model branch, the residua of the resonance functions were normalized by the Fermi constant. With this approach the actual residua are contained in the partial widths. Comparing the two, one can derive the relation between the partial widths for the two different definitions of the Z propagator from (3.13):

$$\bar{\Gamma}_f = \frac{\Gamma_f}{\sqrt{1 + (\Gamma_Z/M_Z)^2}}. \quad (4.19)$$

This relation is in full accordance with the corresponding relation for the total width (3.12).

4.3 S-Matrix

Besides the approach to the effective Born cross section based on the Standard Model or on one of its extensions, there is only one accurate model-independent approach to the Z line shape. One can derive this *rigorous* model-independent formula either starting from an analysis of the Standard Model results [58] or from S-matrix theory.

An early application of the S-matrix formalism to LEP I physics may be found in [59]. Recently, it has been proposed to use S-matrix theory for a global description of the hard-scattering process [35, 14]. Such an ansatz has the advantage that it contains no special assumptions on the dynamics beyond general principles and the existence of both photon and Z boson. In [14] the necessary formalism has been described. One starts from the incoherent sum of four squared matrix elements for the scattering of helicity fermion states ($e_L^- e_R^+ \rightarrow f_L \bar{f}_R$, $e_L^- e_R^+ \rightarrow f_R \bar{f}_L$, $e_R^- e_L^+ \rightarrow f_R \bar{f}_L$, $e_R^- e_L^+ \rightarrow f_L \bar{f}_R$) as seen in fig. 13.

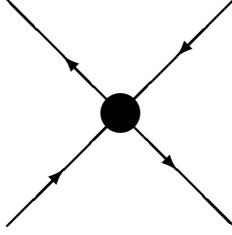


Figure 13: *Scattering in the S-matrix approach.*

All have the following structure:

$$\mathcal{M}_i(s) = \frac{R_\gamma}{s} + \frac{R_Z^i}{s - s_Z} + F_i(s_Z) + (s - s_Z)F_i'(s_Z) + (s - s_Z)^2 F_i''(s_Z) + \dots \quad (4.20)$$

The location of the Z -boson pole is given by s_Z in the complex energy plane, and R_γ and R_Z^i represent constant complex residuals. The cross section is:

$$\sigma_T^{o,S}(s) = \frac{1}{4} \sum_{i=1}^4 s |\mathcal{M}^i(s)|^2. \quad (4.21)$$

In order to fit the cross section, it is perhaps useful to decompose the above into a series of real-valued terms with rising powers of $(s - M_Z^2)$ ¹⁴:

$$\sigma_T^{o,S}(s) = \frac{r_\gamma}{s} + \frac{M_Z^2 R + (s - M_Z^2) I}{|s - s_Z|^2} + \frac{r_0}{M_Z^2} + (s - M_Z^2) \frac{r_1}{M_Z^4} + (s - M_Z^2)^2 \frac{r_2}{M_Z^6} + \dots \quad (4.22)$$

where we defined the constants to be dimensionless and

$$r_\gamma = |R_\gamma|^2, \quad (4.23)$$

$$R_\gamma = \begin{cases} Q_e \sqrt{3Q_d^2 + 2Q_u^2} \sqrt{\frac{4\pi}{3}} c_f R_{\text{QCD}} \alpha(M_Z^2) & \text{for hadrons at LEP I} \\ Q_e Q_f \sqrt{\frac{4\pi}{3}} \alpha(M_Z^2) & \text{for leptons.} \end{cases} \quad (4.24)$$

Here r_γ depends only on the dynamics of the photon, while the other parameters ($M_Z, \Gamma_Z, R, I, r_0, \dots$) depend also on the Z . The ansatz (4.22) may be compared with the notation used in the foregoing sections:

$$\begin{aligned} \sigma_T^{o,S}(s) &= \sigma_T^{o,S}(s; \gamma, \gamma) + \sigma_T^{o,S}(s; \gamma, Z) + \sigma_T^{o,S}(s; Z, Z) \\ &= \mathcal{I}_T^S(\gamma, \gamma; s) + \Re \left[\mathcal{I}_T^S(\gamma, Z; s) \mathcal{K}_Z(s) \right] + \mathcal{I}_T^S(Z, Z; s) |\mathcal{K}_Z(s)|^2. \end{aligned} \quad (4.25)$$

¹⁴ Each of the coefficients itself is then a series in the variable Γ_Z/M_Z .

Here,

$$\mathcal{I}_T^S(\gamma, \gamma; s) = \frac{r_\gamma}{s} + \dots, \quad (4.26)$$

$$\mathcal{I}_T^S(\gamma, Z; s) \equiv \frac{\mathcal{J}}{s} = \frac{I - R}{s} + \dots, \quad (4.27)$$

$$\mathcal{I}_T^S(Z, Z; s) = \frac{R}{s} + \dots \quad (4.28)$$

The dots indicate contributions from the Taylor coefficients; for instance, the photon-exchange contribution collects not only the r_γ but also small additional terms due to the dependence of the running QED coupling on s or s' ¹⁵. The leading contribution to the γZ interference comes from the combination $\mathcal{J} = I - R$; in order to simplify the s dependence of the ansatz, R has been introduced in (4.22) with a coefficient of M_Z^2 instead of s .

In order to get an intuitive feeling for the meaning of the S-matrix parameters, it may be helpful to contrast this approach with that of the effective couplings discussed in section 4.1. The cross section for muon production (4.22) in this *approximation* is given by fixing:

$$R = c^2(\hat{v}_e^2 + \hat{a}_e^2)(\hat{v}_\mu^2 + \hat{a}_\mu^2), \quad (4.29)$$

$$I = R + \mathcal{J}, \quad (4.30)$$

$$\mathcal{J} = 2cR_\gamma \hat{v}_e \hat{v}_\mu, \quad (4.31)$$

$$r_i = 0, \quad i = 0, 1, \dots \quad (4.32)$$

with

$$c = \sqrt{\frac{4\pi}{3}} \frac{G_\mu}{\sqrt{2}} \frac{M_Z^2}{8\pi}. \quad (4.33)$$

Contrasting the S-matrix to the partial width approach, one obtains instead:

$$R = 12\pi\Gamma_e\Gamma_f + \dots, \quad (4.34)$$

and the γZ interference part has to be fixed by a relation analogous to (4.30) (see the lengthy discussion in section 4.2). An exact treatment would enlarge the number of parameters to be fitted, and weaken the numerical result.

The general form of the above parameters (R, I, r_0, \dots) may be found in [14] (they were not made dimensionless there as is done here). In a quantum field theory, the constants (r_0, r_1, \dots) are non-vanishing, owing due to non-resonating quantum corrections. A careful analysis of their calculation in accordance with the S-matrix properties has been performed in [35].

An ansatz quite similar to (4.22) has been derived in [58], starting from an on-mass-shell renormalization of the Standard Model; for the production of flavor f :

$$\sigma_T^{o,S}(s) = \frac{12\pi\Gamma_e\Gamma_f}{|s - s_Z|^2} \left\{ \frac{s}{M_Z^2} + \mathcal{R}_f \frac{s - M_Z^2}{M_Z^2} + \mathcal{I}_f \frac{\Gamma_Z}{M_Z} + \dots \right\} + \sigma_{\text{QED}}^f, \quad (4.35)$$

where terms of higher order in $(s - M_Z^2)/M_Z^2$ and in Γ_Z/M_Z are dropped. There is a simple one-to-one correspondence to the terms in (4.22), with exclusion of the \mathcal{I}_f ; the dominating

¹⁵ Strictly speaking, the residuum of the photon pole (4.24) is not $\alpha(M_Z^2)$ but the QED coupling constant α at zero momentum; the difference is related to non-leading terms and may be absorbed by a redefinition of r_i .

part of this correction is due to the imaginary part of the running QED coupling $\alpha(s)$. The corresponding contribution in our notations may be found in the exact definition of R :

$$R = \frac{1}{4} \sum_i |R_Z^i|^2 + 2 \frac{\Gamma_Z}{M_Z} \Im m R_\gamma^* \left(\frac{1}{4} \sum_i R_Z^i \right) + \dots \quad (4.36)$$

As in the aforementioned branches, the definitions of mass and width of the Z boson are correlated and deserve special attention.

The possibility to describe asymmetries is mentioned in [14].

5 Beyond the Standard Model

In recent years, many searches for possible effects from *New Physics* have been undertaken in precision experiments at LEP I. Reviews of the present status and of the literature may be found in [61]–[65]. Here, we would like to restrict ourselves to some hints on the possible use of ${}_{ZF} \overline{I} T_{ER}$ for corresponding searches.

To start with, let us assume that some more general theory leads to predictions for the scattering of two fermions into two fermions. This may be described by an additional matrix element \mathcal{M}_E , to be added to \mathcal{M}_γ and \mathcal{M}_Z :

$$\mathcal{M}_E(s, \cos \vartheta) \sim C_E [u_\rho L_\beta \otimes L^\beta + u_e \gamma_\beta \otimes L^\beta + u_f L_\beta \otimes \gamma^\beta + u_{ef} \gamma_\beta \otimes \gamma^\beta], \quad (5.37)$$

and the C_E, u_a can depend on s and $\cos \vartheta$. An instructive example for new physics at the Born level is an additional heavy neutral gauge boson Z' with mass $M_{Z'}$, width $\Gamma_{Z'}$, vector and axial-vector couplings v'_f, a'_f , and coupling constant $g_{Z'}$. As long as this Z' does not mix with the ordinary Z , the influence on the scattering process is due to \mathcal{M}_E and thus limited to higher energy [66]:

$$C_E = C_{Z'} \equiv \frac{g_{Z'}^2}{s - M_{Z'}^2 + i M_{Z'} \Gamma_{Z'}}, \quad (5.38)$$

$$u_\rho = a'_e a'_f \rho'_{ef}, \quad u_f = (v'_f - a'_f) \rho'_{ef} \kappa'_f, \quad u_{ef} = (v'_e - a'_e) (v'_f - a'_f) \rho'_{ef} \kappa'_{ef}, \quad (5.39)$$

with $\rho' = \kappa' = 1$ for Z' Born physics.

In general, the corrections u_a may also be due to some loop insertions to the Z matrix element from a generalized renormalizable theory, or even simply due to some Standard Model corrections not yet included in the definitions of the weak form factors. An example of the latter case had been given in the Z -vertex corrections from t -quark exchange, see (3.46)–(3.48). Usually, the additional loop corrections are incorporated into the Z matrix element (3.37):

$$\mathcal{M}(Z, E) = \mathcal{M}_Z + \mathcal{M}_E, \quad (5.40)$$

$$\begin{aligned} \mathcal{M}(Z, E)(s, \cos \vartheta) \sim C_Z \left\{ \left[\bar{a}_e \bar{a}_f + \frac{C_E}{C_Z} u_\rho \right] \gamma_\beta \gamma_5 \otimes \gamma^\beta \gamma_5 + \left[\bar{v}_e \bar{a}_f + \frac{C_E}{C_Z} (u_\rho + u_e) \right] \gamma_\beta \otimes \gamma^\beta \gamma_5 \right. \\ \left. + \left[\bar{a}_e \bar{v}_f + \frac{C_E}{C_Z} (u_\rho + u_f) \right] \gamma_\beta \gamma_5 \otimes \gamma^\beta + \left[\bar{v}_{ef} + \frac{C_E}{C_Z} (u_\rho + u_e + u_f + u_{ef}) \right] \gamma_\beta \otimes \gamma^\beta \right\} \quad (5.41) \end{aligned}$$

$$C_Z = \frac{G_\mu}{s - M_Z^2 + iM_Z\Gamma_Z}. \quad (5.42)$$

In case of loop corrections to the Z propagator, the ratio C_E/C_Z is free of the resonating s dependence around the Z peak, and in some scenarios the corrections are even constant.

In general, however, this is not the case. Coming back to the example of an additional Z' , there is evidently a potentially remarkable s dependence of the insertions, being even resonating near the Z' peak.

In any case, one can go a step further and include the non-standard corrections into the form factors introduced in (3.35) by the following replacements:

$$\rho_{ef} \rightarrow \rho_{ef}(Z, E) = \rho_{ef} \left(1 + \frac{C_E}{C_Z} \frac{u_\rho}{\rho_{ef} a_e a_f} \right), \quad (5.43)$$

$$\kappa_f \rightarrow \kappa_f(Z, E) = \frac{\rho_{ef}}{\rho_{ef}(Z, E)} \kappa_f \left[1 + \frac{C_E}{C_Z} \frac{u_f}{\rho_{ef} \kappa_f a_e (v_f - a_f)} \right], \quad (5.44)$$

$$\kappa_{ef} \rightarrow \kappa_{ef}(Z, E) = \frac{\rho_{ef}}{\rho_{ef}(Z, E)} \kappa_{ef} \left[1 + \frac{C_E}{C_Z} \frac{u_{ef}}{\rho_{ef} \kappa_{ef} (v_e - a_e)(v_f - a_f)} \right]. \quad (5.45)$$

The above replacements ensure the interpretation of the weak form factors as finite renormalizations of Fermi constant and weak mixing angle; see (3.41), (3.42). They can, however, drastically change the numerical behaviour of the form factors, which now need no longer be small. The advantage of the above formulae is two-fold. Besides the compact notation and simple interpretation, they may be used not only for the description of the fermion pair production process (1.1). Without changes, they describe also the effects of new physics in Bhabha scattering or in the crossed channel, i.e. ep scattering.

Besides the neutral current amplitude \mathcal{M}_E , new physics may show up also in other phenomena, thus influencing fermion pair production in an indirect way. It is well-known that e.g. a Z' , which mixes with the ordinary Z boson, may influence the Z and W mass ratio and the Z vector and axial-vector couplings – it is these effects, which may be searched for at LEP I. How they can be covered in the language of form factors has been explained in the references quoted above. In addition, a careful derivation of the weak form factors following the notations used in the present paper may be found in [15], where the use of ${}_{ZF}I^T T_{ER}$ for a Z' search is explained¹⁶. The main consequences are contained in the following replacements in the definitions of weak form factors ρ_f^Z, κ_f^Z for partial widths and $\rho_{ef}, \kappa_f, \kappa_{ef}$ for the cross sections:

$$\begin{aligned} \rho_f^Z &\rightarrow \rho_{\text{mix}}(1 - y_f)^2 \rho_f^Z, \\ \kappa_f^Z &\rightarrow (1 - x_f) \kappa_f^Z, \end{aligned} \quad (5.46)$$

$$\begin{aligned} \rho_{ef} &\rightarrow \rho_{\text{mix}}(1 - y_e)(1 - y_f) \rho_{ef}, \\ \kappa_f &\rightarrow (1 - x_f) \kappa_f, \\ \kappa_{ef} &\rightarrow (1 - x_e)(1 - x_f) \kappa_{ef}. \end{aligned} \quad (5.47)$$

Here, x_f, y_f are small corrections to the Z -boson couplings due to the Z, Z' mixing, and ρ_{mix} is due to the related slight Z mass shift:

$$\rho_{\text{mix}} = \frac{M_W^2}{M_Z^2 \cos^2 \theta_W} = \frac{M_0^2}{M_Z^2} = 1 + \sin^2 \theta_M \left(\frac{M_{Z'}^2}{M_Z^2} - 1 \right). \quad (5.48)$$

¹⁶ See also the package ZEFIT [15] at ZFITTER@CERNVM.

The parameter M_0 is the Z mass of the standard model without Z, Z' mixing. The ρ_{mix} influences the widths and cross sections directly, since we have replaced in (3.17) and in (3.35),(3.37) the coupling constant α of the on-mass-shell scheme by the Fermi constant G_μ . These are related as follows (see (3.16)):

$$\frac{\pi\alpha}{2\sin^2\theta_W\cos^2\theta_W} = \frac{G_\mu}{\sqrt{2}}M_0^2(1-\Delta r) = \frac{G_\mu}{\sqrt{2}}M_Z^2\rho_{\text{mix}}(1-\Delta r). \quad (5.49)$$

In the same way as $(1-\Delta r)$ becomes part of ρ_f^Z and ρ_{ef} without mixing, the factor $\rho_{\text{mix}}(1-\Delta r)$ becomes part of the form factors when Z and Z' mix.

Another, completely different source of deviations from the standard model are self-energy corrections Π due to new physics, which may lead to the following changes of the weak form factors [42]:

$$\Delta\rho_{ef}(s) = \Delta\rho(0) + \Pi_{ZZ}(M_Z^2) - \frac{s\Pi_{ZZ}(s) - M_Z^2\Pi_{ZZ}(M_Z^2)}{s - M_Z^2}, \quad (5.50)$$

$$\Delta\rho_W(s) = \Pi_{WW}(M_W^2) - \frac{s\Pi_{WW}(s) - M_W^2\Pi_{WW}(M_W^2)}{s - M_W^2}, \quad (5.51)$$

$$\Delta\kappa(s) = \Delta\kappa(M_Z^2) - \frac{\cos\theta_W}{\sin\theta_W} [\Pi_{\gamma Z}(s) - \Pi_{\gamma Z}(M_Z^2)]. \quad (5.52)$$

For completeness, the corrections for the charged-current form factor have been added. The corrections at LEP I may be obtained from the above expressions by setting $s = M_Z^2$.

A different starting point has been used e.g. in [60, 65]. There it is studied how one can disentangle new physics from the possibly large, unknown t-quark corrections of leading order $G_\mu m_t^2$; see section 3.4. For this purpose one can introduce three new parameters:

$$\epsilon_1 = \Delta\rho, \quad (5.53)$$

$$\epsilon_2 = c_0^2\Delta\rho + \frac{s_0^2\Delta r_W}{(c_0^2 - s_0^2)} - 2s_0^2\Delta k', \quad (5.54)$$

$$\epsilon_3 = c_0^2\Delta\rho + (c_0^2 - s_0^2)\Delta k'. \quad (5.55)$$

The quantities $\Delta\rho, \Delta r_W, \Delta k', s_0^2$ may be identified with quantities used in ${}_{ZF}{}^T T_{ER}$ and introduced above¹⁷:

$$\Delta r_W = 1 - (1 - \Delta r)\frac{\alpha(M_Z^2)}{\alpha}, \quad (5.56)$$

$$g_a = -\frac{\sqrt{\rho}}{2} = -\frac{1}{2}(1 + \frac{1}{2}\Delta\rho), \quad (5.57)$$

$$\frac{g_v}{g_a} = 1 - 4s_w^{2,\text{eff}} = 1 - 4(1 + \Delta\kappa')s_0^2, \quad (5.58)$$

$$s_0^2 c_0^2 = \frac{\pi\alpha(M_Z^2)}{\sqrt{2}G_\mu M_Z^2}. \quad (5.59)$$

It is up to the user of ${}_{ZF}{}^T T_{ER}$ to decide which of the various coupling definitions available in the program and described in sections 3.2, 3.3, 4 are used as couplings g_v, g_a in the above definitions. The running QED coupling is defined in (3.33). Thus, while it may appear that

¹⁷Here, we exactly follow the notations of [65]; see also the package ZFEPSON [67] at ZFITTER@CERNVM.

the ϵ parameters are merely rearrangements of previously defined quantities, their merit lies in separating out the m_t -dependent effects in ϵ_1 and other (Higgs) effects in ϵ_3 . Furthermore, for an analysis of LEP I data alone, the ϵ_2 parameter may be ignored.

Besides the notations introduced so far, there are several similar ones used in the literature, often in quite a different context. As one important example, we quote the following notation which introduces again some self-energy corrections, but now calculated before γ, Z mixing [63]:

$$\alpha S \approx -4e^2 \frac{d}{dq^2} [\Pi_{30}(q^2)]|_{q^2=0}, \quad (5.60)$$

$$\alpha T \approx \frac{e^2}{\sin^2 \theta_W M_W^2} [\Pi_{11}(0) - \Pi_{33}(0)], \quad (5.61)$$

$$\alpha U \approx 4e^2 \frac{d}{dq^2} [\Pi_{11}(q^2) - \Pi_{33}(q^2)]|_{q^2=0}. \quad (5.62)$$

The relation to the above notations is [64]:

$$\epsilon_1 = \alpha T, \quad \epsilon_2 = -\frac{\alpha}{4 \sin^2 \theta_W} U, \quad \epsilon_3 = \frac{\alpha}{4 \sin^2 \theta_W} S. \quad (5.63)$$

Further relations between different notations may be found in [61].

6 Initialization of $ZFI^T T_{ER}$

$ZFI^T T_{ER}$ is coded in FORTRAN 77 and it has been implemented on IBM, IBM PC, VAX, and APOLLO. It must be used with DIZET and BHANG. Double-precision variables have been used throughout the program in order to obtain maximum accuracy, which is especially important for resonance physics. In all, the package ($ZFI^T T_{ER}$, DIZET and BHANG) contains about 11500 lines of FORTRAN code. A block diagram of $ZFI^T T_{ER}$ is shown in fig. 14.

The following routines are normally called in the initialization phase of programs using the $ZFI^T T_{ER}$ package. Normally they are called in the order listed below.

6.1 Subroutine ZUINIT

Subroutine ZUINIT is used to initialize variables to their default values. This routine *must* be called before any other $ZFI^T T_{ER}$ routine.

```
CALL ZUINIT
```

6.2 Subroutine ZUFLAG

Subroutine ZUFLAG is used to modify the default values of flags which control various $ZFI^T T_{ER}$ options.

```
CALL ZUFLAG(CHFLAG, IVALUE)
```

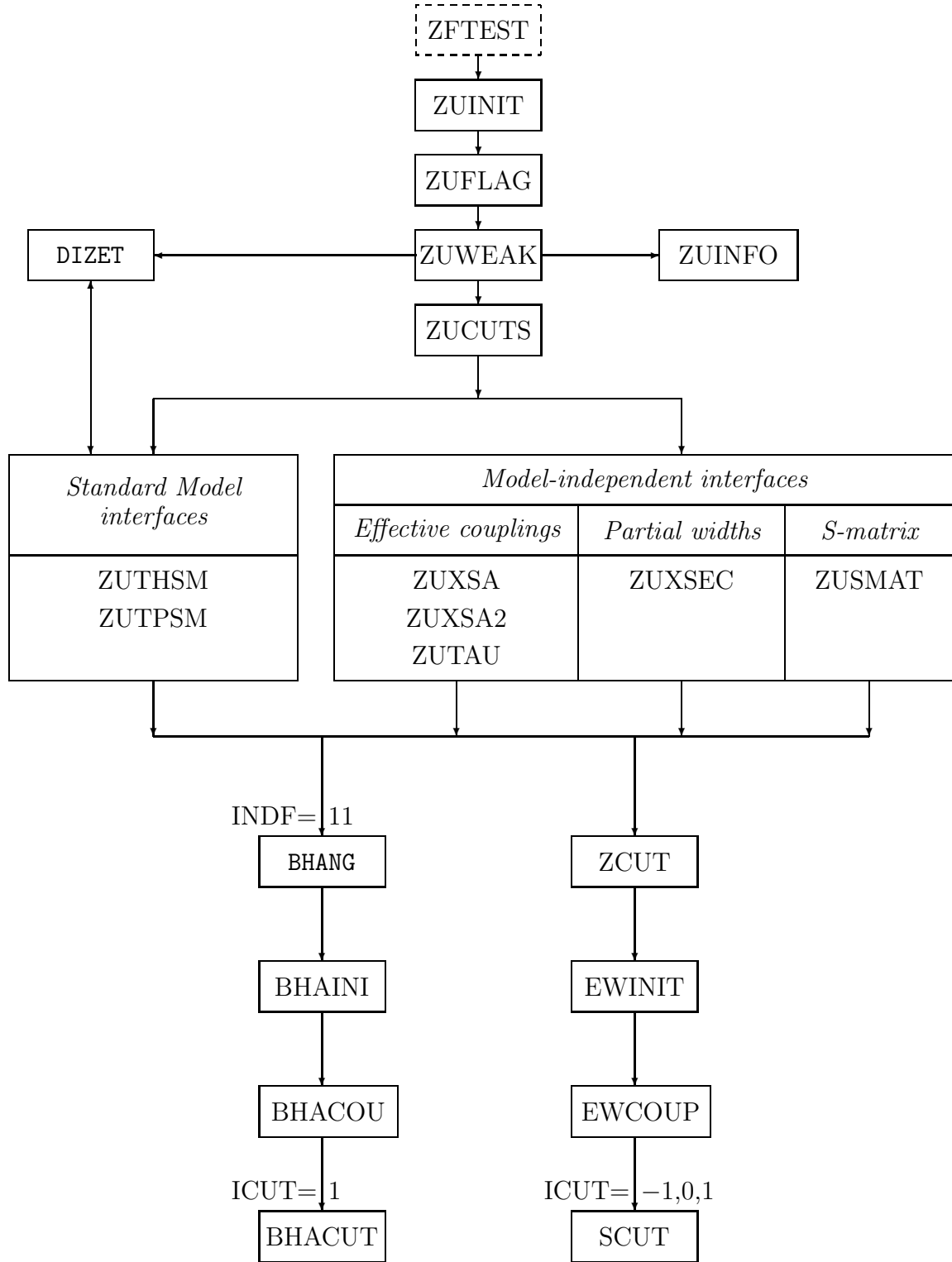



Figure 14: The structure of zF^T_{ER} . $ICUT=-1$ gives observables without any cuts, $ICUT=0,1$ with cuts.

Input Arguments:

CHFLAG is the character identifier of a $ZF^T T_{ER}$ flag (see table 9).

IVALUE is the value of the flag.

CHFLAG	IVALUE		CHFLAG	IVALUE		CHFLAG	IVALUE	
AFBC	1	1	ALPH	0	0	ALST	1	0
AMT4	3	3	BORN	0	0	BOXD	0	1
CONV	0	1	FINR	1	1	FOT2	1	2
GAMS	1	1	INCL	1	0;1	INTF	1	1
PART	0	0	POWR	1	1	PRNT	0	-
QCDC	1	2	QCDC3	1	1	VPOL	3	3
WEAK	1	1						

Table 9: Flag settings for $ZF^T T_{ER}$; the values shown are: in the first column the default, recommended settings optimized for LEP I physics and in the second the ‘best’ settings, recommended for use in a broader energy region.

Possible combinations of CHFLAG and IVALUE are listed below:

CHFLAG=‘AFBC’ Controls the calculation of the forward backward asymmetry for interface ZUTHSM.

IVALUE=0 Asymmetry calculation is inhibited (can speed up the program if asymmetries are not desired).

IVALUE=1 (default) Asymmetry calculation is done.

CHFLAG=‘ALPH’ Controls the calculation of $\alpha_s(q^2, \Lambda_{\overline{MS}})$ for R_{QCD} (3.25, 3.79)-(3.83) and for the $\mathcal{O}(\alpha\alpha_s)$ corrections (section 3.4); see also flag ALST.

IVALUE=0 (default) ALPHA4 is used to calculate α_s , where $\Lambda_{\overline{MS}}$ is calculated according to table 6; user input is defined by ALST.

IVALUE=1 ALPHA5 relies on 5 quark flavors and is used to calculate α_s .

CHFLAG=‘ALST’ Determines how the strong coupling constant α_s runs as a function of s in R_{QCD} , (3.25). Form factor corrections $\mathcal{O}(\alpha\alpha_s)$ are calculated corresponding to ALST=0. ALFAS is input by the user in calls to ZUWEAK, ZUTHSM and ZUTPSM.

IVALUE=0 Calculation of $\alpha_s = \text{ALPHAn}(q^2, \Lambda_{\overline{MS}})$ corresponding to (3.81) with $q^2 = M_Z^2$ for the Z width and with $q^2 = s$ for the cross sections. Where n is determined according to the flag ALPH. For $n = 4$, $\Lambda_{\overline{MS}}$ is calculated from the input $\Lambda_{\overline{MS}}^{(4)} = \text{ALFAS}$, while for $n = 5$, $\Lambda_{\overline{MS}} \equiv \Lambda_{\overline{MS}}^{(5)} = \text{ALFAS}$.

IVALUE=1 (default) In R_{QCD} , the strong coupling constant runs as follows: $\alpha_s(q^2) = \alpha_s(M_Z^2) [\text{ALPHAn}(q^2, \Lambda_{\overline{MS}}^{(n)}) / \text{ALPHAn}(M_Z^2, \Lambda_{\overline{MS}}^{(n)})]$, with $\alpha_s(M_Z^2) = \text{ALFAS}$. Here, $\Lambda_{\overline{MS}}^{(n)}$ is fixed at 185 MeV for $n = 4$ and at 122 MeV for $n = 5$.

CHFLAG='AMT4' Controls calculation of leading $\mathcal{O}(\alpha^2 m_t^4)$ terms for Δr and the weak form factors as discussed in section 3.4 ¹⁸.

IVALUE=0 No resummation. $\Delta r, \rho, \kappa$ as introduced in sections 3.1, 3.2, 3.3 are calculated to order $\mathcal{O}(\alpha)$, with possible inclusion of the $\mathcal{O}(\alpha\alpha_s)$ corrections depending on another flag;

IVALUE=1 Leading $\mathcal{O}(\alpha^2 m_t^4)$ corrections are included in $\Delta\rho$ and $\bar{\delta}\rho$, (3.71), (3.73), while the $\mathcal{O}(\alpha\alpha_s)$ terms and X_0, X are neglected there. The latter remain in the remainder part of the form factors;

IVALUE=2 Common resummation of leading $\mathcal{O}(\alpha^2 m_t^4)$ and $\mathcal{O}(\alpha\alpha_s)$ terms; only the X_0, X are neglected;

IVALUE=3 (default) Resummation as described in [52, 18, 20]; $\Delta\rho$ and $\bar{\delta}\rho$ as defined in (3.71), (3.73).

CHFLAG='BORN' Controls calculation of QED and Born observables.

IVALUE=0 (default) QED convoluted observables.

IVALUE=1 Non-convoluted 'effective' Born observables.

CHFLAG='BOXD' Determines if the ZZ and WW box contributions (see fig. 10) are calculated.

IVALUE=0 (default) No box contributions are calculated.

IVALUE=1 ZZ and WW box diagrams are calculated.

CHFLAG='CONV' Controls the energy scale of running α .

IVALUE=0 (default) For WEAK=1, α is calculated at the energy scale s and for WEAK=0 it is not running at all.

IVALUE=1 α is calculated at the energy scale s' and convoluted.

CHFLAG='FINR' Controls the calculation of final-state radiation.

IVALUE=0 Final-state radiation is included as in (1.11).

IVALUE=1 (default) Include complete treatment of final-state radiation with common soft-photon exponentiation as in (1.10), (2.1).

CHFLAG='FOT2' Controls second-order leading log and next-to-leading log QED corrections.

IVALUE=0 Second-order QED corrections are not included.

IVALUE=1 (default) Second-order QED corrections are included as described in [21, 26]; constant terms $\mathcal{O}(\alpha^2)$ omitted.

IVALUE=2 Second-order QED corrections are included as described in [21, 26].

CHFLAG='GAMS' Controls the s dependence of \mathcal{G}_Z , the Z -width function, introduced in (3.3).

IVALUE=0 Forces \mathcal{G}_Z to be constant. Propagator definition (3.9) is used.

¹⁸ To reproduce results presented in [31], one has to choose AMT4=-1 together with VPOL=2. This combination of flags gives a reasonable result only at LEP I energies.

IVALUE=1 (default) Allows \mathcal{G}_Z to vary as a function of s as in (3.6)-(3.8).

CHFLAG='INCL' Influences the treatment of final-state bremsstrahlung *exclusively* for quarks and hadrons.

IVALUE=0 Same as FINR=1.

IVALUE=1 (default) For quarks and hadrons, final-state bremsstrahlung is treated as with FINR=INTF=0.

CHFLAG='INTF' Determines if the $\mathcal{O}(\alpha)$ initial-final state QED interference terms are calculated. These terms are very small near the Z peak; however, they can become significant if severe kinematic cuts are applied.

IVALUE=0 The interference term is ignored.

IVALUE=1 (default) The interference term is included.

CHFLAG='PART' Controls the calculation of various parts of Bhabha scattering.

IVALUE=0 (default) Calculation of full Bhabha cross section and asymmetry.

IVALUE=1 Only s channel.

IVALUE=2 Only t channel.

IVALUE=3 Only s-t interference.

CHFLAG='PRNT' Controls ZUWEAK printing.

IVALUE=0 (default) Printing by subroutine ZUWEAK is suppressed.

IVALUE=1 Each call to ZUWEAK produces some output.

CHFLAG='POWR' Controls inclusion of final-state masses in kinematical factors.

IVALUE=0 Lepton and light-quark masses are set to zero in (3.17), (3.22), (3.55), (3.52), (4.4); $m_c = 1.5, m_b = 4.5$ GeV.

IVALUE=1 (default) Lepton and light-quark masses as taken in the calculation of vacuum polarization. In combination with VPOL=1: $m_u = .062, m_d = .083, m_s = .215$ GeV, and with VPOL=2,3: $m_u = .04145, m_d = .04146, m_s = .15$ GeV.

CHFLAG='QCDC' Controls how $\mathcal{O}(\alpha\alpha_s)$ corrections related to the t-quark mass are treated within weak form factors. The leading $\mathcal{O}(\alpha\alpha_s m_t^2)$ term of this QCD correction is explicitly given in (3.73).

IVALUE=0 $\mathcal{O}(\alpha\alpha_s)$ corrections to weak form factors are not calculated. This setting must be used for numerical comparisons with the tables shown in [31, 11, 20].

IVALUE=1 (default) They are included and determined with a fast approximate calculation as described in [51]. It should be noted that this approximation is only valid for $s < m_t^2$.

IVALUE=2 Same as 1 except that exact calculations of the Feynman diagrams are performed as in [51]¹⁹. No restriction on s .

¹⁹ An alternative calculation [68] agrees numerically to 12 digits.

CHFLAG='QCD3' Controls the inclusion of the $\mathcal{O}(\alpha_s^3)$ in (3.79), (3.80).

IVALUE=0 (default) This term is not included.

IVALUE=1 The calculation is made to $\mathcal{O}(\alpha_s^3)$.

CHFLAG='WEAK' Determines if weak loop calculations are to be performed.

IVALUE=0 No weak loop corrections to the cross sections are calculated and weak parameters are forced to their Born values, i.e. $\rho_{ef} = \kappa_{e,f,ef} = 1$.

IVALUE=1 (default) Weak loop corrections to the cross sections are calculated.

CHFLAG='VPOL' Controls, which parametrization of the hadronic vacuum polarization contribution α_{had} to the photon propagator (3.33) is used. Three different parametrizations are available.

IVALUE=1 Selects a parametrization taken from [69, 61].

IVALUE=2 Quarks are treated like leptons and their effective masses are as in the second set quoted in the description of the flag POWR. This choice was used to obtain the results presented in [31]²⁰.

IVALUE=3 (default) Selects a parametrization that uses the hadronic vacuum polarization calculations described in [70].

6.3 Subroutine ZUWEAK

Subroutine ZUWEAK is used to perform the weak sector calculations. These are done internally with DIZET [10]. The routine calculates a number of important electroweak parameters (i.e. $\sin^2 \theta_W$, the partial Z widths, fermionic vacuum polarization, F_A , and weak form factors for the cross section), which are stored in common blocks for later use (see appendix A). If any $ZF^T T_{ER}$ flags are to be modified this must be done before calling ZUWEAK.

```
CALL ZUWEAK(ZMASS, TMASS, HMASS, ALFAS)
```

Input Arguments:

ZMASS is the Z mass (M_Z) in GeV.

TMASS is the top quark mass (m_t) in GeV, [10-400].

HMASS is the Higgs mass (M_H) in GeV, [10-1000].

ALFAS is the value of the strong coupling constant (α_s) at $q^2 = M_Z^2$ (see also flag ALST).

A tremendous saving in computing time can be realized by performing weak sector calculations only once during initialization of the $ZF^T T_{ER}$ package. This is possible because weak parameters are nearly independent of s near the Z peak, e.g. $\sim \ln s/M_Z^2$.

²⁰In addition, the value of the AMT4 flag was set to -1 .

6.4 Subroutine ZUCUTS

Subroutine ZUCUTS is used to define kinematic and geometric cuts for each fermion channel. In terms of the internal structure of $z_F \overline{f} T_{ER}$, this routine is used to select the appropriate QED calculational *chain*.

CALL ZUCUTS(INDF, ICUT, ACOL, EMIN, S_PR, ANGO, ANG1)

Input Arguments:

INDF is the fermion index (see table 10).

INDF	Final-state fermions
0	$\nu\bar{\nu}$
1	e^+e^-
2	$\mu^+\mu^-$
3	$\tau^+\tau^-$
4	$u\bar{u}$
5	$d\bar{d}$
6	$c\bar{c}$
7	$s\bar{s}$
8	$t\bar{t}$
9	$b\bar{b}$
10	hadrons
11	Bhabha

Table 10: Indices used by $z_F \overline{f} T_{ER}$ interface routines to select the final-state fermion pair. Note that INDF=1 returns only s-channel observables, INDF=8 always returns zero, and INDF=10 indicates a sum over all open quark channels.

ICUT controls the kinds of cuts (*chain*) to be used.

- =-1: (default) no cuts at all are to be used (fastest).
- = 0: allows for a cut on the acollinearity of the $f\bar{f}$ pair and the minimum energy of both fermion and antifermion.
- = 1: allows for a cut on the minimum invariant mass of the $f\bar{f}$ pair.

ACOL is the maximum acollinearity angle (ξ^{\max}) of the $f\bar{f}$ pair in degrees (ICUT = 0).

EMIN is the minimum energy (E_f^{\min}) of the fermion and antifermion in GeV (ICUT = 0).

S_PR is minimum allowed invariant $f\bar{f}$ mass (s') in GeV (ICUT = 1). This is related to the maximum photon energy by (2.5), (2.6).

ANGO (default = 0°) is the minimum polar angle (ϑ) in degrees of the final-state antifermion.

ANG1 (default = 180°) is the maximum polar angle (ϑ) in degrees of the final-state antifermion.

6.5 Subroutine ZUINFO

Subroutine ZUINFO prints the values of $ZF I^T T_{ER}$ flags and cuts.

```
CALL ZUINFO(MODE)
```

Input Argument:

MODE controls the printing of $ZF I^T T_{ER}$ flag and cut values.

=0: Prints all flag values.

=1: Prints all cut values.

7 Interface Routines of $ZF I^T T_{ER}$

Each calculational branch of $ZF I^T T_{ER}$ has corresponding interfaces. These interfaces will be described below. For the Standard Model branch the cross section and asymmetry interface is subroutine ZUTHSM, while for the tau polarization it is subroutine ZUTPSM. Subroutines ZUXSA, ZUXSA2 and ZUTAU are interfaces for the effective coupling's branch. The interfaces for the partial widths and S-matrix branches are ZUXSEC and ZUSMAT, respectively.

Note that subroutine ZUWEAK must be called prior to any of the interfaces to be described below. As a consequence, flags used in this subroutine can influence the calculation of cross sections and asymmetries in the interfaces described now.

7.1 Subroutine ZUTHSM

Subroutine ZUTHSM is used to calculate Standard Model cross sections and forward-backward asymmetries as described in section 3.

```
CALL ZUTHSM(INDF, SQRS, ZMASS, TMASS, HMASS, ALFAS, XS*, AFB*)
```

Input Arguments:

INDF is the fermion index (see table 10).

SQRS is the centre-of-mass energy (\sqrt{s}) in GeV.

ZMASS is the Z mass (M_Z) in GeV.

TMASS is the top quark mass (m_t) in GeV, [10-400].

HMASS is the Higgs mass (M_H) in GeV, [10-1000].

ALFAS is the value of the strong coupling constant (α_s) at $q^2 = M_Z^2$ (see also flag ALST).

Output Arguments:²¹

XS is the total cross section (σ_T) in nb.

AFB is the forward-backward asymmetry (A_{FB}).

²¹An asterisk (*) following an argument in a calling sequence is used to denote an output argument.

7.2 Subroutine ZUTPSM

Subroutine ZUTHSM is used to calculate the Standard Model tau polarization and tau polarization asymmetry as described in section 3.

```
CALL ZUTPSM(SQRS,ZMASS,TMASS,HMASS,ALFAS,TAUPOL*,TAUAFB*)
```

Input Arguments:

SQRS is the centre-of-mass energy (\sqrt{s}) in GeV.

ZMASS is the Z mass (M_Z) in GeV.

TMASS is the top quark mass (m_t) in GeV, [40-300].

HMASS is the Higgs mass (M_H) in GeV, [10-1000].

ALFAS is the value of the strong coupling constant (α_s) at $q^2 = M_Z^2$ (see also flag ALST).

Output Arguments:

TAUPOL is the tau polarization (A_{pol}) of (3.67).

TAUAFB is the tau polarization forward-backward asymmetry (A_{FB}^{pol}) as defined in (3.68).

7.3 Subroutine ZUXSA

Subroutine ZUXSA is used to calculate the cross section and asymmetry described in section 4.1 as a function of \sqrt{s} , M_Z , Γ_Z , and the weak couplings (4.8), (4.9), (4.10).

```
CALL ZUXSA(INDF,SQRS,ZMASS,GAMZ,MODE,GVE,XE,GVF,XF,XS*,AFB*)
```

Input Arguments:

INDF is the fermion index (see table 10), (1:9,11).

SQRS is the centre-of-mass energy (\sqrt{s}) in GeV.

ZMASS is the Z mass (M_Z) in GeV.

GAMZ is the total Z width (Γ_Z) in GeV.

MODE determines which weak couplings are used:

=0: XE (XF) is the effective axial-vector coupling (\hat{g}_a) for electrons (final-state fermions).

=1: XE (XF) is the effective weak neutral-current amplitude normalization ($\hat{\rho}$) for electrons (final-state fermions).

GVE is the effective vector coupling for electrons (\hat{g}_v^e).

XE is the effective axial-vector coupling (\hat{g}_a^e) or weak neutral-current amplitude normalization ($\hat{\rho}_e$) for electrons (see **MODE**).

GVF is the effective vector coupling for the final-state fermions (\hat{g}_v^f).

XF is the effective axial-vector coupling (\hat{g}_a^f) or weak neutral-current amplitude normalization ($\hat{\rho}_f$) for the final-state fermions (see **MODE**).

Output Arguments:

XS is the cross section (σ_T) in nb.

AFB is the forward–backward asymmetry (A_{FB}).

7.4 Subroutine ZUXSA2

Subroutine **ZUXSA2** is used to calculate the lepton cross section and asymmetry as a function of \sqrt{s} , M_Z , Γ_Z , and the weak couplings *assuming lepton universality*. This routine is similar to **ZUXSA** except that the couplings are squared.

`CALL ZUXSA2(INDF,SQRS,ZMASS,GAMZ,MODE,GV2,X2,XS*,AFB*)`

Input Arguments:

INDF is the fermion index (see table 10) (1-3,11).

SQRS is the centre-of-mass energy (\sqrt{s}) in GeV.

ZMASS is the Z mass (M_Z) in GeV.

GAMZ is the total Z width (Γ_Z) in GeV.

MODE determines which weak couplings are used:

=0: **X2** is the square of the effective axial-vector coupling (\hat{g}_a^l) for leptons.

=1: **X2** is the square of the effective neutral-current amplitude normalization ($\hat{\rho}_l$) for leptons.

GV2 is the square of the effective vector coupling (\hat{g}_v^l) for leptons.

X2 is the square of the effective axial-vector coupling (\hat{g}_a^l) or neutral-current amplitude normalization ($\hat{\rho}_l$) for leptons (see **MODE**).

Output Arguments:

XS is the cross section (σ_T) in nb.

AFB is the forward–backward asymmetry (A_{FB}).

7.5 Subroutine ZUTAU

Subroutine ZUTAU is used to calculate the τ^+ polarization as a function of \sqrt{s} , M_Z , Γ_Z , and the weak couplings (see discussion in section 4.1).

```
CALL ZUTAU(SQRS,ZMASS,GAMZ,MODE,GVE,XE,GVF,XF,TAUPOL*,TAUAFB*)
```

Input Arguments:

SQRS is the centre-of-mass energy (\sqrt{s}) in GeV.

ZMASS is the Z mass (M_Z) in GeV.

GAMZ is the total Z width (Γ_Z) in GeV.

MODE determines which weak couplings are used:

=0: XE (XF) is the effective axial-vector coupling (\hat{g}_a) for electrons (final-state fermions).

=1: XE (XF) is the effective weak neutral-current amplitude normalization ($\hat{\rho}$) for electrons (final-state fermions).

GVE is the effective vector coupling for electrons (\hat{g}_v^e).

XE is the effective axial-vector coupling (\hat{g}_a^e) or weak neutral-current amplitude normalization ($\hat{\rho}_e$) for electrons (see MODE).

GVF is the effective vector coupling for the final-state fermions (\hat{g}_v^f).

XF is the effective axial-vector coupling (\hat{g}_a^f) or weak neutral-current amplitude normalization ($\hat{\rho}_f$) for the final-state fermions (see MODE).

Output Arguments:

TAUPOL is the tau polarization (λ_τ) defined in (3.67).

TAUAFB is the forward-backward asymmetry for polarized tau's (A_{FB}^{pol}) as defined in (3.68).

7.6 Subroutine ZUXSEC

Subroutine ZUXSEC is used to calculate the cross section as a function of \sqrt{s} , M_Z , Γ_Z , Γ_e and Γ_f as was described in section 4.2.

```
CALL ZUXSEC(INDF,SQRS,ZMASS,GAMZO,GAMEE,GAMFF,XS*)
```

Input Arguments:

INDF is the fermion index (see table 10).

SQRS is the centre-of-mass energy (\sqrt{s}) in GeV.

ZMASS is the Z mass (M_Z) in GeV.

GAMZ0 is the total Z width (Γ_Z) in GeV.

GAMEE is the partial Z decay width (Γ_e) in GeV.

GAMFF is the partial Z decay width (Γ_f) in GeV; if INDF=10, GAMFF= Γ_h .

Output Argument:

XS is the cross section (σ_T) in nb.

7.7 Subroutine ZUSMAT

Subroutine ZUSMAT is used to calculate the cross section from the S-matrix approach (see section 4.3).

```
CALL ZUSMAT(INDF, SQRS, ZMASS, GAMZ, RR, RI, RO, R1, R2, RG, XS*)
```

Input Arguments:

INDF is the fermion index (see table 10), [2,10].

SQRS is the centre-of-mass energy (\sqrt{s}) in GeV.

ZMASS is the Z mass (M_Z) in GeV.

GAMZ is the total Z width (Γ_Z) in GeV.

RR-R2 six parameters in S-matrix approach, (RR, RI, RG, R0, ...) = ($R, I, r_\gamma, r_0, \dots$), introduced in (4.22).

Output Argument:

XS is the cross section (σ_T) in nb.

Note that the default Z mass and width definitions correspond to (3.9) and thus differ from those of the other $ZF^I T_{ER}^I$ interfaces.

8 Comparisons

In this section, we compare the predictions of the Standard Model branch of $ZF^I T_{ER}^I$ with other programs. For this comparison we use the following parameter values, unless explicitly stated otherwise: $M_Z = 91.18$, $m_t = 150$, $M_H = 100$ GeV, and $\alpha_s = 0.12$. The section is broken up into two parts:

1. A comparison of the weak mixing angle (with its various definitions) as well as the partial and total Z widths.
2. A comparison of total cross sections and forward–backward asymmetries.

In the past many comparisons of this sort have been made. In particular an earlier version of $ZF^I T_{ER}^I$, the ZBIZON [71] package, was used in the 1989 Workshop on Z Physics at LEP 1 [31] for numerous comparisons [12, 13, 71]. In addition to these comparisons, others did not explicitly include the ZBIZON code [72]. At that time, the predictions from all of these programs agreed to within 0.5%. Since then, new codes have been developed and the quality of several of the existing programs has been improved; among these is the $ZF^I T_{ER}^I$ package.

8.1 Weak Mixing Angles and Partial Z Widths

Throughout the Standard Model branch of ${}_{ZF}^T T_{ER}$, we use the on-shell definition (3.15) of the weak mixing angle $\sin^2 \theta_W$. For the sake of this comparison, we take into account two additional definitions of the weak mixing angle: the ‘effective’ weak mixing angle, $s_W^{2,\text{eff}}$, introduced in (3.20), and the weak mixing angle of the $\overline{\text{MS}}$ renormalization scheme given below:

$$\sin^2 \theta_W = 1 - \frac{M_W^2}{M_Z^2}, \quad (8.1)$$

$$s_W^{2,\text{eff}} = \kappa_e^Z \sin^2 \theta_W, \quad (8.2)$$

$$\sin^2 \theta_W^{\overline{\text{MS}}} = \left[1 + \frac{\cos^2 \theta_W}{\sin^2 \theta_W} \delta\bar{\rho} \right] \sin^2 \theta_W, \quad (8.3)$$

where $\delta\bar{\rho}$ has been introduced in (3.73). In table 11, we compare predictions from ${}_{ZF}^T T_{ER}$ with those obtained by W. Hollik [17] and G. Degrossi, S. Fanchiotti, A. Sirlin [18].

The agreement of the different calculations for these three cases is impressive. From the table it is apparent that the mixing angles $s_W^{2,\text{eff}}$ and $\sin^2 \theta_W^{\overline{\text{MS}}}$ depend to a lesser extent on the unknown top and Higgs masses than does $\sin^2 \theta_W$. For a detailed discussion of the different approaches see for instance [73, 60, 52, 20, 46, 42].

When using data to determine an effective weak mixing angle, one must be careful, since measurements of mixing angles from different observables may yield results that cannot be directly compared. This delicate point was addressed in sections 3.2 and 4.1 [see also (3.43)-(3.45)] and has been discussed in detail in [43]. It has been demonstrated that a proper formulation of the hard-scattering subprocess and a correct unfolding of the leptonic forward-backward, b-quark forward-backward, and tau polarization asymmetries lead to results which are very close to each other and to the value of $s_W^{2,\text{eff}}$ expected from Γ_e , as defined in (3.20).

In table 12, we compare partial, hadronic and total Z widths with numbers of other authors: as W. Hollik [19] and G. Degrossi, A. Sirlin [20]. Shown in the second and third lines are the digits which differ from ${}_{ZF}^T T_{ER}$ – as one can see the deviations are very small.

m_t	M_H	$\sin^2 \theta_W$	$s_W^{2,\text{eff}}$	$\sin^2 \theta_W^{\overline{\text{MS}}}(M_Z^2)$
100	100	0.23056	0.23362	0.23351
		44	52	7
		62	66	42
	500	0.23266	0.23447	0.23438
		53	37	43
		73	51	29
	1000	0.23371	0.23485	0.23477
		60	77	83
		81	91	0
150	100	0.22483	0.23217	0.23213
		74	07	25
		87	23	0
	500	0.22690	0.23300	0.23299
		81	291	309
		5	6	5
	1000	0.22794	0.23337	0.23337
		88	0	49
		802	45	5
200	100	0.21782	0.23025	0.23024
		78	17	41
		7	35	8
	500	0.21985	0.23106	0.23108
		3	099	24
		91	16	10
	1000	0.22088	0.23142	0.23144
		7	37	63
		96	54	9
250	100	0.20919	0.22786	0.22785
		21	1	808
		25	800	96
	500	0.21118	0.22865	0.22866
		22	0	89
		26	79	76
	1000	0.21217	0.22899	0.22901
		25	7	26
		28	916	13

Table 11: Comparison of $\sin^2 \theta_W$, $s_W^{2,\text{eff}}$ and $\sin^2 \theta_W^{\overline{\text{MS}}}(M_Z^2)$ from $z_F \overline{I} T_{ER}$ (first line), Hollik [17] (second line), and Degrassi, Fanchiotti, Sirlin [18] (third line); with flags AMT4=3, QCDC=0, QCD3=0, $M_Z=91.170$ GeV, m_t and M_H in GeV.

m_t	M_H	Γ_ν	Γ_e	Γ_μ	Γ_τ	Γ_u	Γ_d	Γ_c	Γ_s	Γ_b	Γ_{had}	Γ_{tot}
100	100	166.3	83.42 4 4*	83.42 4	83.23 - -	296.0	382.2 1	295.6 - -	382.2 - -	377.5 6 -	1733.5 - -	2482.4 - -
	500	166.1	83.29 30 3*	83.29 30 -	83.10 - -	295.3 2 2	381.4 2 3	294.8 - -	381.4 - -	376.7 - -	1729.5 - -	2477.5 - -
	1000	166.0	83.22 3 2*	83.22 3 -	83.03 - -	294.8 7 -	380.9 7 8	294.4 - -	380.9 - -	376.2 3 -	1727.3 - -	2474.8 - -
150	100	166.9 7.0	83.81 3 8*	83.81 3 -	83.62 - -	298.0 7.9 7.9	384.4	297.5 - -	384.4 - -	376.5 6 -	1740.8 - -	2492.9 - -
	500	166.8	83.68 9 7*	83.68 9 -	83.49 - -	297.2	383.6 5	296.8 - -	383.6 - -	375.7 8 -	1736.9 - -	2488.0 - -
	1000	166.6 7	83.61 6*	83.61 -	83.42 - -	296.8 7 7	383.1 0	296.4 - -	383.1 - -	375.3 - -	1734.7 - -	2485.3 - -
200	100	167.9 8	84.37 8 4*	84.37 8 -	84.18 - -	300.6 5	387.4	300.2 - -	387.4 - -	375.3 - -	1750.9 - -	2507.4 - -
	500	167.7	84.24 3*	84.24 -	84.04 - -	299.9 8 8	386.6	299.4 - -	386.6 - -	374.5 - -	1747.1 - -	2502.6 - -
	1000	167.6 5	84.16 2*	84.16 -	83.97 - -	299.5 4 4	386.2 1 1	299.0 - -	386.2 - -	374.1 - -	1745.0 - -	2499.9 - -
250	100	169.0 1	85.10 1 1*	85.10 1 -	84.91 - -	304.0 3.8	391.4 3	303.6 - -	391.4 - -	373.7 5 -	1764.0 - -	2526.3 - -
	500	168.9 8	84.96 7 5.0*	84.96 7 -	84.77 - -	303.3 1	390.6 5	302.9 - -	390.6 - -	373.0 2.8 -	1760.2 - -	2521.5 - -
	1000	168.8 7	84.89 9*	84.89 -	84.69 - -	302.9 7 8	390.1	302.5 - -	390.1 - -	372.6 4 -	1758.2 - -	2518.9 - -

Table 12: *Partial and total widths of the Z boson in MeV from $z_F^{\text{IT}} T_{ER}$ (first line), Hollik [19] (second line) and Degraasi, Sirlin [20] (third line). Shown are only the digits which differ, a dash means no entry, an asterisk no digit available. Flags as in table 11, $M_Z=91.170$ GeV, m_t and M_H in GeV.*

8.2 Cross Sections and Asymmetries

In this section the cross sections and asymmetries for processes (1.1) and (1.2) predicted by $_{ZF}i^T T_{ER}$ are compared with those of ZSHAPE 2.0 [21, 74] and of ALIBABA 2.0 [23]. Earlier comparisons of $_{ZF}i^T T_{ER}$ with the Cahn package [75] can be found in [76]; with ALIBABA in [77]; and with ZSHAPE, ALIBABA, and KORALZ 3.8 [78] in [79].

For (1.1), all packages include weak corrections of at least $\mathcal{O}(\alpha)$. In ZSHAPE, QED contributions of $\mathcal{O}(\alpha^2)$ to the initial-state are calculated exactly, while in the other programs a leading-log approximation is used. In addition, all programs include final-state radiation corrections to $\mathcal{O}(\alpha)$ and common exponentiation of initial- and final-state soft-photon emission. Initial-final interference is contained only in ALIBABA and $_{ZF}i^T T_{ER}$. The additional t-channel terms (including s-t interference), which are necessary in order to calculate Bhabha scattering (1.2), are available in both ALIBABA and $_{ZF}i^T T_{ER}$. In the latter, this is done via the BHANG package, which only contains some of the higher-order t-channel QED corrections that have been implemented in ALIBABA. On the other hand, $_{ZF}i^T T_{ER}$ contains higher-order weak and QCD corrections as explained in section 3.4, which are not available in the other two packages. As can be seen in more detail from the references, the three codes allow for different applications of kinematic cuts due to their different theoretical basis.

Since the other two programs (ALIBABA and ZSHAPE) perform only Standard Model calculations, we have restricted these comparisons to the corresponding branch of $_{ZF}i^T T_{ER}$. In this context, we have used the ‘recommended’ $_{ZF}i^T T_{ER}$ flags of table 9. In addition, we perform comparisons using flag settings shown in table 13, which have been chosen such that the corrections realized in $_{ZF}i^T T_{ER}$ most closely resemble that of the other programs.

CHFLAG	IVALUE		CHFLAG	IVALUE		CHFLAG	IVALUE	
AFBC	1	1	ALPH	1	1	ALST	1	1
AMT4	0	0	BORN	0	0	BOXD	0	1
CONV	1	1	FINR	1	1	FOT2	2	2
GAMS	1	1	INCL	0	0	INTF	0	1
PART	0	0	POWR	0	0	PRNT	-	-
QCDC	0	0	QCD3	0	0	VPOL	2	2
WEAK	1	1						

Table 13: *Flag settings in $_{ZF}i^T T_{ER}$ for comparisons of cross sections and asymmetries; the values shown are: first column - best agreement with ZSHAPE, second column - best agreement with ALIBABA.*

We performed three series of comparisons:

- I. A comparison of the total $_{ZF}i^T T_{ER}$ and ZSHAPE cross sections with an s' cut and no angular acceptance cut.
- II. Comparisons of $_{ZF}i^T T_{ER}$ and ALIBABA muon pair production cross section and forward-backward asymmetry with E_f^{\min} , ξ^{\max} and angular acceptance cuts.
- III. As above, except that here the comparison is done for Bhabha scattering.

For case I, we have compared quark and muon cross sections over a large energy range, [10-100] GeV. Due to ZSHAPE limitations, only cross-section comparisons up to LEP I energies can be performed. In fig. 15, we show the ratio of hadron and muon cross sections as a function of the centre-of-mass energy for different values of s' . As can be seen in the figure, the agreement at LEP I energies is excellent even though some higher-order weak corrections are not realized in ZSHAPE²². As the energy decreases from LEP I, deviations begin to appear, which reach 2% in magnitude for the hadronic cross section. For muons, the deviation goes to 1% when s' is at the kinematic limit and 0.5% otherwise, approaching in the latter case nearly exact agreement at small energies where pure QED dominates.

A considerable improvement in the agreement of these two programs can be realized through a judicious choice of ${}_{ZF}I^T T_{ER}$ flags (see table 13). If various enhancements to ${}_{ZF}I^T T_{ER}$, which have been realized since the 1989 workshop, are inhibited, then a dramatic improvement in the agreement of the two programs is observed. These enhancements are mainly concerned with QCD corrections, higher order weak corrections and the handling of light-quark thresholds. As can be seen from fig. 16, the disagreement shrinks to 0.1% for both muon and hadron production cross sections and for different cuts.

In case II, we compare the predictions of ${}_{ZF}I^T T_{ER}$ with ALIBABA for the muon production cross section and forward-backward asymmetry with cuts on minimum fermion energy (E_f^{\min}) and acollinearity (ξ^{\max}). We restrict this comparison to muons since ALIBABA has no hadron option. In figs. 17 and 18, we contrast the predictions for these programs using the ‘recommended’ ${}_{ZF}I^T T_{ER}$ flags and another set of flags (table 13) chosen to minimize the differences in the calculations performed by these programs. The differences in the predictions, for the value of m_t chosen, is minor in both cases. For the ‘recommended’ flags, over the large energy interval covered in fig. 17, the cross sections agree to within 0.7%; at LEP I energies the agreement is good to within 0.2%. For the asymmetry, the difference of the two predictions is smaller than 0.2% over the full energy range and well within 0.1% at LEP I energies.

For case III, we compare in fig. 19 the cross-section ratio and forward-backward asymmetry for Bhabha scattering for ${}_{ZF}I^T T_{ER}$ (via BHANG) and ALIBABA with the same cuts as described above for case II. Since BHANG contains several approximations adapted to applications at LEP I, we restrict the energy range of the comparison correspondingly. As may be seen from the figure, the programs agree to within 1.5% for the cross-section ratio and within 1% for the asymmetry difference.

²² Very recently, a new version of ZSHAPE was developed, which now also contains higher-order electroweak corrections connected with the t quark. The agreement of the program with ${}_{ZF}I^T T_{ER}$, with the corresponding flag settings, is not worse than shown here [80].

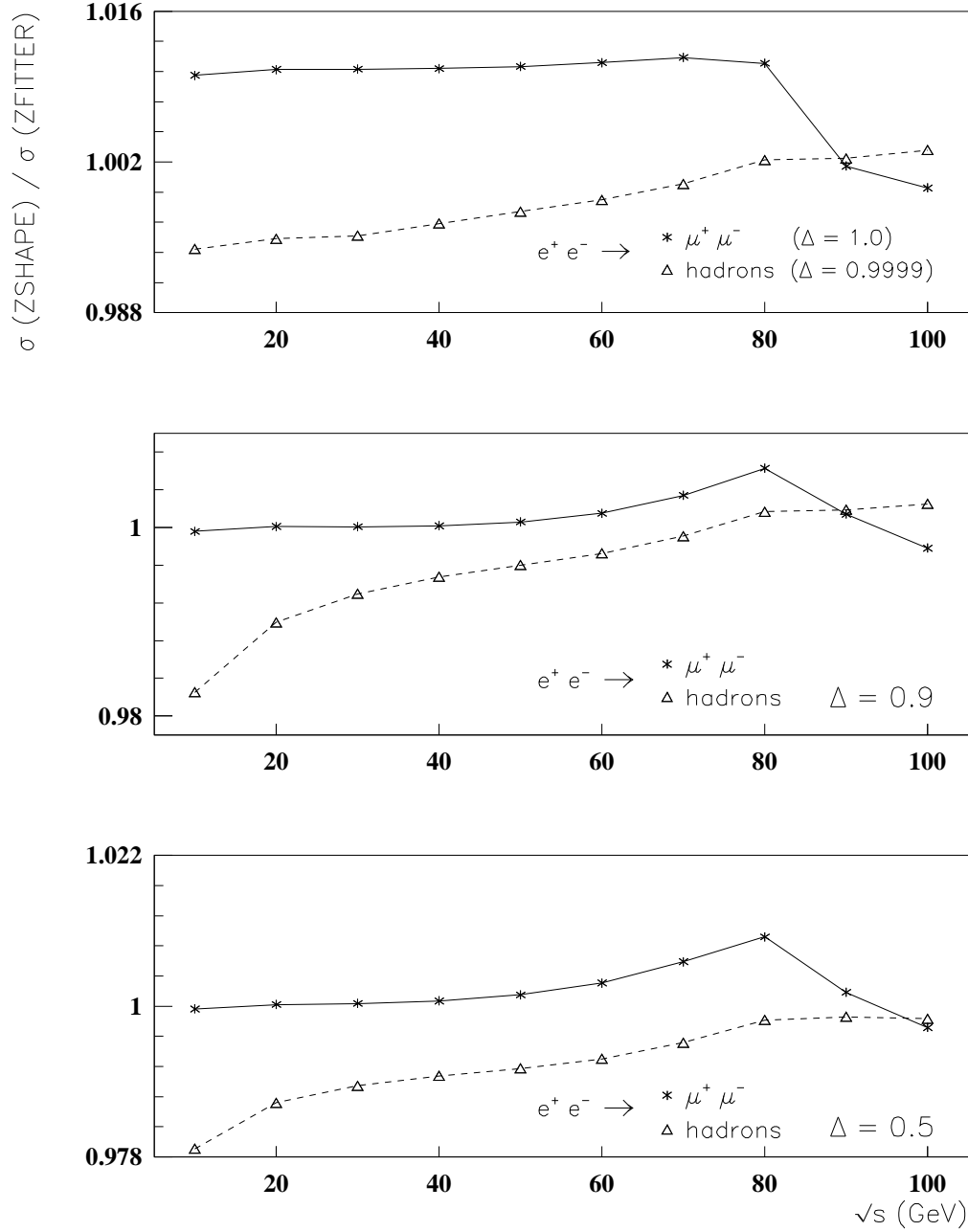


Figure 15: Ratio of cross section predictions from ZFITTER and ZSHAPE for muon and hadron production, as a function of the centre-of-mass energy, for three different values of $\Delta = 1 - s'_{\min}/s$; both programs with their ‘recommended’ choice of flags.

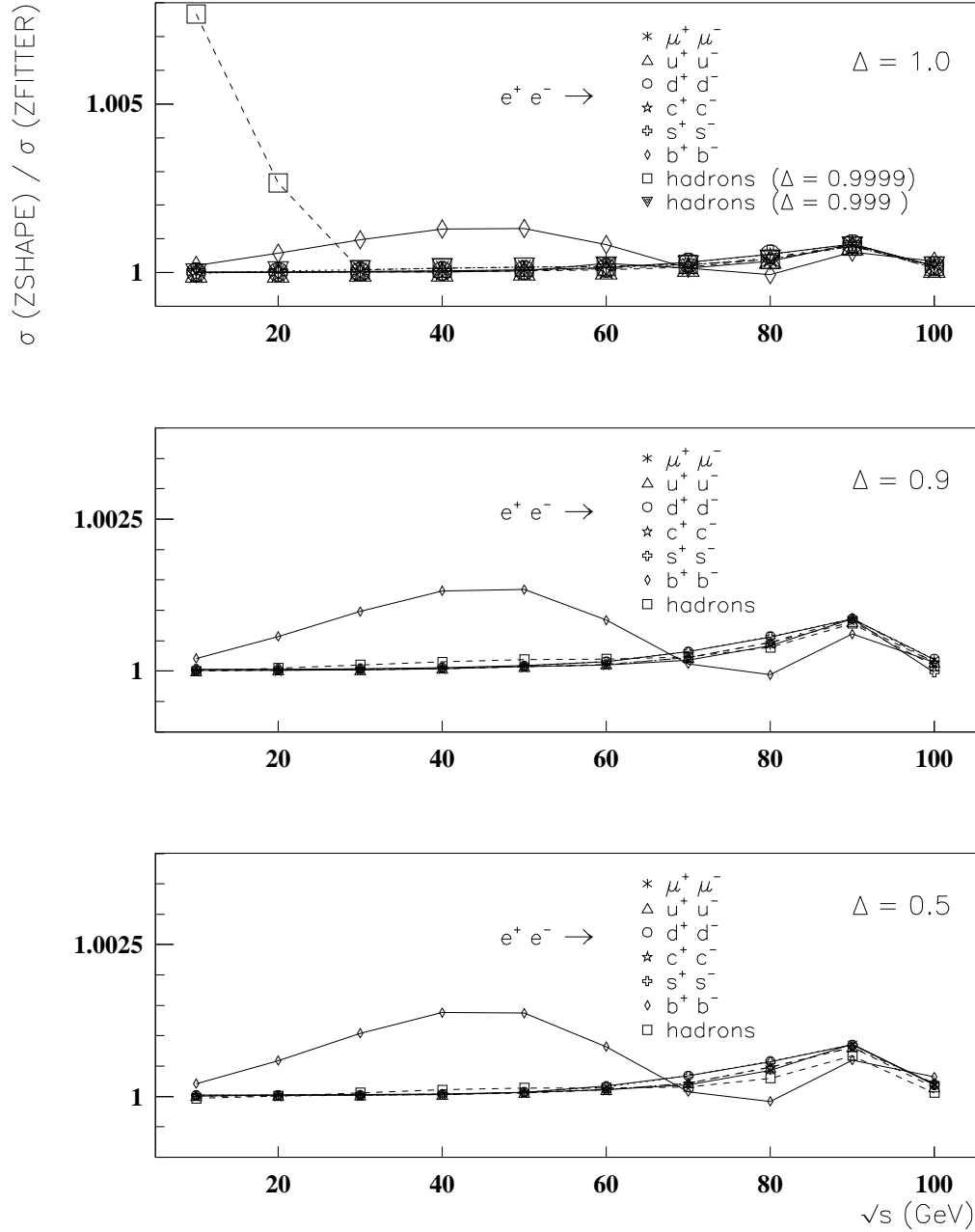


Figure 16: Ratio of cross-section predictions from $ZFITTER$ and ZSHAPE for muon and quark production, as a function of the centre-of-mass energy, as in fig. 15, but here flags are chosen such that the theoretical assumptions of both programs are as similar as possible.

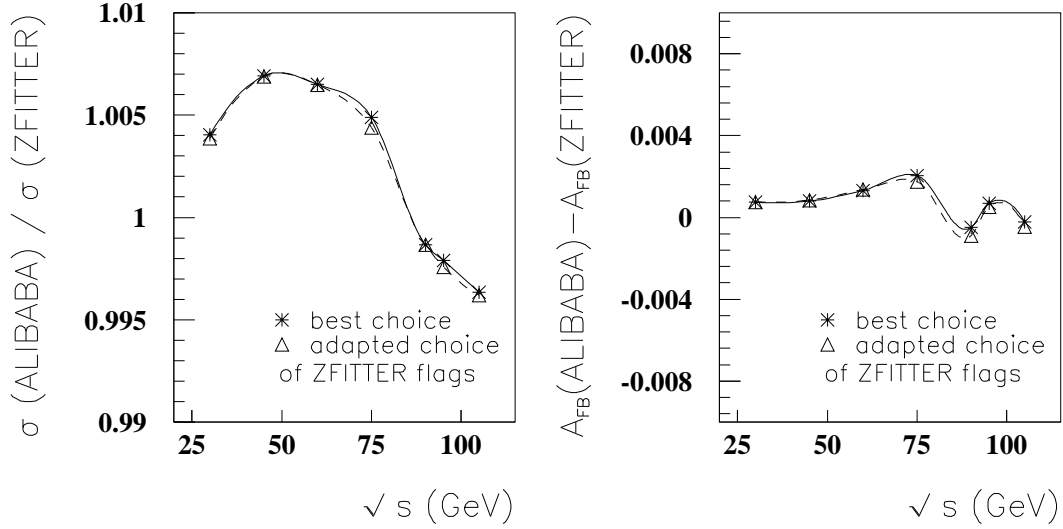


Figure 17: Ratio of cross sections, σ^μ , and difference of forward-backward asymmetries, A_{FB}^μ , as predicted by $\text{ZFITTER}_{\text{ER}}$ and ALIBABA, as a function of the centre-of-mass energy. An acceptance cut of $44^\circ \leq \vartheta \leq 136^\circ$, an acollinearity cut of $\xi \leq 25^\circ$ and a muon energy cut of $E_f^{\text{min}} = 5$ GeV have been employed. The comparison is made for both the ‘recommended’ $\text{ZFITTER}_{\text{ER}}$ flag values and those listed in table 13.

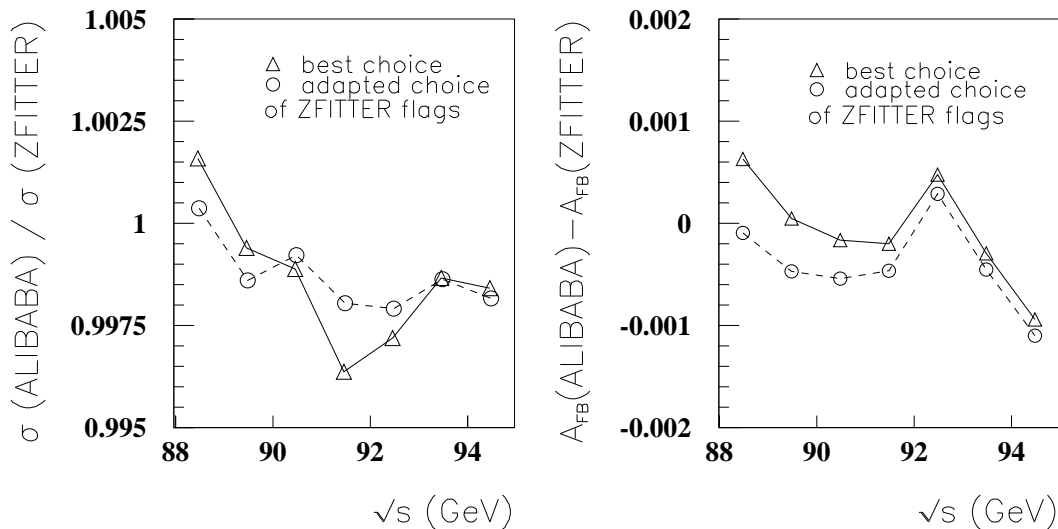


Figure 18: Same as in fig. 17, for LEP I energies explicitly.

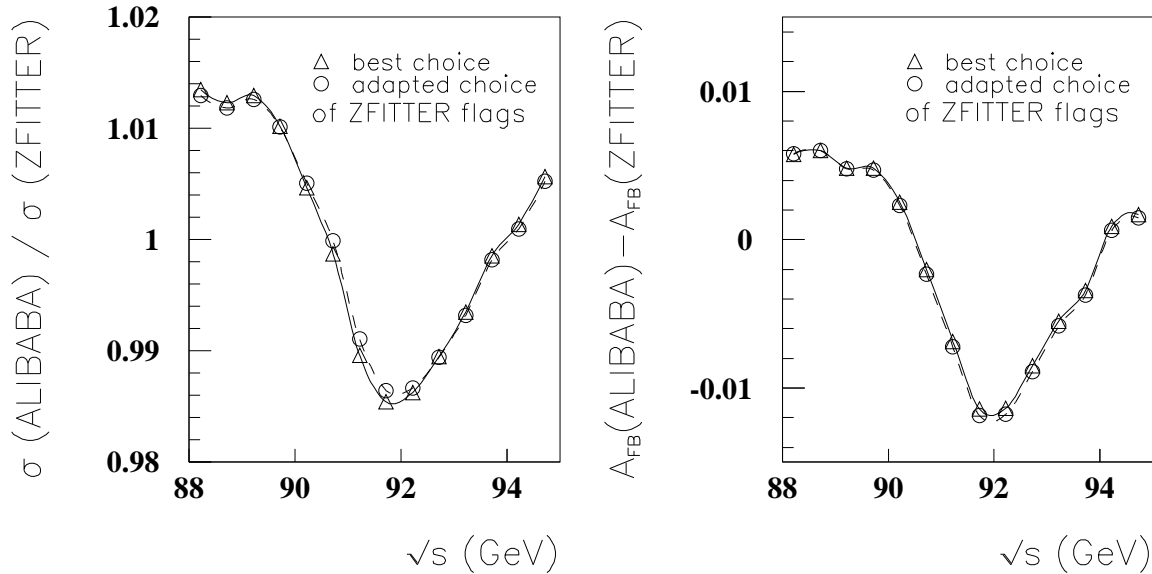


Figure 19: *Same as in fig. 17, for Bhabha scattering at LEP I energies.*

8.3 Conclusions

There exists a wealth of programs, of the semi-analytical and Monte Carlo variety, which can make predictions for the fermion pair production process in e^+e^- collisions. The programs are varied in both their theoretical accuracy (i.e. the order to which the calculations are performed) and in the cuts that one may apply. $ZFITTER$ is a semi-analytic program with large inherent flexibility in both these respects. With a judicious selection of $ZFITTER$ flags, agreement with other programs to the level of 0.5% and better have been reached with the exception of Bhabha scattering where the agreement is slightly worse.

Acknowledgements

We thank S. Kirsch for providing us with the $ZFITTER$ logo. We are grateful to R. Barbieri, P. Ch. Christova, D. Haidt, W. Hollik, B. Kniehl, L. Maiani, K. Mazumdar for fruitful discussions and hints. For allowing us to use unpublished programs, thanks to W. Hollik.

Note added in proof:

Recently, a new package has been published, which allows to calculate the one-loop electroweak radiative corrections to two-fermion production near the Z resonance [81]. The test run output for the unpolarized muon production cross section shown in Sample 2 (p. 62 of [81]) reproduces the effective Born approximation of $ZFITTER$ within 0.01% at the resonance, and within 0.02% in the full energy range covered by Sample 2. The corresponding b-quark production cross section shown in Sample 3 does not agree with the $ZFITTER$ results.

References

- [1] S.L. Glashow, *Nucl. Phys.* **22** (1961) 579;
S. Weinberg, *Phys. Rev. Letters* **19** (1967) 1264;
A. Salam, in: "Elementary Particle Theory", ed. N. Svartholm (Almqvist and Wiksell, Stockholm, 1968), p. 367.
- [2] D. Bardin, M. Bilenky, A. Chizhov, A. Olshevsky, S. Riemann, T. Riemann, M. Sachwitz, A. Sazonov, Yu. Sedykh and I. Sheer,
Fortran code $ZF^T T_{ER}$ version 4.5 (19 April 1992).
- [3] D. Bardin, O. Fedorenko and T. Riemann, JINR Dubna prepr. E2-87-663 (1987);
D. Bardin, M. Bilenky, A. Chizhov, O. Fedorenko, T. Riemann, M. Sachwitz and A. Sazonov,
Analytic approach to the complete set of QED corrections to fermion pair production in e^+e^- annihilation,
Nucl. Phys. **B351** (1991) 1.
- [4] D. Bardin, M. Bilenky, T. Riemann, M. Sachwitz, A. Sazonov and Yu. Sedykh,
QED corrections with partial angular integration to fermion pair production in e^+e^- annihilation,
Phys. Letters **B255** (1991) 290.
- [5] M. Bilenky and A. Sazonov,
QED corrections at Z^0 -pole with realistic kinematical cuts,
JINR Dubna prepr. E2-89-792 (1989).
- [6] M. Bilenky,
Fortran package BHANG, version 2.00 (May 23, 1991),
publication in preparation.
- [7] A. Akhundov, D. Bardin and T. Riemann,
Electroweak one loop corrections to the decay of the neutral vector boson,
Nucl. Phys. **B276** (1986) 1.
- [8] D. Bardin, S. Riemann and T. Riemann,
Electroweak one loop corrections to the decay of the charged vector boson,
Z. Physik **C32** (1986) 121.
- [9] D. Bardin, M. Bilenky, G. Mitselmakher, T. Riemann and M. Sachwitz,
A realistic approach to the standard Z peak,
Z. Physik **C44** (1989) 493.
- [10] A. Akhundov, D. Bardin, M. Bilenky, P. Christova, S. Riemann, T. Riemann, M. Sachwitz and H. Vogt,
Fortran code DIZET version 4.04 (21 Aug 1991);
Version 2.0 (July 1989) was described in: D. Bardin et al., *Comput. Phys. Commun.* **59** (1990) 303.

- [11] D. Bardin, W. Hollik and T. Riemann,
Bhabha scattering with higher-order weak loop corrections,
Z. Physik **C49** (1991) 485.
- [12] F. Berends et al.,
 Z line shape,
in [31], vol. 1, p. 89.
- [13] M. Böhm, W. Hollik et al.,
Forward-backward asymmetries,
in [31], vol. 1, p. 203.
- [14] A. Leike, T. Riemann and J. Rose,
S-matrix approach to the Z line shape,
Phys. Letters **B273** (1991) 513.
- [15] A. Leike, S. Riemann and T. Riemann,
 ZZ' mixing in presence of standard weak loops,
Munich Univ. prepr. LMU-91/06 (Dec 1991) and ZEFIT - a package to be used with
 $_{ZF}I_{ER}^T$.
- [16] The LEP Collaborations: ALEPH, DELPHI, L3 and OPAL,
Electroweak Parameters of the Z Resonance and the Standard Model, *Phys. Letters* **B276**
(1992) 247;
DELPHI Collaboration,
P. Aarnio et al., *Phys. Letters* **B241** (1990) 425; *Phys. Letters* **B260** (1991) 240; prepr.
CERN-PPE/90-119, Contrib. to the Int. HEP Conf., Singapore, Aug 1990; *Nucl. Phys.*
B367 511; prepr. CERN-PPE/91-211 (1991), subm. to *Phys. Letters* **B**;
L3 Collaboration,
B. Adeva et al., *Phys. Letters* **B236** (1990) 109; *Phys. Letters* **B237** (1990) 136; *Phys.*
Letters **B238** (1990) 122; *Phys. Letters* **B247** (1990) 473; *Phys. Letters* **B249** (1990) 341;
Phys. Letters **B250** (1990) 183; *Z. Physik* **C51** (1991) 179;
OPAL Collaboration,
M. Akrawy et al., *Phys. Letters* **B263** (1991) 311;
G. Alexander et al., *Z. Physik* **C52** (1991) 175;
P. Acton et al., *Phys. Letters* **B276** (1992) 379.
- [17] W. Hollik, Fortran package DELTAR, based on [41]; for calculations in the minimal sub-
traction scheme, see also prepr. MPI-Ph/92-116 (1992).
- [18] G. Degrossi, S. Fanchiotti and A. Sirlin, *Nucl. Phys.* **B351** (1991) 49.
- [19] W. Hollik, Fortran package WIDTHS, based on [41].
- [20] G. Degrossi and A. Sirlin, *Nucl. Phys.* **B352** (1991) 342.
- [21] F.A. Berends, G.J.H. Burgers and W.L. van Neerven, *Nucl. Phys.* **B297** (1988) 429; *E:*
Nucl. Phys **B304** (1988) 921.

- [22] W. Beenakker and W. Hollik, in: *Proc. ECFA workshop on LEP 200*, CERN 87-08 (1987), p. 185;
W. Beenakker, thesis, University of Leiden, October 1989.
- [23] W. Beenakker, F.A. Berends and S.C. van der Marck, *Nucl. Phys.* **B349** (1991) 323.
- [24] T. Riemann and Z. Wąs, *Mod. Phys. Letters* **A4** (1989) 2487.
- [25] D. Bardin et al., *Phys. Letters* **B229** (1989) 405.
- [26] W. Beenakker, F.A. Berends and W.L. van Neerven, Applications of Renormalization Group Methods to Radiative Corrections, in: *Proc. Int. Workshop on Radiative Corrections for e^+e^- Collisions*, Schloß Ringberg, Tegernsee, FRG, April 1989, ed. J.H. Kühn (Springer, Berlin, 1989), p. 3.
- [27] G. Bonneau and F. Martin, *Nucl. Phys.* **B27** (1971) 381.
- [28] M. Greco, G. Pancherivi and Y. Srivastava, *Nucl. Phys.* **B101** (1975) 11; *ibid*, **B171** (1980) 118; *E: Nucl. Phys.* **B197** (1982) 543.
- [29] S. Jadach and B.F.L. Ward, *Phys. Rev.* **D40** (1989) 3582.
- [30] M. Caffo and E. Remiddi, Bhabha scattering, in [31], vol. 1, p.171.
- [31] G. Altarelli, R. Kleiss and C. Verzegnassi (eds.), *Z Physics at LEP 1*, CERN 89-08 (Sept. 1989).
- [32] D. Bardin, A. Leike, T. Riemann and M. Sachwitz, *Phys. Letters* **206B** (1988) 539.
- [33] G. Burgers, contrib. to the LEP Physics Workshop 1987, unpublished.
- [34] S. Willenbrock and G. Valencia, *Phys. Letters* **B259** (1991) 373;
- [35] R. Stuart, *Phys. Letters* **B262** (1991) 113; and **B272** (1991) 353; prepr. CERN-TH.6261/91 (1991).
- [36] G.J. Gounaris and J.J. Sakurai, *Phys. Rev. Letters* **21** (1968) 244.
- [37] A. Sirlin, *Phys. Letters* **B267** (1991) 240; *Phys. Rev.* **D67** (1991) 2127.
- [38] B.F.L. Ward, Trieste prepr. IC/91/161 (1991).
- [39] D. Bardin, P. Christova and O. Fedorenko, *Nucl. Phys.* **B197** (1982) 1.
- [40] D. Bardin and B. Kniehl, private communication (1991).
- [41] W. Hollik, *Fortschr. Physik* **38** (1990) 165.
- [42] W. Hollik et al., Electroweak parameters: Theoretical aspects, contrib. to the *Workshop on physics at HERA*, DESY, Hamburg, Sept. 1991, prepr. MPI-Ph/92-30 (1992) (to appear in the proceedings).
- [43] S. N. Ganguli, TIFR/EHEP 91-15 and L3-note #1042 (Oct. 1991).

- [44] G. Mann and T. Riemann, *Annalen d. Physik* **40** (1983) 334.
- [45] W. Beenakker and W. Hollik, *Z. Physik* **C40** (1988) 141.
- [46] J. Bernabéu, A. Pich and A. Santamaria, *Phys. Letters* **B200** (1988) 569; *Nucl. Phys.* **B363** (1991) 326.
- [47] A. Djouadi, G. Girardi, W. Hollik, F. Renard and C. Verzegnassi, in: *Report of the working group on high luminosities at LEP*, eds. E. Blucher et al., CERN 91-02 (1991), p. 135.
- [48] T. Riemann and M. Sachwitz, in: *Proc. Int. Topical Meeting on Physics of e^+e^- Interactions at Lep Energies*, ed. D. Bardin (Dubna, 1987), p. 101; see also: Zeuthen prepr. PHE 87-12 (1987).
- [49] M. Consoli, W. Hollik and F. Jegerlehner, *Phys. Letters* **B227** (1989) 167;
 J. van der Bij and F. Hoogeveen, *Nucl. Phys.* **B283** (1987) 477;.
 M. Consoli, W. Hollik and F. Jegerlehner, in: [31], vol. 1, p. 7;
 W. Hollik, Lectures at the CERN-JINR School of Physics 1989, Egmond-aan-Zee, Netherlands, in: CERN 91-07 (1991).
- [50] A. Djouadi and C. Verzegnassi, *Phys. Lett.* **B195** (1987) 265;
 A. Djouadi, *Nuovo Cim.* **A100** (1988) 357.
- [51] D. Bardin and A. Chizhov, in: *Proc. Int. Topical Meeting on Physics of e^+e^- Interactions at LEP Energies*, ed. D. Bardin (Dubna, 1988), JINR Dubna E2-89-525 (1989), p. 42.
- [52] S. Fanchiotti and A. Sirlin, prepr. NYU-TH-91-02-04 (1991), in: *M.A.B. Beg Memorial Volume*, eds. A. Ali et al. (World Scientific, Singapore, 1991), p. 58.
- [53] S. Gorishny, A. Kataev and S. Larin, *Phys. Letters* **B259** (1991) 144.
- [54] B. Kniehl and J. Kühn, *Nucl. Phys.* **B329** (1990) 547; in $ZF^T T_{ER}$ the coding of E. Lange is used.
- [55] W. J. Marciano, *Phys. Rev.* **D29** (1984) 580.
- [56] Subroutines ALPHA4, ALPHA5 are based on [55, 57]; a coding by B. Kniehl is used.
- [57] A. D. Martin, R. G. Roberts and W. J. Stirling, *Phys. Rev.* **D43** (1991) 3648.
- [58] A. Borrelli, L. Maiani, M. Consoli and R. Sisto, *Nucl. Phys.* **B333** (1990) 357.
- [59] A. Martin, *Phys. Letters* **B156** (1985) 411.
- [60] G. Burgers and F. Jegerlehner, Δr , or the relation between the electroweak couplings and the weak vector boson masses, in: [31], vol. 1, p. 55.
- [61] F. Jegerlehner, Physics of precision experiments with Zs, in: *Prog. Part. Nucl. Phys.*, vol. 27, p. 1, ed. A. Faessler (Pergamon Press, Oxford, U.K., 1991).
- [62] P. Langacker, M. Luo and A. K. Mann, *Rev. Mod. Phys.* **64** (1992) 87.

- [63] A. De Rújula, M.B. Gavela, P. Hernandez and E. Masso, prepr. CERN-TH.6272/91 (1991).
- [64] J. Ellis, *Status of the electroweak interaction*, talk at LP-HEP '91 Conference, Geneva, 25 July–1 August 1991, prepr. CERN-TH.6193/91 (1991), to appear in the proceedings.
- [65] G. Altarelli, R. Barbieri and S. Jadach, *Nucl. Phys.* **B369** (1992) 3;
 G. Altarelli, *Limits on new physics from precision electroweak data*, talk at LP-HEP '91 Conference, Geneva, 25 July–1 August 1991, prepr. CERN-TH.6245/91 (1991), to appear in the proceedings; *Theoretical implications of precision electroweak data*, talk at 4th Int. Symp. on Heavy Flavor Physics, Orsay, June 1991, prepr. CERN-TH.6206/91 (1991); *The standard electroweak theory and its experimental tests*, Lectures given at the LVth Les Houches Summer School, France, 30 June – 26 July, 1991, prepr. CERN-TH.6305/91 (1991).
- [66] A. Djouadi, A. Leike, T. Riemann, D. Schaile and C. Verzegnassi, Signals of new gauge bosons at future e^+e^- colliders, prepr. CERN-TH.6350/91 (1991), to appear in: *Proc. of the Workshop on e^+e^- Collisions at 500 GeV: The Physics Potential*, DESY, ed. P. Zerwas.
- [67] A. Gurtu, Fortran package ZFEPSLON - a package to be used with $ZF\overline{I}T_{ER}$.
- [68] B. Kniehl, *Comput. Phys. Commun.* **58** (1990) 293.
- [69] F. Jegerlehner, Renormalizing the Standard Model, in: *Testing the Standard Model – Proceedings of the 1990 Theoretical Advanced Study Institute in Elementary Particle Physics*, Boulder, Colorado, June 1990, eds. M. Cvetič and P. Langacker (World Scientific, Singapore, 1991), p. 476.
- [70] H. Burkhardt, F. Jegerlehner, G. Penso and C. Verzegnassi, *Z. Physik* **C43** (1989) 497.
- [71] D. Bardin et al., ZBIZON package, in [31], vol. 3, p. 60;
- [72] R. Kleiss et al., in: [31], vol. 3, p. 102. DELPHI note 89-71; L3-note 679 (1989).
- [73] A. Sirlin, *Phys. Letters* **B232** (1989) 123.
- [74] R. Kleiss et al., in: [31], vol. 3, p. 50.
- [75] R.N. Cahn, *Phys. Rev.* **D36** (1987) 2666.
- [76] S. Ganguli, A. Gurtu, K. Mazumdar and M. Sachwitz, L3 Note #797 (1990).
- [77] W. Beenakker, F.A. Berends and S.C. van der Marck, *Phys. Lett.* **B251** (1990) 299.
- [78] S. Jadach, B. Ward and Z. Wąs, *Comput. Phys. Commun.* **66** (1991) 276.
- [79] S. Riemann, Zeuthen prepr. PHE 91-04 (1991).
- [80] W. Beenakker and S. Riemann, private communication (1992).
- [81] B. A. Kniehl and R. G. Stuart, Fortran package ZOPOLE, prepr. CERN-TH.6439/92 (March 1992);

A Common Blocks

A.1 $ZFI^T T_{ER}$ Common Blocks

$ZFI^T T_{ER}$ common blocks of potential interest to the user are documented here.

```
COMMON /ZUPARS/QDF, QCDCOR, QCDCOB, ALPHST, SIN2TW, S2TEFF(0:11),
& WIDTHS(0:11)
```

The common block /ZUPARS/ contains some $ZFI^T T_{ER}$ parameters:

QDF is the final-state radiation factor $\frac{3}{4} \frac{\alpha}{\pi}$ introduced in (1.11) and (3.23).

QCDCOR is a QCD correction for all final quark states except $b\bar{b}$ defined in (3.79).

QCDCOB is a QCD correction for $b\bar{b}$ final states defined in (3.80).

ALPHST is $\alpha_s(M_Z^2)$ and is calculated as defined by flag ALST.

SIN2TW is $\sin^2 \theta_W$ as in (3.15).

S2TEFF are the values of $s_W^{2,\text{eff}}$ for each fermion channel (see (3.21) and table 10). Note that S2TEFF(10:11) are not defined.

WIDTHS are the partial decay widths (3.17) of the Z for fermion channels defined in table 10 (WIDTHS(11) is the total Z width).

```
COMMON/EWFORM/XALLCH(5,4), XFOTF
COMPLEX*16 XALLCH, XFOTF
```

Electroweak form factors are stored in the common block /EWFORM/.

XALLCH(I, J) contains the form factors ρ , κ_e , κ_f and κ_{ef} ($J = 1-4$) for neutrinos, leptons, u and c quarks, d and s quarks, and b quarks ($I = 1-5$). These have been introduced in (3.35).

XFOTF is $1 + \Delta\alpha(s)$ as used in (3.33).

```
COMMON/ZFCHMS/ALLCH(0:11), ALLMS(0:11)
```

The common block /ZFCHMS/ contains the charges and masses of the fermions (see table 10).

ALLCH the fermion charges.

ALLMS the fermion masses.

Note that ALLCH(10) and ALLMS(10) are undefined.

We would also like to mention that the variables FAA, FZA, FZZ which are introduced as DATA in subroutine EWCOUP allow us to switch on/off the $\gamma\gamma$, γZ , ZZ parts of the cross sections, respectively.

A.2 DIZET Common Blocks

Two DIZET internal common blocks of potential interest to the user are documented here.

```
COMMON/CDZRKZ/ARROFZ(0:10),ARKAFZ(0:10),ARVEFZ(0:10),ARSEFZ(0:10)
```

Weak form factors, ρ_f^Z and κ_f^Z , and vector couplings, \bar{v}_f^Z for partial Z widths (3.17) as calculated in subroutine ZWRATE. The indices correspond to those of table 10.

ARROFZ ρ_f^Z , introduced in (3.17).

ARKAFZ κ_f^Z , introduced in (3.17).

ARVEFZ \bar{v}_f^Z as defined in (3.19).

ARSEFZ Effective weak mixing angles $s_W^{2,f}$ as in (3.21).

Note that the 10th element of these arrays is undefined.

```
COMMON/CDZXKF/XROKF
```

This variable is the ratio of two different definitions of the weak mixing angle as defined in (8.3):

$$\Re XROKF = \frac{\sin^2 \theta_W^{\overline{MS}}}{\sin^2 \theta_W}.$$

B Subroutine ZFTEST

The $ZF\overline{I}T_{ER}$ distribution package includes subroutine ZFTEST which serves essentially three purposes:

1. It is an example of how to use $ZF\overline{I}T_{ER}$.
2. It is an internal consistency check of the different $ZF\overline{I}T_{ER}$ branches.
3. It allows one to check that $ZF\overline{I}T_{ER}$ has been properly installed on the machine.

The routine creates a table of cross sections and asymmetries as a function of \sqrt{s} near the Z peak.

To run ZFTEST the user needs to create the following main program:

```
PROGRAM ZFMAIN
CALL ZFTEST
END
```

After compiling and linking it to ZFITR4_5, DIZET and BHANG the results presented in appendix B.2 should be obtained. The corresponding Fortran files may be found at ZFITTER@CERNVM.

B.1 Subroutine ZFTEST

```
      SUBROUTINE ZFTEST
      =====
*****
*
*   SUBR. ZFTEST
*
*   Example program to demonstrate the use of the ZFITTER package.
*
*****
*
      IMPLICIT REAL*8(A-H,O-Z)
      COMPLEX*16 XVPOL
      DIMENSION XS(0:11,5),AFB(0:11,4),TAUPOL(2),TAUAFB(2)
*
* constants
*
      PARAMETER(GMU=1.166388D-5,ALFAI=137.0359895D0,ALFA=1.D0/ALFAI,
+             CONS=1.D0)
      PARAMETER(ZMASS=91.175D0,TMASS=140.D0,HMASS=300.D0)
      PARAMETER(AME=0.511D-3,AMU=0.106D0,AMT=1.784D0,ALFAS=.120D0)
      PARAMETER(RSMN=87.D0,DRS=1.D0,NRS=9)
      PARAMETER(ANG0=35D0,ANG1=145D0)
      PARAMETER(QE=-1.D0,AE=-.5D0,QU= 2.D0/3.D0,AU= .5D0,
+             QD=-1.D0/3.D0,AD=-.5D0)
*
* ZFITTER common blocks
*
      COMMON /ZUPARS/QDF,QCDCOR,QCDCOB,ALPHST,SIN2TW,S2TEFF(0:11),
& WIDTHS(0:11)
      COMMON /CDZRKZ/ARROFZ(0:10),ARKAFZ(0:10),ARVEFZ(0:10),ARSEFZ(0:10)
      COMMON /EWFORM/XALLCH(5,4),XFOTF
      COMPLEX*16 XALLCH,XFOTF
*
*-----
*
* initialize
*
      CALL ZUINIT
*
* set ZFITTER flags and print flag values
*
      CALL ZUFLAG('PRNT',1)
      CALL ZUINFO(0)
*
* do weak sector calculations
*
      CALL ZUWEAK(ZMASS,TMASS,HMASS,ALFAS)
*
```

```

* define cuts for fermion channels and print cut values
*
  CALL ZUCUTS( 1,0,15.DO,20.DO,0.DO,ANGO,ANG1)
  CALL ZUCUTS( 2,0,15.DO,20.DO,0.DO,ANGO,ANG1)
  CALL ZUCUTS( 3,0,15.DO,20.DO,0.DO,ANGO,ANG1)
  CALL ZUCUTS(11,0,15.DO,20.DO,0.DO,ANGO,ANG1)
  CALL ZUINFO(1)
*
* make table of cross sections and asymmetries
*
  PI   = DACOS(-1.DO)
  GAMZ = WIDTHS(11)/1000.
  GAME = WIDTHS( 1)/1000.
  GAE  = SQRT(ARROFZ(1))/2.
  GVE  = ARVEFZ(1)*GAE
  DO I = 1,NRS
    RS = RSMN+REAL(I-1)*DRS
* table header
  PRINT *, ' SQRT(S) = ',REAL(RS)
  PRINT *, '          <----- Cross Section ----->',
+ ' <----- Asymmetry ----->', ' <---TauPol--->'
  PRINT *, 'INDF  ZUTHSM  ZUXSEC  ZUXSA  ZUXSA2  ZUSMAT',
+ '  ZUTHSM  ZUXSA  ZUXSA2  ZUTPSM  ZUTAU'
* loop over fermion indices
  DO INDF = 0,11
    S=RS**2
* standard model interf. (INTRF=1)
    CALL ZUTHSM(INDF,RS,ZMASS,TMASS,HMASS,ALFAS,
+   XS(INDF,1),AFB(INDF,1))
    IF(INDF.EQ.3) CALL ZUTPSM(RS,ZMASS,TMASS,HMASS,ALFAS,
+   TAUPOL(1),TAUAFB(1))
* cross section interf. (INTRF=2)
    GAMF = WIDTHS(INDF)/1000.
    IF(INDF.EQ.11) GAMF = WIDTHS( 1)/1000.
    CALL ZUXSEC(INDF,RS,ZMASS,GAMZ,GAME,GAMF,XS(INDF,2))
* cross section & forward--backward asymmetry interf. (INTRF=3)
    IF(INDF.NE.0 .AND. INDF.NE.10) THEN
      GAF = SQRT(ARROFZ(INDF))/2.
      GVF = ARVEFZ(INDF)*GAF
      IF(INDF.EQ.11) THEN
        GAF = SQRT(ARROFZ(1))/2.
        GVF = ARVEFZ(1)*GAF
      ENDIF
      CALL ZUXSA(INDF,RS,ZMASS,GAMZ,0,GVE,GAE,GVF,GAF,
+   XS(INDF,3),AFB(INDF,3))
    ENDIF
* tau polarization interf. (INTRF=3)
    IF(INDF.EQ.3) CALL ZUTAU(RS,ZMASS,GAMZ,0,GVE,GAE,GVF,GAF,
+   TAUPOL(2),TAUAFB(2))
* cross section & forward--backward asymmetry interf. for gv**2 and

```

```

* ga**2 (IBRA=4)
  IF((INDF.GE.1 .AND. INDF.LE.3) .OR. INDF.EQ.11) THEN
    GVF2 = GVF**2
    GAF2 = GAF**2
    CALL ZUXSA2(INDF,RS,ZMASS,GAMZ,0,GVF2,GAF2,
+     XS(INDF,4),AFB(INDF,4))
  ENDIF
* S-matrix interf. (INTRF=5)
* Parameters are fitted with code FITSMA FORTRAN.
  IF(INDF.EQ.2 .OR. INDF.EQ.10) THEN
    IF(INDF.EQ.2) THEN
      AMZS =91.14132D0
      GAMZS= 2.48354D0
      RR=0.14159D0
      RI=0.15092D0
      RG=1.13310D0
    ELSE
      AMZS =91.14126D0
      GAMZS= 2.48406D0
      RR=2.94028D0
      RI=3.15125D0
      RG=2.81462D0
    ENDIF
C The parameters AMZS, GAMZS, RR, RI, RG correspond to:
C     AMZS  = ZMASS-GAMZ**2/2.DO/ZMASS
C     GAMZS = GAMZ -GAMZ**3/2.DO/ZMASS**2
C     VE    = -.5D0+2.DO*SIN2TW
C     VU    = 0.5D0-4.DO/3.DO*SIN2TW
C     VD    = -0.5D0+2.DO/3.DO*SIN2TW
C     AKAPPA = GMU*AMZS1*AMZS1/(SQRT(2.DO)*2.DO*PI*ALFA)
C     XVPOL  = 1.DO/(2.DO-XFOTF)
C     IF(INDF.LE.3) THEN
C         RZ = CONS*AKAPPA**2*(AE**2+VE**2)**2*(1.DO+.75D0*ALFA/PI)
C         SZ = CONS*AKAPPA*VE**2*(1.DO+.75D0*ALFA/PI)
C         RG = CONS*CDABS(XVPOL)**2*(1.DO+.75D0*ALFA/PI)
C     ELSE
C         RZ = CONS*AKAPPA**2*(AE**2+VE**2)*3.DO*
+         (2.DO*(AU**2+VU**2)+3.DO*(AD**2+VD**2))
C         SZ = CONS*AKAPPA*3.DO*QE*VE*(2.DO*VU*QU+3.DO*VD*QD)
C         RG = CONS*CDABS(XVPOL)**2*3.DO*11.DO/9.DO
C     ENDIF
C     RR = RZ
C     RI = RZ+2.DO*SZ*DREAL(XVPOL)
c
    R1 = 0d0
    R2 = 0d0
    R3 = 0d0
    CALL ZUSMAT(INDF,RS,AMZS,GAMZS,RR,RI,R0,R1,R2,RG,XS(INDF,5))
  ENDIF
* results

```

```

      IF(INDF.EQ.0) THEN
        PRINT 9000,INDF,(XS(INDF,J),J=1,2)
      ELSEIF(INDF.EQ.1 .OR. INDF.EQ.11) THEN
        PRINT 9010,INDF,(XS(INDF,J),J=1,4),AFB(INDF,1),
+       (AFB(INDF,J),J=3,4)
      ELSEIF(INDF.EQ.2) THEN
        PRINT 9005,INDF,(XS(INDF,J),J=1,5),AFB(INDF,1),
+       (AFB(INDF,J),J=3,4)
      ELSEIF(INDF.EQ.3) THEN
        PRINT 9015,INDF,(XS(INDF,J),J=1,4),AFB(INDF,1),
+       (AFB(INDF,J),J=3,4),(TAUPOL(J),J=1,2)
      ELSEIF(INDF.EQ.10) THEN
        PRINT 9025,INDF,(XS(INDF,J),J=1,2),XS(INDF,5)
      ELSE
        PRINT 9020,INDF,(XS(INDF,J),J=1,3),AFB(INDF,1),
+       AFB(INDF,3)
      ENDIF
    ENDDO
  PRINT *
  ENDDO
  RETURN
9000 FORMAT(1X,I4,2F8.4)
9005 FORMAT(1X,I4,9F8.4)
9010 FORMAT(1X,I4,4F8.4,8X,3F8.4)
9015 FORMAT(1X,I4,4F8.4,8X,5F8.4)
9020 FORMAT(1X,I4,3F8.4,16X,2F8.4)
9025 FORMAT(1X,I4,2F8.4,16X,F8.4)
*
      END
      END ZFTEST

```

B.2 ZFTEST Results

```
*****
*****
**          This is ZFITTER version 4.5          **
**          92/04/19                             **
*****
** The authors of the ZFITTER package are:      **
**                                               **
** D.Bardin      (Dubna)                       **
** M.Bilenky     (Dubna)                       **
** A.Chizhov     (Dubna)                       **
** A.Olshevsky   (Dubna)                       **
** S.Riemann     (Zeuthen)                     **
** T.Riemann     (Zeuthen)                     **
** M.Sachwitz    (Zeuthen)                     **
** A.Sazonov     (Dubna)                       **
** Yu.Sedykh     (Dubna)                       **
** I.Sheer       (UC San Diego)                **
**                                               **
*****
** Questions and comments to ZFITTER@CERNVM.CERN.CH **
*****
```

ZUINIT> ZFITTER defaults:

ZFITTER flag values:

AFBC: 1 ALPH: 0 ALST: 1 AMT4: 3 BORN: 0
BOXD: 0 CONV: 0 FINR: 1 FOT2: 1 GAMS: 1
INCL: 1 INTF: 1 DUMY: 0 PART: 0 POWR: 1
PRNT: 0 QCD3: 1 QCDC: 1 VPOL: 3 WEAK: 1

ZFITTER cut values:

INDF	ICUT	ACOL	EMIN	S_PR	ANGO	ANG1
0	-1	0.00	0.0000	0.0000	0.00	180.00
1	-1	0.00	0.0000	0.0000	0.00	180.00
2	-1	0.00	0.0000	0.0000	0.00	180.00
3	-1	0.00	0.0000	0.0000	0.00	180.00
4	-1	0.00	0.0000	0.0000	0.00	180.00
5	-1	0.00	0.0000	0.0000	0.00	180.00
6	-1	0.00	0.0000	0.0000	0.00	180.00
7	-1	0.00	0.0000	0.0000	0.00	180.00
8	-1	0.00	0.0000	0.0000	0.00	180.00
9	-1	0.00	0.0000	0.0000	0.00	180.00
10	-1	0.00	0.0000	0.0000	0.00	180.00
11	-1	0.00	0.0000	0.0000	0.00	180.00

ZFITTER flag values:

AFBC: 1 ALPH: 0 ALST: 1 AMT4: 3 BORN: 0
BOXD: 0 CONV: 0 FINR: 1 FOT2: 1 GAMS: 1
INCL: 1 INTF: 1 DUMY: 0 PART: 0 POWR: 1
PRNT: 1 QCD3: 1 QCDC: 1 VPOL: 3 WEAK: 1

ZMASS = 91.17500; TMASS = 140.00000
 HMASS = 300.00000; ALFAS = 0.12000
 ALPHST = 0.12000; SIN2TW = 0.22817
 QCDCOR = 1.03954; QCDCOB = 1.04020

CHANNEL	WIDTH
-----	-----
nu,nubar	166.6
e+,e-	83.6
mu+,mu-	83.6
tau+,tau-	83.4
u,ubar	296.6
d,dbar	382.9
c,cbar	296.2
s,sbar	382.9
t,tbar	0.0
b,bbar	375.7
hadron	1734.2
total	2484.7

ZFITTER cut values:

INDF	ICUT	ACOL	EMIN	S_PR	ANGO	ANG1
0	-1	0.00	0.0000	0.0000	0.00	180.00
1	0	15.00	20.0000	0.0000	35.00	145.00
2	0	15.00	20.0000	0.0000	35.00	145.00
3	0	15.00	20.0000	0.0000	35.00	145.00
4	-1	0.00	0.0000	0.0000	0.00	180.00
5	-1	0.00	0.0000	0.0000	0.00	180.00
6	-1	0.00	0.0000	0.0000	0.00	180.00
7	-1	0.00	0.0000	0.0000	0.00	180.00
8	-1	0.00	0.0000	0.0000	0.00	180.00
9	-1	0.00	0.0000	0.0000	0.00	180.00
10	-1	0.00	0.0000	0.0000	0.00	180.00
11	0	15.00	20.0000	0.0000	35.00	145.00

SQRT(S) = 87.0000000

```
<----- Cross Section -----> <----- Asymmetry ----->
INDF  ZUTHSM  ZUXSEC  ZUXSA  ZUXSA2  ZUSMAT  ZUTHSM  ZUXSA  ZUXSA2
  0  0.2363  0.2364
  1  0.0935  0.0935  0.0935  0.0935      -0.3521 -0.3521 -0.3521
  2  0.0954  0.0954  0.0954  0.0954  0.0954 -0.3522 -0.3521 -0.3521
  3  0.0961  0.0961  0.0961  0.0961      -0.3525 -0.3524 -0.3524
  4  0.4504  0.4504  0.4505
  5  0.5480  0.5480  0.5481      -0.0097 -0.0097
  6  0.4414  0.4414  0.4415      -0.1837 -0.1837
  7  0.5472  0.5472  0.5473      -0.0097 -0.0097
  8  0.0000  0.0000  0.0000      0.0000  0.0000
  9  0.5346  0.5346  0.5347      -0.0103 -0.0103
 10  2.5217  2.5217      2.5217
 11  0.4405  0.4404  0.4404  0.4406      0.6259  0.6258  0.6258
<---TauPol--->
INDF  ZUTPSM  ZUTAU
  3  -0.0825 -0.0826
```

SQRT(S) = 88.0000000

```
<----- Cross Section -----> <----- Asymmetry ----->
INDF  ZUTHSM  ZUXSEC  ZUXSA  ZUXSA2  ZUSMAT  ZUTHSM  ZUXSA  ZUXSA2
  0  0.3826  0.3827
  1  0.1461  0.1461  0.1461  0.1461      -0.2723 -0.2722 -0.2722
  2  0.1489  0.1489  0.1490  0.1490  0.1489 -0.2724 -0.2723 -0.2723
  3  0.1500  0.1500  0.1501  0.1501      -0.2727 -0.2726 -0.2726
  4  0.7092  0.7091  0.7093
  5  0.8831  0.8831  0.8832      0.0149  0.0149
  6  0.7000  0.6999  0.7001      -0.1255 -0.1255
  7  0.8824  0.8823  0.8825      0.0149  0.0149
  8  0.0000  0.0000  0.0000      0.0000  0.0000
  9  0.8635  0.8633  0.8635      0.0145  0.0145
 10  4.0381  4.0378      4.0381
 11  0.5124  0.5122  0.5122  0.5124      0.5569  0.5568  0.5569
<---TauPol--->
INDF  ZUTPSM  ZUTAU
  3  -0.0951 -0.0952
```

SQRT(S) = 89.0000000

	<----- Cross Section ----->					<----- Asymmetry ----->		
INDF	ZUTHSM	ZUXSEC	ZUXSA	ZUXSA2	ZUSMAT	ZUTHSM	ZUXSA	ZUXSA2
0	0.7007	0.7007						
1	0.2609	0.2608	0.2609	0.2609		-0.1870	-0.1868	-0.1868
2	0.2658	0.2658	0.2659	0.2659	0.2658	-0.1870	-0.1869	-0.1869
3	0.2677	0.2677	0.2678	0.2678		-0.1873	-0.1871	-0.1871
4	1.2733	1.2731	1.2734			-0.0662	-0.0661	
5	1.6126	1.6124	1.6127			0.0388	0.0388	
6	1.2634	1.2633	1.2635			-0.0666	-0.0666	
7	1.6118	1.6117	1.6120			0.0388	0.0388	
8	0.0000	0.0000	0.0000			0.0000	0.0000	
9	1.5792	1.5789	1.5792			0.0385	0.0385	
10	7.3403	7.3394			7.3402			
11	0.6562	0.6558	0.6561	0.6562		0.4592	0.4591	0.4593

<---TauPol--->

INDF	ZUTPSM	ZUTAU
3	-0.1071	-0.1072

SQRT(S) = 90.0000000

	<----- Cross Section ----->					<----- Asymmetry ----->		
INDF	ZUTHSM	ZUXSEC	ZUXSA	ZUXSA2	ZUSMAT	ZUTHSM	ZUXSA	ZUXSA2
0	1.4868	1.4867						
1	0.5452	0.5451	0.5453	0.5453		-0.0993	-0.0992	-0.0992
2	0.5555	0.5553	0.5555	0.5555	0.5554	-0.0994	-0.0992	-0.0992
3	0.5593	0.5592	0.5593	0.5593		-0.0996	-0.0994	-0.0994
4	2.6703	2.6698	2.6704			-0.0086	-0.0085	
5	3.4173	3.4169	3.4175			0.0617	0.0617	
6	2.6586	2.6581	2.6587			-0.0086	-0.0085	
7	3.4166	3.4161	3.4167			0.0617	0.0617	
8	0.0000	0.0000	0.0000			0.0000	0.0000	
9	3.3503	3.3495	3.3501			0.0614	0.0615	
10	15.5131	15.5104			15.5119			
11	0.9678	0.9669	0.9677	0.9679		0.3302	0.3301	0.3303

<---TauPol--->

INDF	ZUTPSM	ZUTAU
3	-0.1181	-0.1182

SQRT(S) = 91.0000000

```
<----- Cross Section -----> <----- Asymmetry ----->
INDF  ZUTHSM  ZUXSEC   ZUXSA  ZUXSA2  ZUSMAT  ZUTHSM  ZUXSA  ZUXSA2
  0  2.8218  2.8214
  1  1.0295  1.0292  1.0295  1.0295          -0.0155 -0.0153 -0.0153
  2  1.0484  1.0481  1.0485  1.0485  1.0484 -0.0155 -0.0153 -0.0153
  3  1.0556  1.0552  1.0556  1.0556          -0.0156 -0.0154 -0.0154
  4  5.0483  5.0472  5.0483          0.0453  0.0454
  5  6.4869  6.4858  6.4870          0.0826  0.0827
  6  5.0335  5.0323  5.0335          0.0454  0.0455
  7  6.4862  6.4850  6.4862          0.0826  0.0827
  8  0.0000  0.0000  0.0000          0.0000  0.0000
  9  6.3635  6.3617  6.3629          0.0825  0.0825
 10 29.4183 29.4120          29.4150
 11  1.3601  1.3581  1.3600  1.3601          0.2053  0.2052  0.2054
<---TauPol--->
INDF  ZUTPSM  ZUTAU
  3  -0.1274 -0.1275
```

SQRT(S) = 92.0000000

```
<----- Cross Section -----> <----- Asymmetry ----->
INDF  ZUTHSM  ZUXSEC   ZUXSA  ZUXSA2  ZUSMAT  ZUTHSM  ZUXSA  ZUXSA2
  0  2.3301  2.3295
  1  0.8526  0.8523  0.8525  0.8525          0.0530  0.0532  0.0532
  2  0.8681  0.8677  0.8680  0.8680  0.8681  0.0529  0.0531  0.0531
  3  0.8739  0.8735  0.8738  0.8738          0.0529  0.0531  0.0531
  4  4.1794  4.1783  4.1793          0.0884  0.0885
  5  5.3632  5.3620  5.3630          0.0993  0.0994
  6  4.1661  4.1650  4.1660          0.0886  0.0887
  7  5.3624  5.3612  5.3622          0.0994  0.0994
  8  0.0000  0.0000  0.0000          0.0000  0.0000
  9  5.2618  5.2601  5.2611          0.0993  0.0994
 10 24.3329 24.3266          24.3329
 11  0.9720  0.9701  0.9719  0.9719          0.1624  0.1624  0.1626
<---TauPol--->
INDF  ZUTPSM  ZUTAU
  3  -0.1341 -0.1341
```

SQRT(S) = 93.0000000

	<----- Cross Section ----->					<----- Asymmetry ----->		
INDF	ZUTHSM	ZUXSEC	ZUXSA	ZUXSA2	ZUSMAT	ZUTHSM	ZUXSA	ZUXSA2
0	1.3333	1.3329						
1	0.4914	0.4912	0.4913	0.4913		0.1013	0.1015	0.1015
2	0.5002	0.5000	0.5001	0.5001	0.5002	0.1013	0.1015	0.1015
3	0.5035	0.5033	0.5035	0.5035		0.1013	0.1015	0.1015
4	2.4063	2.4056	2.4062			0.1182	0.1183	
5	3.0742	3.0734	3.0740			0.1110	0.1111	
6	2.3957	2.3950	2.3956			0.1186	0.1187	
7	3.0735	3.0727	3.0733			0.1111	0.1111	
8	0.0000	0.0000	0.0000			0.0000	0.0000	
9	3.0156	3.0145	3.0151			0.1111	0.1112	
10	13.9653	13.9612			13.9658			
11	0.5607	0.5595	0.5606	0.5606		0.2113	0.2113	0.2115

<---TauPol--->

INDF	ZUTPSM	ZUTAU
3	-0.1381	-0.1380

SQRT(S) = 94.0000000

	<----- Cross Section ----->					<----- Asymmetry ----->		
INDF	ZUTHSM	ZUXSEC	ZUXSA	ZUXSA2	ZUSMAT	ZUTHSM	ZUXSA	ZUXSA2
0	0.8343	0.8340						
1	0.3102	0.3100	0.3101	0.3101		0.1358	0.1360	0.1360
2	0.3157	0.3156	0.3157	0.3157	0.3157	0.1357	0.1359	0.1359
3	0.3178	0.3177	0.3178	0.3178		0.1357	0.1359	0.1359
4	1.5173	1.5168	1.5172			0.1390	0.1391	
5	1.9272	1.9267	1.9270			0.1193	0.1194	
6	1.5081	1.5076	1.5080			0.1397	0.1398	
7	1.9266	1.9260	1.9264			0.1194	0.1194	
8	0.0000	0.0000	0.0000			0.0000	0.0000	
9	1.8899	1.8892	1.8895			0.1195	0.1196	
10	8.7692	8.7663			8.7692			
11	0.3862	0.3854	0.3861	0.3862		0.3006	0.3006	0.3008

<---TauPol--->

INDF	ZUTPSM	ZUTAU
3	-0.1404	-0.1403

SQRT(S) = 95.0000000

	<----- Cross Section ----->					<----- Asymmetry ----->		
INDF	ZUTHSM	ZUXSEC	ZUXSA	ZUXSA2	ZUSMAT	ZUTHSM	ZUXSA	ZUXSA2
0	0.5808	0.5805						
1	0.2180	0.2178	0.2179	0.2179		0.1617	0.1619	0.1619
2	0.2218	0.2217	0.2218	0.2218	0.2219	0.1615	0.1617	0.1617
3	0.2233	0.2232	0.2233	0.2233		0.1615	0.1617	0.1617
4	1.0652	1.0648	1.0650			0.1542	0.1542	
5	1.3442	1.3438	1.3441			0.1255	0.1256	
6	1.0567	1.0563	1.0566			0.1552	0.1553	
7	1.3436	1.3432	1.3434			0.1256	0.1257	
8	0.0000	0.0000	0.0000			0.0000	0.0000	
9	1.3177	1.3171	1.3174			0.1258	0.1259	
10	6.1274	6.1252			6.1271			
11	0.3061	0.3056	0.3060	0.3061		0.3902	0.3902	0.3904
	<---TauPol--->							
INDF	ZUTPSM	ZUTAU						
3	-0.1417	-0.1416						